



CHESTER

Compressed Heat Energy
Storage for Energy
from Renewable sources

D2.3 Requirements of the overall CHEST system

PROJECT	CHESTER
PROJECT NO.	764042
DELIVERABLE NO.	D2.3
DOCUMENT VERSION	V2.1
DOCUMENT PREPARATION DATE	08/02/2019
RESPONSIBLE PARTNER	PlanEnergi
DISSEMINATION LEVEL	Public

Type of Deliverable		
R	Document, Report	X
DEM	Demonstrator, pilot, prototype	
DEC	Websites, patent fillings, videos, etc.	
OTHER		
ETHICS	Ethics requirements	
ORDP	Open Research Data Pilot	



This project has received funding from the European Union's Horizon 2020 research and innovation programme under grant agreement No. 764042.

This deliverable reflects only the author's views and neither Agency nor the Commission are responsible for any use that may be made of the information contained therein.

EC Grant Agreement	No.764042
Project Acronym	CHESTER
Project Title	Compressed Heat Energy Storage for Energy from Renewable sources
Programme	HORIZON 2020
Start Date of Project	01-04-2018
Duration	48 Months

Financial/Administrative Coordinator

Project Coordinator Organization Name	TECNALIA
Address	Parque Tecnológico de Bizkaia C/ Astondo, Edificio 700 (Spain)
Phone Numbers	+34 946 430 850
E-mail Address	eduardo.zabala@tecnalia.com
Project web-site	www.chester-project.eu

Version Management

Filename	CHESTER D2.3 Requirements of the overall CHEST system		
Authors	F. Bava, M. Kowalska, S. Stark, H. Jockenhöfer, S. Amelio		
Reviewed by	Silvia Alonso		
Approved by	Eduardo Zabala		
Revision No.	Date	Author	Modification description
V0.1	09/01/2019	F. Bava	Common update of the TRNSYS model + specific model update for Turin and Ispaster
V0.2	18/01/2019	M. Kowalska, F. Bava	Addition of Ispaster case study
V0.3	20/01/2019	S. Stark, H. Jockenhöfer	Addition of Barcelona case study
V0.4	21/01/2019	S. Amelio, F. Bava	Addition of Turin case study
V1.0	25/01/2019	F. Bava	Complete draft of full report
V1.1	30/01/2019	S. Stark	Update of Barcelona cases study
V2.0	31/01/2019	A. Carrera	Internal revision
V2.1	05/02/2019	S. Alonso	Final review

Contents

1.	Introduction.....	10
1.1.	Purpose and Scope	10
1.2.	Structure of the document.....	10
2.	Update of the TRNSYS model	11
2.1.	Common features of the updated TRNSYS model	11
2.1.1.	Condensation to the environment	12
2.1.2.	Updated clean-up strategy of the HT-TES	13
2.2.	Specific features in the individual TRNSYS models.....	14
2.2.1.	Case Study #1: Turin, Italy	14
2.2.2.	Case Study #3: Ispaster, Spain	19
2.2.3.	Case Study #4: Barcelona, Spain.....	25
3.	Simulation results	31
3.1.	Variable HT-HP and ORC capacities with infinite HT-TES	31
3.1.1.	Case Study #1: Turin	31
3.1.2.	Case Study #3: Ispaster.....	34
3.1.3.	Case Study #4: Barcelona	38
3.1.4.	General discussion.....	41
3.2.	Variable HT-HP and ORC capacities with finite HT-TES	43
3.2.1.	Case Study #1: Turin	43
3.2.2.	Case Study #3: Ispaster.....	44
3.2.3.	Case Study #4: Barcelona	47
3.2.4.	General discussion.....	52
3.3.	Blow-off operation against condensation to the environment.....	54
3.3.1.	Case Study #1: Turin	54
3.3.2.	Case Study #3: Ispaster.....	54
3.3.3.	Case Study #4: Barcelona	57
3.3.4.	General discussion.....	61
3.4.	Working fluid: R1233zd(E) against Butene	62
3.5.	RES electricity production and electricity demand	67
3.5.1.	Case Study #1: Turin	67
3.5.2.	Case Study #3: Ispaster.....	68
3.5.3.	Case Study #4: Barcelona	70
4.	Conclusions.....	73
4.1.1.	Case Study #1: Turin	73
4.1.2.	Case Study #3: Ispaster.....	73



4.1.3. Case study #4: Barcelona..... 74

4.1.4. General conclusions..... 75

5. Appendix A 77

References..... 79

List of Figures

Figure 1: TRNSYS model of the CHEST system as used in the CHESTER deliverable D2.2.....	11
Figure 2: Distribution of deviation between actual production and commitment of the Moncalieri 3GT plant in Turin case during the year (8760 hours).	15
Figure 3: Distribution of the unbalanced power (production - commitment) of the Moncalieri 3GT plant (unbalances equal to 0 are not counted in the corresponding bin (-1,0]).	15
Figure 4: TRNSYS model used for Turin case study.	16
Figure 5: Monthly-average temperatures of the Po river at the Moncalieri plant during the year.	17
Figure 6: Profiles of the DH demand and of the electricity production from 3GT in 2017.	18
Figure 7: TRNSYS model used for Ispaster case study.....	20
Figure 8: Monthly average dry bulb temperatures of air in Santander city over a year.....	21
Figure 9: Electricity demand profile and electricity output from PV plant in Ispaster case.....	23
Figure 10: Profiles of the DH heat load and heat output from the solar collectors in the scenario without the CHEST system in Ispaster case.....	24
Figure 11: TRNSYS model used for Barcelona case study.	26
Figure 12: Ambient air temperatures of Barcelona and monthly-average temperatures of the sea water in Barcelona during the year.	26
Figure 13: Profiles of the RES electricity production and the electricity demand used in Barcelona case.....	27
Figure 14: Profiles of the DH heat demand and RES heat availability used in Barcelona case.	27
Figure 15: Electricity absorbed by the HT-HP and produced by the ORC as function of the HT-HP capacity for a fixed ORC relative capacity of 0.4 (infinite HT-TES size).	31
Figure 16: Electricity production of the ORC as a function of the ORC relative capacity for different sizes of HT-HP (legend entries, in MW) and infinite HT-TES size.	32
Figure 17: Full-load hours of the ORC as function of the ORC relative capacity for different sizes of HT-HP (legend entries, in MW) and infinite HT-TES size.	32
Figure 18: COP of the HT-HP as a function of the HT-HP capacity for a fixed ORC relative capacity of 0.4 (infinite HT-TES size).	33
Figure 19: P2P ratio of the CHEST system as a function of the HT-HP capacity for a fixed ORC relative capacity of 0.4 (infinite HT-TES size).	34
Figure 20: Distribution of electric surplus and electric deficit in Ispaster case during the year (8760 hours).35	
Figure 21: Full-load hours of the ORC as a function of its relative capacity for different sizes of the HT-HP (infinite HT-TES size).	36
Figure 22: HT-HP electricity consumption and ORC electricity output as a function of the HT-HP capacity (infinite HT-TES size).	36
Figure 23: Full-load hours of the HT-HP as a function of its capacity (infinite HT-TES size).	37
Figure 24: COP of the HT-HP, the efficiency of the ORC and P2P ratio as a function of the HT-HP capacity (infinite HT-TES size).	37
Figure 25: Additional heat production from the DH boiler with respect to the case without CHEST and condensing heat dissipated to the environment.	38
Figure 26: Distribution of the electricity surplus and the electricity deficit in the Barcelona case study during a year (8760 hours).....	38
Figure 27: Electricity absorbed by the HT-HP as a function of the ORC relative capacity for different HT-HP capacities (infinite HT-TES size).	39
Figure 28: Electricity produced by the ORC as a function of the ORC relative capacity for different HT-HP capacities (infinite HT-TES size).	39
Figure 29: Electricity absorbed by the HT-HP and produced by the ORC as a function of the HT-HP capacity, for an ORC relative capacity of 0.50 (infinite HT-TES size).	40

Figure 30: COP, ORC efficiency and P2P ratio as a function of the HT-HP capacity, for an ORC relative capacity of 0.50 (infinite HT-TES size). 40

Figure 31: Electricity absorbed by the HT-HP as a function of the HT-TES capacity for different HT-HP capacities and ORC relative capacities. 43

Figure 32: Full-load hours of the HT-HP as a function of the HT-TES capacity for different HT-HP capacities and ORC relative capacities. 44

Figure 33: Full-load hours of the ORC as a function of the HT-TES capacity for different HT-HP capacities and ORC relative capacities. 44

Figure 34: Full-load hours of the HT-HP (solid lines) and the ORC (dashed lines) as a function of the HT-TES capacity. The legend entries denote the capacity of the HT-HP (ORC relative capacity = 1). 45

Figure 35: COP of the HT-HP as a function of the HT-TES capacity. The legend entries denote the capacity of the HT-HP (ORC relative capacity = 1). 45

Figure 36: Full-load hours of the HT-HP as a function of the ORC relative capacity for 1 kW and 9 kW HT-HP, and an 8 h and 12 h HT-TES. 46

Figure 37: ORC electricity production as a function of the ORC relative capacity for 1 kW and 9 kW HT-HP, and an 8 h and a 12 h HT-TES. 47

Figure 38: Additional heat output from the boiler compared to reference scenario without CHEST as function of the ORC relative capacity for 1 kW and 9 kW HT-HP, and an 8 h and 12 h HT-TES. 47

Figure 39: Electricity absorbed by the HT-HP as a function of the HT-TES size for different HT-HP capacities (ORC relative capacity = 1). 48

Figure 40: Electricity produced by the ORC as a function of the HT-TES size for different HT-HP capacities (ORC relative capacity = 1). 48

Figure 41: P2P ratio as a function of the HT-TES size for different HT-HP capacities (ORC relative capacity = 1). 49

Figure 42: Electricity absorbed by the HT-HP as a function of the ORC relative capacity for different HT-HP capacities and different HT-TES sizes. 49

Figure 43: Electricity produced by the ORC as a function of the ORC relative capacity for different HT-HP capacities and different HT-TES sizes. 50

Figure 44: COP of the HT-HP as a function of the ORC relative capacity for different HT-HP capacities and different HT-TES sizes. 50

Figure 45: ORC efficiency as a function of the ORC relative capacity for different HT-HP capacities and different HT-TES sizes. 51

Figure 46: P2P ratio as a function of the ORC relative capacity for different HT-HP capacities and different HT-TES sizes. 51

Figure 47: Boiler output as a function of the ORC relative capacity for different HT-HP capacities and 2 different HT-TES sizes. 52

Figure 48: ORC efficiency in different condensation modes as a function of the HT-HP capacity. 54

Figure 49: Temperature at the bottom of the LT-TES over a year for the operation of 3 kW and 5 kW HT-HP at partial condensation mode. 55

Figure 50: Heat production from the DH boiler and heat blown-off to the environment from the ORC loop. 56

Figure 51: Heat production from the DH boiler and heat dissipated to the environment by the ambient condenser. 56

Figure 52: Heat production from the DH boiler, heat blown-off to the environment from the ORC loop and heat dissipated to the environment by the ambient condenser in partial condensation mode. 56

Figure 53: “Electric efficiency” of the CHEST system in three different ORC condensation modes. 57

Figure 54: Electricity absorbed by the HT-HP as a function of the HT-HP capacity for a HT-TES of 12 h, an ORC relative capacity of 0.50 and different condensation modes. 58

Figure 55: Electricity produced by the ORC as a function of the HT-HP capacity for a HT-TES of 12 h, an ORC relative capacity of 0.50 and different condensation modes.....	59
Figure 56: COP of the HT-HP as a function of the HT-HP capacity for a HT-TES of 12 h, an ORC relative capacity of 0.50 and different condensation modes.....	59
Figure 57: ORC efficiency as a function of the HT-HP capacity for a HT-TES of 12 h, an ORC relative capacity of 0.50 and different condensation modes.....	59
Figure 58: P2P ratio as a function of the HT-HP capacity for a HT-TES of 12 h, an ORC relative capacity of 0.50 and different condensation modes.	59
Figure 59: Boiler output as a function of the HT-HP capacity for a HT-TES of 12 h, an ORC relative capacity of 0.50 and different condensation modes.	60
Figure 60: “Electric efficiency” as a function of the HT-HP capacity for a HT-TES of 12 h, an ORC relative capacity of 0.50 and different condensation modes.....	60
Figure 61: Electricity absorbed by the HT-HP as a function of the ORC relative capacity for different working fluids, a HT-HP capacity of 1 MW, HT-TES sizes of 6 and 12 h.	62
Figure 62: Electricity produced by the ORC as a function of the ORC relative capacity for different working fluids, a HT-HP capacity of 1 MW, HT-TES sizes of 6 and 12 h.	63
Figure 63: COP of the HT-HP as a function of the ORC relative capacity for different working fluids, a HT-HP capacity of 1 MW, HT-TES sizes of 6 and 12 h.....	63
Figure 64: ORC efficiency as a function of the ORC relative capacity for different working fluids, a HT-HP capacity of 1 MW, HT-TES sizes of 6 and 12 h.....	63
Figure 65: P2P ratio as a function of the ORC relative capacity for different working fluids, a HT-HP capacity of 1 MW, HT-TES sizes of 6 and 12 h.	64
Figure 66: COP of the HT-HP as a function of the ORC relative capacity for 2 different working fluids, a HT-HP capacity of 1 MW, HT-TES sizes of 6 and 12 h.	64
Figure 67: ORC efficiency as a function of the ORC relative capacity for 2 different working fluids, a HT-HP capacity of 1 MW, HT-TES sizes of 6 and 12 h.....	65
Figure 68: P2P ratio as a function of the ORC relative capacity for 2 different working fluids, a HT-HP capacity of 1 MW, HT-TES sizes of 6 and 12 h.....	65
Figure 69: Electricity absorbed by the HT-HP as function of the HT-TES capacity.....	67
Figure 70: COP of the HT-HP for the different HT-HP capacities in for a solar collector area of 54 m ² (S=100%), 108 m ² (S=200%) and 162 m ² (S=300%), and ORC relative capacity of 0.15.....	68
Figure 71: Electricity output from the ORC as function of the ORC relative capacity for the different HT-HP capacities for a solar collector area.....	69
Figure 72: Annual heat production from the DH boiler as a function of the HT-HP capacity in the reference case and for a solar collector area with the CHEST system in operation.....	70
Figure 73: Electricity absorbed by the HT-HP as a function of the ORC relative capacity for different HT-HP capacities, a HT-TES of 12 h and 3 different ratios R of RES electricity production to electricity demand. ...	71
Figure 74: Electricity produced by the ORC as a function of the ORC relative capacity for different HT-HP capacities, a HT-TES of 12 h and 3 different ratios R of RES electricity production to electricity demand. ...	71
Figure 75: COP of the HT-HP as a function of the ORC relative capacity for different HT-HP capacities, a HT-TES of 12 h and 3 different ratios R of RES electricity production to electricity demand.....	71
Figure 76: ORC efficiency as a function of the ORC relative capacity for different HT-HP capacities, a HT-TES of 12 h and 3 different ratios R of RES electricity production to electricity demand.	72
Figure 74: Technical datasheet of the PV module (REC250PE) used in Ispaster case.....	77
Figure 78: Technical datasheet of the CPC collector (STAR 19/49) used in Ispaster case.....	78

List of Tables

Table 1: General parameters for Turin case (on an annual basis).....	19
Table 2: Overview of the main parameters varied in the different parametric analyses.	19
Table 3: General parameters for Ispaster case (yearly basis).	22
Table 4: Overview of the main parameters varied in the different parametric analyses.	22
Table 5: General parameters for Barcelona case during the 2 nd year of operation (on an annual basis).....	28
Table 6: Overview of the main parameters varied in the different parametric analyses presented in the following sections of this deliverable.	29
Table 7: General parameters for Turin case (on an annual basis).....	67
Table 8: Overview of the amounts of heat and electricity in three different scenarios.	75

Glossary, Abbreviations and Acronyms

CHEST	Compressed Heat Energy Storage
COP	Coefficient of Performance
CPC	Compound Parabolic Collector
DH	District Heating
HP	Heat Pump
HT	High Temperature
HX	Heat Exchanger
LT	Low Temperature
P2P	Power-to-power
ORC	Organic Rankine Cycle
RES	Renewable Energy Source
TES	Thermal Energy Storage
TRNSYS	Transient System Simulation (software) ©
WtE	Waste-to-Energy (plant)

1. Introduction

1.1. Purpose and Scope

This deliverable describes the simulation of the CHEST system's integration in three case studies with different boundary conditions: a high-temperature DH network as in the case of Turin (Italy), a 100 % RES small DH loop as in the case of Ispaster (Spain) and a small DH network using excess heat from a WtE plant as in the case of Barcelona (Spain).

Deliverable D2.2 explained the TRNSYS simulation model of the CHEST system, and its application to case studies #2 (Aalborg) and #5 (Alpha Ventus). Later an updated and improved model has been developed and has been used for these three case studies described in D2.3.

CHESTER's case studies are described in D2.1.

The main updates introduced in the TRNSYS model used for the simulations presented in this deliverable, compared to the previously developed model described in the CHESTER deliverable D2.2, are:

1. added possibility of making the ORC condense to the environment instead of the DH network;
2. improved clean-up strategy of the latent and sensible part of the HT-TES.

The three case studies are investigated synoptically, in order to identify general trends and impacts that the variation of certain parameters can have on the performance of the CHEST system. Thereby, it has been possible to identify specifications and requirements of the overall system and partly of the individual components in the different case studies.

1.2. Structure of the document

This document is divided in two main sections.

The first of these (Section 2) describes how the TRNSYS model (as described in the CHESTER deliverable D2.2) has been updated to be used for the simulations presented in the present deliverable. Of the newly introduced features, some are implemented in the overall model and hence are common to all three case studies for which the model is applied (see Subsection 2.1); others are specific to a case study under investigation and are used to better reproduce the boundary conditions of the case (see Subsection 2.2).

The next section (Section 3) presents the simulation results obtained when running the TRNSYS model using the boundary conditions specific to the three case studies of Turin, Ispaster and Barcelona. The section is divided into subsections, in which a specific parameter (or a combination of parameters) is investigated to identify its role and effect on the overall performance of the CHEST system. For most of the subsections, results are shown for the three above-mentioned case studies to highlight common characteristics and/or differences from one case study to another.

Finally, Section 4 summarizes and lists the main results and conclusions of the deliverable.

2. Update of the TRNSYS model

2.1. Common features of the updated TRNSYS model

The TRNSYS model used for the simulations presented in this report is mainly based on the TRNSYS model previously used in the CHESTER deliverable D2.2 (Figure 1). The reader should refer to the CHESTER deliverable D2.2 for a detailed description of the TRNSYS model. Here below we simply summarize a few points from the CHESTER deliverable D2.2, which will make it easier to read and understand the content of this deliverable.

- Electricity surplus refers to the positive difference between the RES electricity production and the simultaneous electricity demand. The HT-HP only runs on electricity surplus.
- Electricity deficit refers to the positive difference between the electricity demand and the simultaneous RES electricity production. The ORC operates only in presence of an electricity deficit, so to compensate (partially or totally) for the deficit.

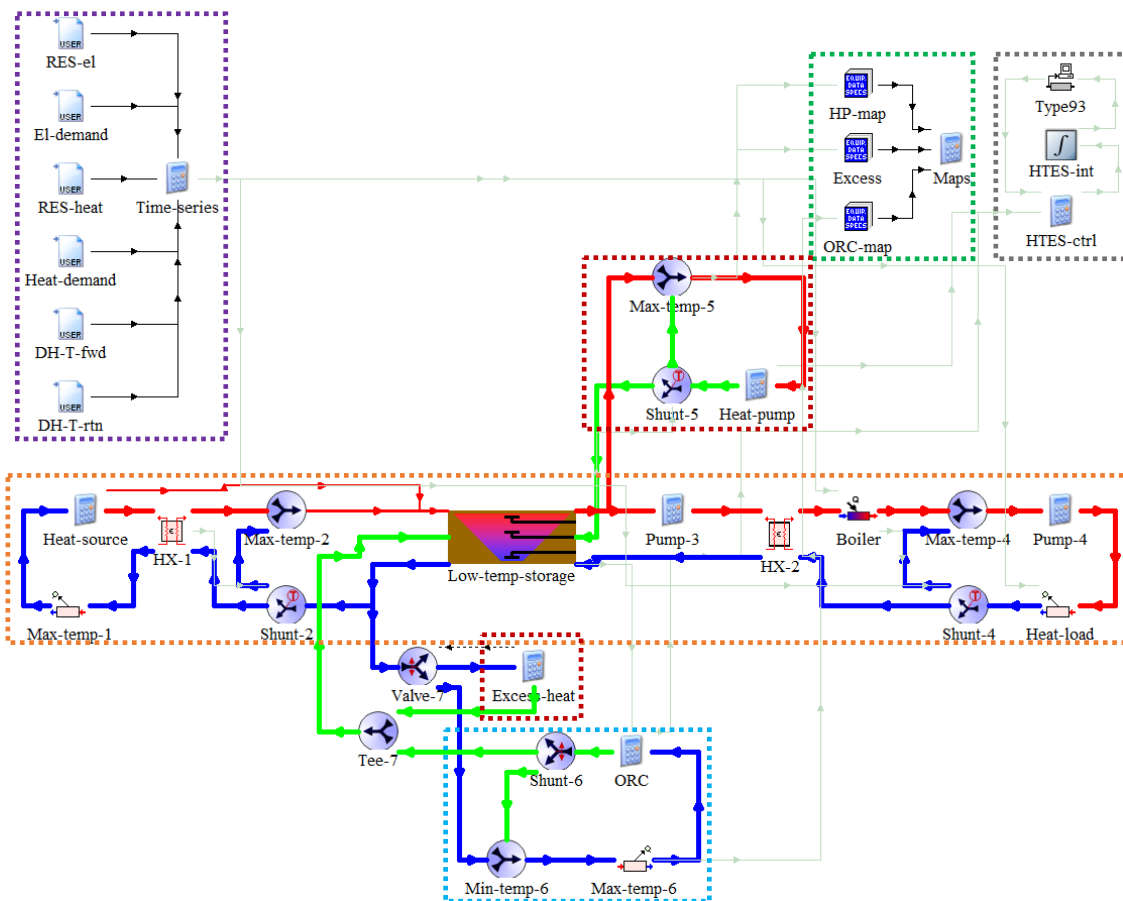


Figure 1: TRNSYS model of the CHEST system as used in the CHESTER deliverable D2.2.

- The number of full-load hours of the HT-HP is defined as the ratio between the electricity absorbed by the HT-HP and the HT-HP capacity. Similarly, the number of full-load hours of the ORC is defined as the ratio between the electricity produced by the ORC and the ORC capacity.

- As *ORC relative capacity* we refer to the ratio between the ORC electrical nominal capacity and the HT-HP electrical nominal capacity in the same simulation run. So, for example it is said that the HT-HP has a capacity of 10 MW and the ORC has a relative capacity of 0.2, it means that the ORC has a capacity 0.2 times that of the HT-HP, i.e. $0.2 \cdot 10 \text{ MW} = 2 \text{ MW}$
- The power-to-power (P2P) ratio of the CHEST system is defined as the ratio between the electricity produced by the ORC and that absorbed by the HP.
- The storage capacity (i.e. the maximum energy content) of the HT-TES can be measured in MWh (or another unit of measure for energy). In this report the storage capacity of the HT-TES in each case was calculated as (1):

$$C_{HT-TES} = W_{p,HP} \cdot COP_{ref} \cdot \Delta t \quad (1)$$

Where C_{HT-TES} is the overall (latent + sensible) storage capacity of the HT-TES (in MWh);

$W_{p,HP}$ is the nominal capacity of the HT-HP (in MW);

COP_{ref} is a reference COP assumed for the HT-HP;

Δt is the time (in hours) that a HT-HP with capacity $W_{p,HP}$ and COP COP_{ref} needs to run at full capacity to completely fill the HT-TES.

In this report the HT-TES capacity is expressed in hours, because we always refer to the Δt parameter, so to normalize the storage capacity to the capacity of the HT-HP and make it easier to compare CHEST cases with different HT-HP sizes.

2.1.1. Condensation to the environment

The first difference consists in the added possibility that the ORC could condense to the environment rather than in the return pipe of the DH network. This allows the ORC operation also in cases of high return temperatures from the DH network (such as in the case of Turin), which otherwise would have required a lot of heat to be dissipated by the component *Max-temp-6* (Figure 1), simply to lower the DH return temperature to the maximum temperature allowed at the inlet of the condenser of the ORC. Additionally, when the ORC condenses to the environment at lower condensing temperatures, its electric efficiency increases, thereby favouring the overall P2P ratio of the CHEST system. The resulting ORC loop after the addition of the ambient condensation option can be seen in Figure 4, which shows the TRNSYS model as used in the Turin case study.

Compared to Figure 1, three new components are present in the updated ORC loop (Figure 4): the controlled flow diverter *Valve-8*, the equation block *Condensation* and the converging tee junction *Tee-8*. In the *Condensation* equation block, two setpoint temperatures are defined — *Cond_T_limit_min* and *Cond_T_limit_max* (with the former lower than the latter)—, which control the flow diverter *Valve-8*, hence determining if the ORC condensation occurs to the ambient, to the DH network or a mixed of the two. Three scenarios can be identified:

- if the fluid temperature coming from the bottom of the LT-TES (*Cond_T_pit*) is higher than the temperature *Cond_T_limit_max*, then *Valve-8* is completely open towards the *Condensation* equation block, and the ORC condenses completely to the environment. In this deliverable, this operation mode is referred to as “*ambient condensation*”;

- if the fluid temperature coming from the bottom of the LT-TES ($Cond_T_pit$) is lower than the temperature $Cond_T_limit_min$, then *Valve-8* is completely open toward the converging tee junction *Tee-7*, and the ORC condenses completely to the LT-TES. This operation mode is referred to as blow-off operation;
- if the fluid temperature coming from the bottom of the LT-TES ($Cond_T_pit$) is between $Cond_T_limit_min$ and $Cond_T_limit_max$, then *Valve-8* will be partially opened toward the *Condensation* equation block. The fraction of the flow at the inlet of *Valve-8* that is sent toward the *Condensation* equation block is given by the following relation (2):

$$Control_{valve\ 8} = \max\left(0, \min\left(1, \frac{Cond_T_pit - Cond_T_limit_min}{Cond_T_limit_max - Cond_T_limit_min}\right)\right) \quad (2)$$

The remaining part of the inlet flow is sent toward the converging tee junction *Tee-7*. This operation mode is referred to as “*partial condensation*”.

The temperature of the water at the outlet of the *Condensation* equation block ($Cond_T_out$), which is supplied to the converging tee junction *Tee-8*, is given by the following relation (3):

$$Cond_T_out = Cond_T_ambient + Cond_DT_out \quad (3)$$

where $Cond_T_out$ (°C) is the temperature of the water at the outlet of the *Condensation* equation block;

$Cond_T_ambient$ (°C) is temperature of the environment used for the condensation, hence it can be the temperature of the ambient air, sea water or river water, depending on the specific boundary conditions and on the case study;

$Cond_DT_out$ (K) is the difference between the temperature of the water at the outlet of the *Condensation* equation block and the temperature of the environment. It is, therefore, the minimum temperature difference across the ambient condensation heat exchanger, and it can be assumed to be 10 K for liquid-to-air heat exchangers and 5 K for liquid-to-liquid heat exchangers.

The temperature $Cond_T_out$ has an upper limit represented by the temperature at the inlet of the *Condensation* equation block and a lower limit represented by minimum temperature accepted at the inlet of the ORC condenser (15 °C according to the performance maps shown in the CHESTER deliverable D2.2).

2.1.2. Updated clean-up strategy of the HT-TES

Given the better performance of the clean-up strategy of the sensible part of the HT-TES tested through the simulations of the Aalborg case (Section 3.1.2 in the CHESTER deliverable D2.2), this is implemented as the default in the new TRNSYS model used for the simulations of this deliverable.

When excessive sensible heat is present in the HT-TES, heat is removed from the sensible part of the HT-TES according to the following relation (4):

$$Q_{sensible, cleanup} = \min\left[E_{sensible}, E_{latent} \cdot \left(\frac{E_{sensible}}{E_{latent}} - \frac{1}{R_{LOS_HTTES}}\right)\right] / timestep \quad (4)$$

where $Q_{sensible, cleanup}$ is the thermal power (in MW) which is removed by the sensible part of the HT-TES by the clean-up strategy;
 $E_{sensible}$ and E_{latent} are the amount of heat (in MWh) stored respectively in the sensible heat part and in the latent heat part of the HT-TES;
 R_{LOS_HTTES} is the design ratio between the heat content in the latent part of the HT-TES and the heat content in the sensible part of the HT-TES, which the clean-up strategy will aim to maintain by removing heat from either part of the HT-TES.

On the contrary, when excessive latent heat is present in the HT-TES, heat is removed from the latent part of the HT-TES according to the following relation:

$$Q_{latent, cleanup} = \min \left[E_{latent}, E_{sensible} \cdot \left(\frac{E_{latent}}{E_{sensible}} - R_{LOS_HTTES} \right) \right] / timestep \quad (5)$$

2.2. Specific features in the individual TRNSYS models

2.2.1. Case Study #1: Turin, Italy

In the case study of Turin unfortunately, non-dispatchable renewable electricity production has not been identified under the current boundary conditions. It has been decided to use the actual electricity production from one of the CHP plants supplying the DH network. The actual electricity production from the CHP plant is compared to the electricity that the plant has committed to feed into the electric grid. Deviations between the actual production and the commitment are caused by imperfect control of the gas turbine. Any deviation (both positive and negative) incurs in a penalty to be paid by the plant operator. Hence, an electricity production higher than the commitment represents an excess of electricity that can be exploited by the CHEST's HT-HP at no (or even negative) cost. On the other hand, an electricity production lower than the commitment represents a deficit of electricity that can be compensated by some production from the CHEST's ORC. Of the three CHP units connected to the DH network (Moncalieri 2GT, Moncalieri 3GT and North Turin, see Section 2.1.2 of the CHESTER deliverable D2.1), the 3GT plant is chosen, because, at the lower range of deviations (<10 MW in absolute value), it presents the best compromise in terms of a high amount of electricity surplus and a more favourable ratio between electricity surplus and electricity deficit.

The distribution of the deviation between the actual electricity production and commitment of the Moncalieri 3GT plant is shown in Figure 2. The same distribution is represented in a different way in Figure 3, where for each power bin width (on the x-axis) is shown the number of occurrences (i.e. number of 15-minutes long time slots) over the year (on the y-axis). As an example, the graph shows that the power production from the 3GT plant is lower than the commitment by a difference between 1 MW and 2 MW about 4700 times during the year, i.e. $4700 \cdot 0.25 \text{ h} = 1175 \text{ hours}$.

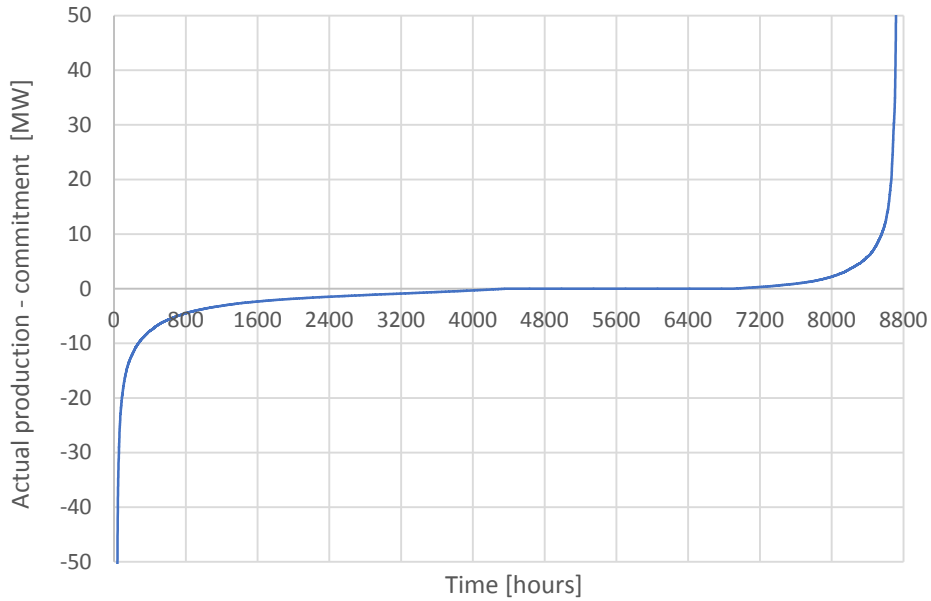


Figure 2: Distribution of deviation between actual production and commitment of the Moncalieri 3GT plant in Turin case during the year (8760 hours).

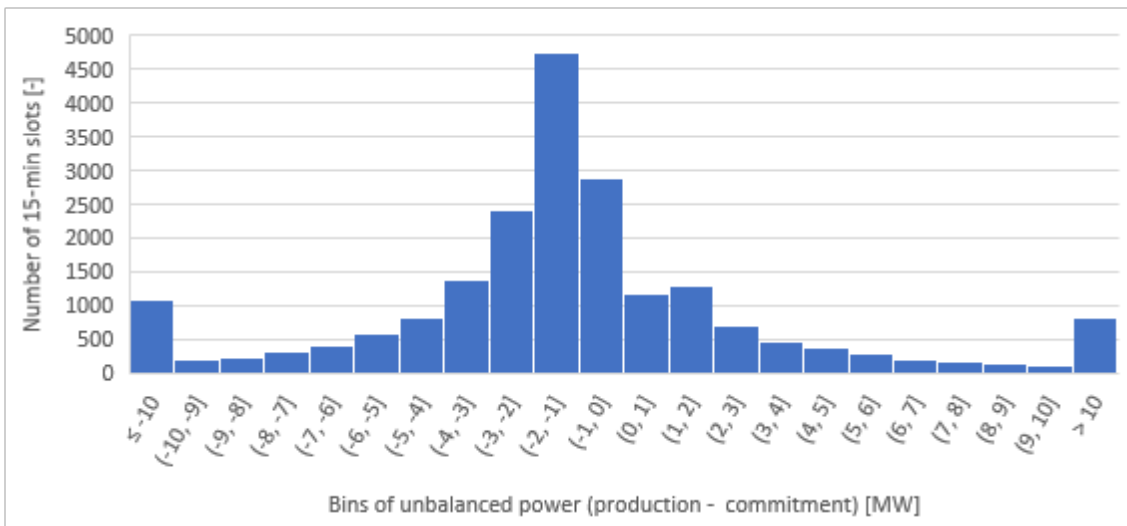


Figure 3: Distribution of the unbalanced power (production - commitment) of the Moncalieri 3GT plant (unbalances equal to 0 are not counted in the corresponding bin $[-1,0]$).

In the case study of Turin, no excess heat realistically usable by the CHEST system can be identified under the current boundary conditions. Instead of assuming a fictitious source of RES heat or waste heat, it is decided to use the return flow of the DH network as the heat source for the HT-HP of the CHEST system. The resulting TRNSYS model used to simulate the Turin case is shown in Figure 4.

The following inputs are used as input files to the TRNSYS model:

- *RES-el*: the electricity production from the 3GT gas turbine for 2017 is used. This is made available as a time series with a timestep of 15 minutes. No scaling is applied. The electricity production profile used in the TRNSYS model is shown in Figure 6.

- *El-demand*: the commitment of electricity production from the 3GT gas turbine for 2017 is used. This is made available as a time series with a timestep of 15 minutes. No scaling is applied.
- RES-heat: none.
- *Heat-demand*: the load profile from Turin DH network is used. No scaling is applied. The DH heat demand profile used in the TRNSYS model is shown in Figure 6.
- *DH-T-fwd*: a constant supply temperature of 120 °C for the DH network is used.
- *DH-T-rtn*: a constant return temperature of 70 °C for the DH network is used.
- *Cond_T_ambient*: the linear interpolation of the monthly average temperature of the Po river is measured at the inlet of the DH plant in Moncalieri is used. The resulting profile used in the TRNSYS model is shown in Figure 5.

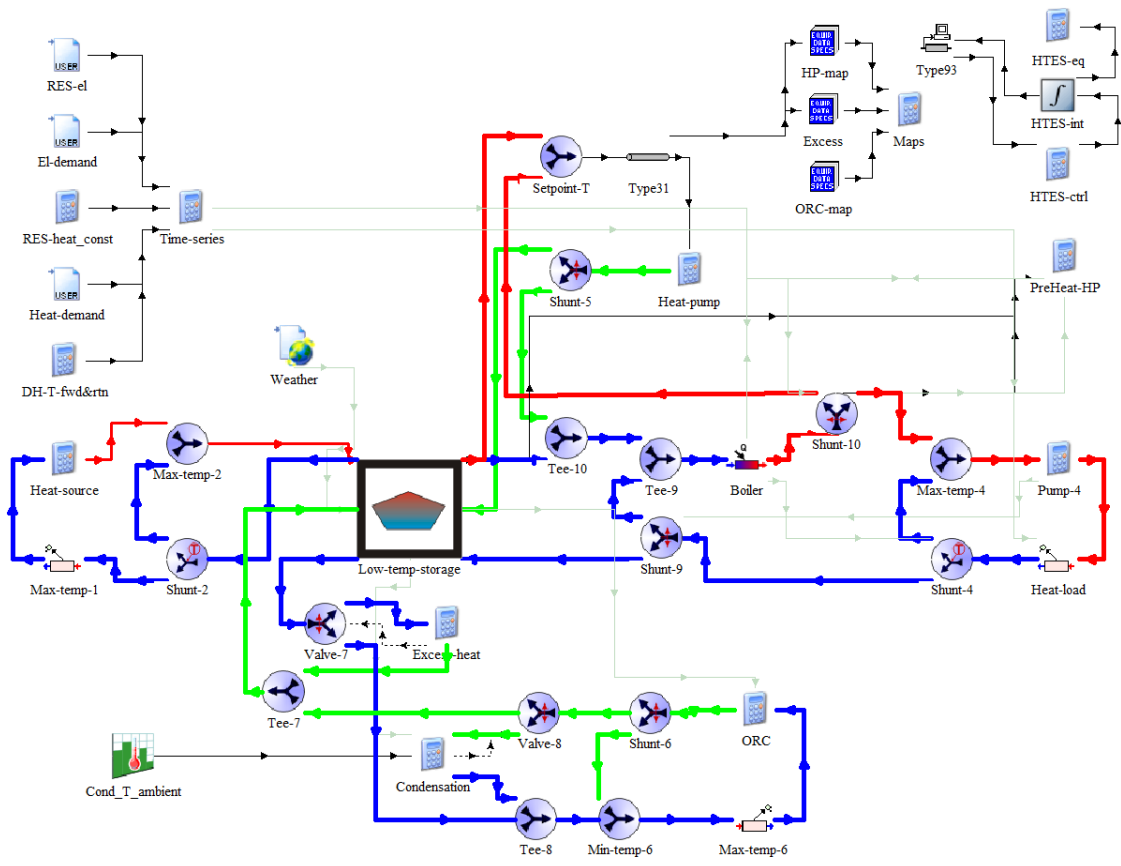


Figure 4: TRNSYS model used for Turin case study.

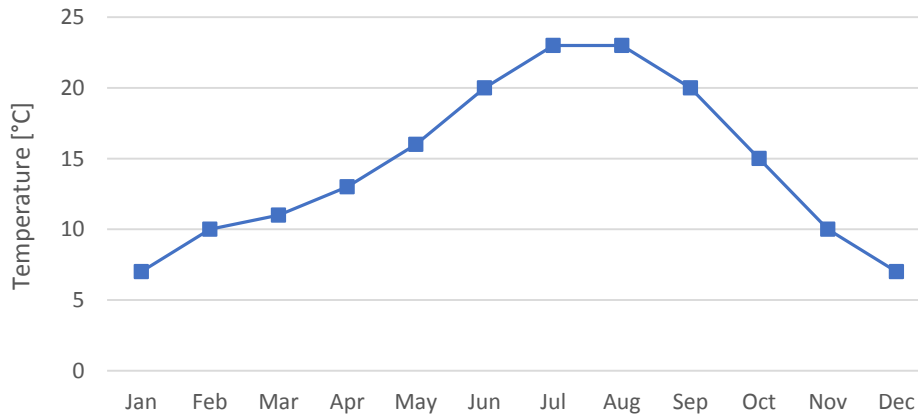


Figure 5: Monthly-average temperatures of the Po river at the Moncalieri plant during the year.

Insulated hot water tanks (of the same type as those currently installed in the DH network in Turin) are assumed to be the LT-TES for the CHEST system. The total volume assumed for the tanks is 10,000 m³. The water circulating in the DH network is the same as that circulating in the LT-TES hydraulic loop, therefore no heat exchanger is needed (compare the TRNSYS schemes in Figure 1 and Figure 4). Instead of the heat exchanger *HX-2* (Figure 1), the tee junctions *Shunt-9* and *Tee-9* are now the interface between the DH network and the LT-TES. The flow that from the DH return pipe is deviated through the LT-TES is set low enough to avoid issues of numerical convergence of type 342 (the LT-TES), but high enough to guarantee the HT-HP heat input.

Comparing the TRNSYS schemes in Figure 1 and Figure 4, it can be seen that the TRNSYS scheme of Turin case presents the additional components *Shunt-10* and *Tee-10*, as well as a different connection of the two tee junctions right before and after the *Heat-pump* equation block (*Setpoint-T* and *Shunt-5*). The new arrangement allows using the high temperature water at the outlet of the *Boiler* component to increase the DH return temperature at the inlet of the HT-HP, thereby improving its COP and reducing the amount of excess heat, which cannot be stored in the HT-TES. For the amount and temperature of excess heat as a function of the temperature at the inlet of the HT-HP's evaporator, the reader should refer to the performance maps shown in Table 5 and Table 7 in the CHESTER deliverable D2.2.

Due to the high return temperature of the DH network (70 °C) in Turin, the ORC always condenses to the environment, using the water of the Po river as heat sink. If the ORC condenses in the DH network (after lowering the DH return temperature through the auxiliary cooling device *Max-temp-6*), it would supply water at 60 °C to the bottom of the LT-TES, lower than the DH return temperature. Therefore, this operation mode, which offers no advantage compared to the ambient condensation mode, is rejected.

The following simulations have been carried out assuming butene as the working fluid in all the presented scenarios and as a reference scenario, a TRNSYS simulation without the CHEST system, to identify the performance of the DH system itself.

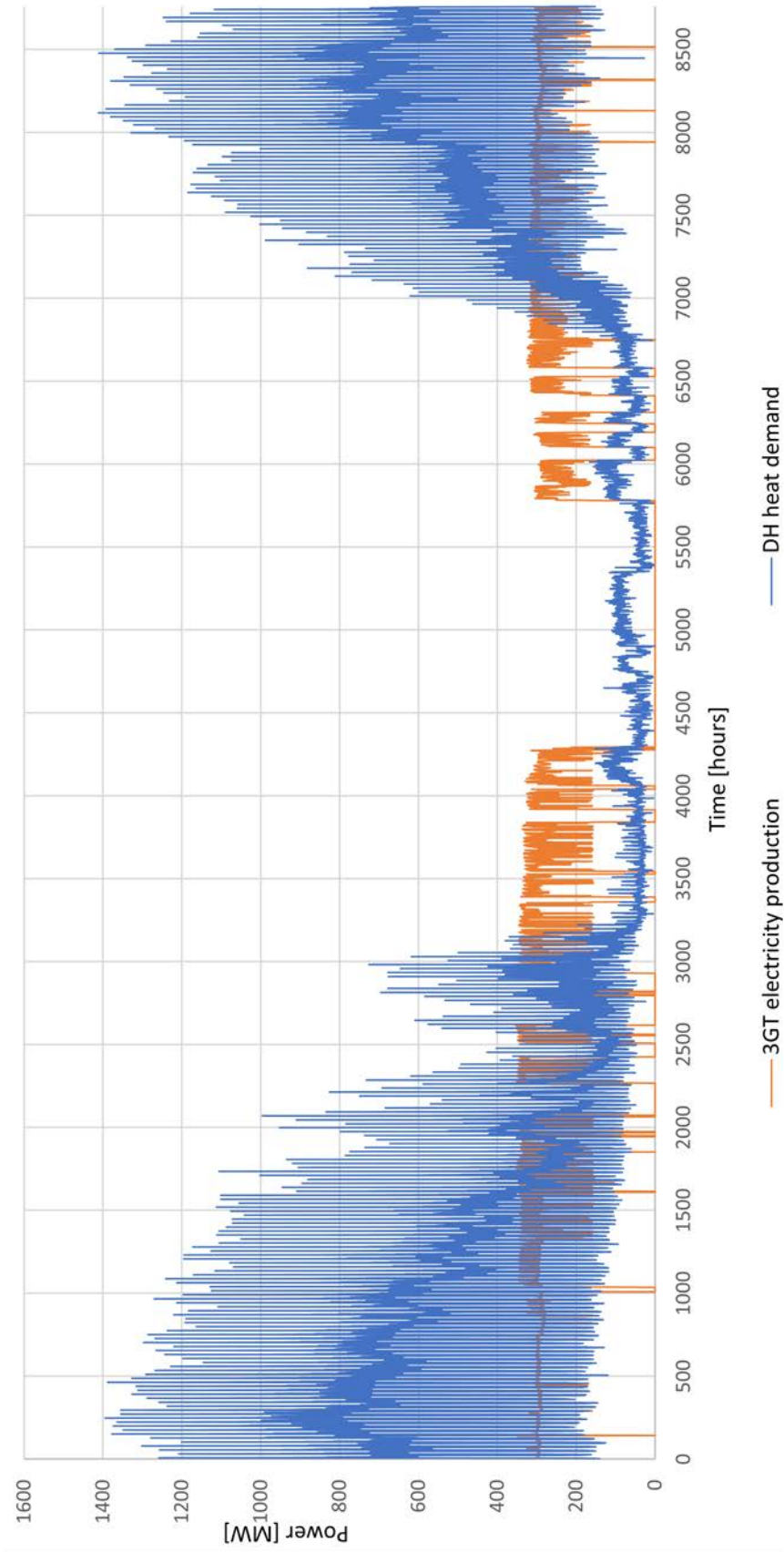


Figure 6: Profiles of the DH demand and of the electricity production from 3GT in 2017.

Under the above-mentioned boundary conditions and energy profiles, the parameters listed in Table 1 are common to all simulations referring to the Turin case, unless otherwise specified. Besides, the listed boiler production refers to the reference case without CHEST system.

Table 1: General parameters for Turin case (on an annual basis).

Energy [MWh]	
GT3 electricity production	1.74E+06
GT3 committed production	1.74E+06
DH heat demand	2.31E+06
Electricity surplus	1.51E+04
Electricity deficit	2.04E+04
RES electricity directly used	1.72E+06
WITHOUT CHEST SYSTEM:	
Boiler production	2.31E+06

An overview of the parameters which are varied in the parametric analyses is presented in Table 2.

Table 2: Overview of the main parameters varied in the different parametric analyses.

Section number		3.1.1	3.2.1	3.5.1
Scaling factor of RES electricity profile	[-]	1	1	0.5
Scaling factor of electricity demand profile	[-]	1	1	0.5
Capacity of HT-TES, Δt	[h]	Infinite	1-20	1, 3, 5
Latent-to-sensible ratio of HT-TES	[-]	-	0.74	0.74
Fluid		Butene	Butene	Butene
HP capacity	[MW]	0.5 - 10	1, 2.5, 5	0.5, 1.25, 2.5
ORC relative capacity	[-]	0.2 - 0.6	0.2 - 0.4	0.2, 0.3, 0.4

2.2.2. Case Study #3: Ispaster, Spain

In the case study of Ispaster, the renewable electricity production is given by the local 100 PV panels, with a total capacity of 25 kWp (see CHESTER deliverable D2.1). The PV panels are installed on the roof of the pelota court, which has a slope of 30° and an azimuth angle of 25° west with respect to the south. The technical specifications of the PV panels, used to calculate their power output, are shown in Figure 74 in Appendix A (model REC250PE). The photovoltaic module type 94 is used to model the PV array in TRNSYS.

The renewable heat production is given by 59 m² (gross area; 54 m² of aperture area) of CPC solar thermal collectors (model: Paradigma STAR 15/49). The solar collectors are installed on the same roof as the PV, so they have the same slope and azimuth. The technical specifications of the solar collectors, used to calculate their power output, are shown in Figure 75 in Appendix A (model STAR 15/49). The evacuated tube collector type 71 is used to model the solar collector array in TRNSYS.

Both the PV component and the solar thermal collector component use the weather boundary conditions (solar radiation, ambient temperature, etc.) contained in the weather file of Santander (about 100 km from Ispaster) available in the TRNSYS weather library.

Additionally, the equations regulating the charge and discharge of the latent part of the HT-TES are modified in such a way that, when the CHEST system is not implemented, the latent part of the HT-TES works as a battery storage connected to the PV array. Based on the information collected on the system in Ispaster in the CHESTER deliverable D2.1 and the technical specifications of the batteries [GNB, 2018], the following assumptions are made:

- overall gross capacity of the battery storage: 197 kWh
- charging efficiency: 100 %
- discharging efficiency: 70 %
- depth-of-discharge: 60 %
- maximum charging/discharging power: 20 kW

The resulting TRNSYS model used to simulate the Ispaster case is shown in Figure 7.

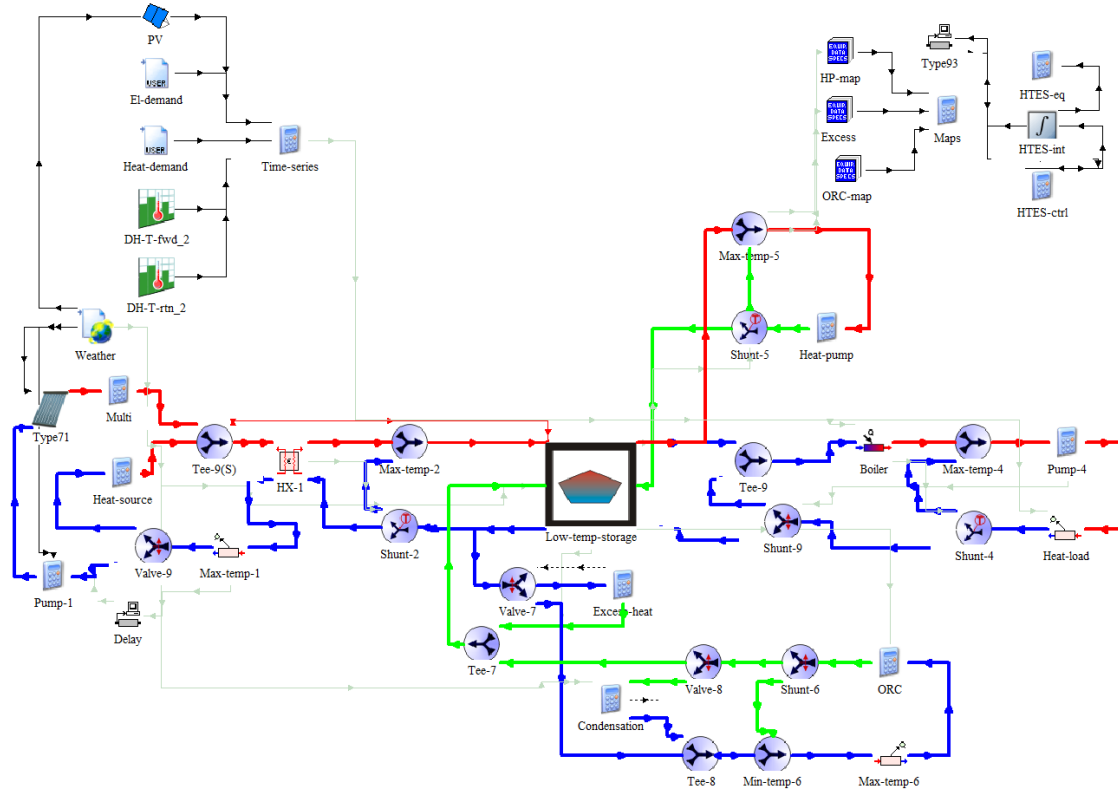


Figure 7: TRNSYS model used for Ispaster case study.

The following inputs are used as input files to the TRNSYS model:

- *RES-el*: the renewable electricity production is calculated within TRNSYS, based on weather conditions and the technical specification of the PV array. The resulting PV production profile is shown in Figure 9.
- *El-demand*: the measured electricity demand profile is not available, so a realistic profile is generated and provided by Goierer to match the yearly electricity demand

and following a realistic usage pattern. The profile used in the TRNSYS model is shown in Figure 9.

- *RES-heat*: the renewable heat production is calculated within TRNSYS, based on weather conditions and the technical specification of the solar collector array. The pump of the solar collector loop is operated in such a way that a constant outlet temperature of 80 °C is aimed at, whenever possible. The resulting solar thermal production profile is shown in Figure 10. This refers to the CHEST system scenario, when the CHEST system is not implemented.
- *Heat-demand*: the measured DH heat demand profile is not available, so a realistic profile is generated and provided by Goiener to match the yearly DH demand and following a realistic usage pattern. The profile used in the TRNSYS model is shown in Figure 10.
- *DH-T-fwd*: a constant supply temperature of 75 °C for the DH network is used.
- *DH-T-rtn*: a constant return temperature of 55 °C for the DH network is used.
- *Cond_T_ambient*: due to the lack of water streams near Ispaster, an air-based heat rejection system is assumed to be used for the ambient-condensation mode. Therefore, the dry bulb air temperature contained in the TRNSYS weather data file of Santander is used. The monthly average air temperature is shown in Figure 8.

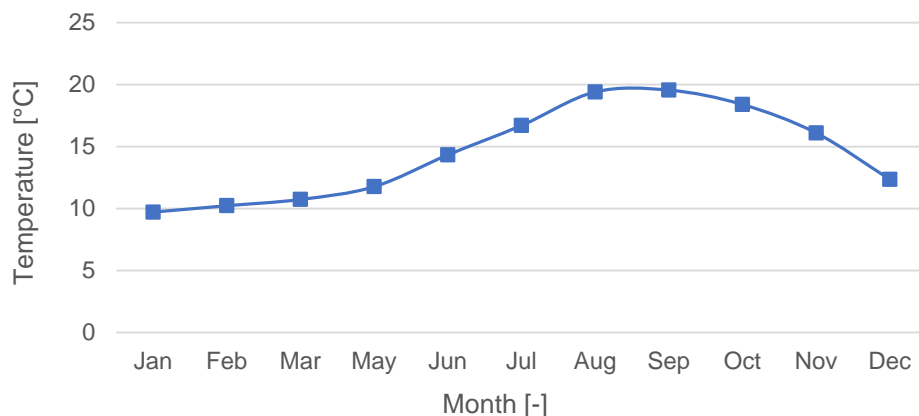


Figure 8: Monthly average dry bulb temperatures of air in Santander city over a year.

In the actual system, the solar collector system is equipped with a 2000 liters buffer tank (see CHESTER deliverable D2.1), which is used as the LT-TES in the CHEST system. For modelling reasons, the volume of the LT-TES is increased to 10,000 liters, to avoid problems of numerical convergence of the type 342 (the LT-TES) when running the TRNSYS model.

The water circulating in the DH network is the same as that circulating in the LT-TES hydraulic loop. Therefore, no hydraulic isolation is needed, so the heat exchanger *HX-2* (Figure 1) is replaced with tee junctions *Shunt-9* and *Tee-9* connecting the DH network with the LT-TES. The flow that is deviated from the DH return pipe through the LT-TES is chosen low enough to avoid issues of numerical convergence of type 342 (the LT-TES), but high enough to guarantee the HT-HP heat input.

Regarding the control of the solar collector loop, the flow rate is regulated so to have an outlet temperature from the collectors as close as possible to the setpoint temperature of 80 °C.

The aggregate figures for the annual energy demand and production are summarized in Table 3. The figures about electricity production/demand/surplus/deficit and those about the DH heat demand are constant in all the presented scenarios, unless otherwise specified. The heat production refers to the reference scenario without the CHEST system. This varies for different CHEST scenarios, as the solar collector output depends on the temperature at the bottom of the LT-TES, which is affected by the CHEST operation. Also, the figures regarding the thermal output from the DH boiler, as well as electricity stored in the electricity charged and discharged from the electric batteries connected to the PV system refer to the scenario without CHEST (no battery storage is assumed in the scenarios where CHEST is implemented).

Table 3: General parameters for Ispaster case (yearly basis).

	Energy [MWh]
RES electricity production	35.6
Electricity demand	61.3
DH heat demand	86.0
Electricity surplus	13.0
Electricity deficit	38.7
RES electricity directly used	22.6
WITHOUT CHEST SYSTEM:	
RES-heat available	37.5
Boiler heat production	57.3
Energy stored in battery	9.7
Energy released from battery	6.6

Assuming butene as working fluid in all the simulations of Ispaster case, an overview of the parameters which are varied in the parametric analyses is presented in Table 4.

Table 4: Overview of the main parameters varied in the different parametric analyses.

Section number		3.1.2	3.2.2	3.3.2	3.5.2
Scaling factor of RES electricity profile	[-]	1.0	1.0	1.0	1.0
Scaling factor of RES heat profile	[-]	1.0	1.0	1.0	1.0; 2.0, 3.0
Capacity of HT-TES, Δt	[h]	Infinite	8, 12	Infinite	12
Latent-to-sensible ratio of HT-TES	[-]	0.74	0.74	0.74	0.74
Fluid		Butene	Butene	Butene	Butene
HP capacity	[MW]	0.001 - 0.009	0.001 - 0.009	0.001 - 0.009	0.001 - 0.009
ORC relative capacity	[-]	0.25-1.0	0.10-0.50	1.0	0.10-0.25
ORC condensation mode		Ambient	Ambient	Ambient, Blow-off, Partial	Blow-off

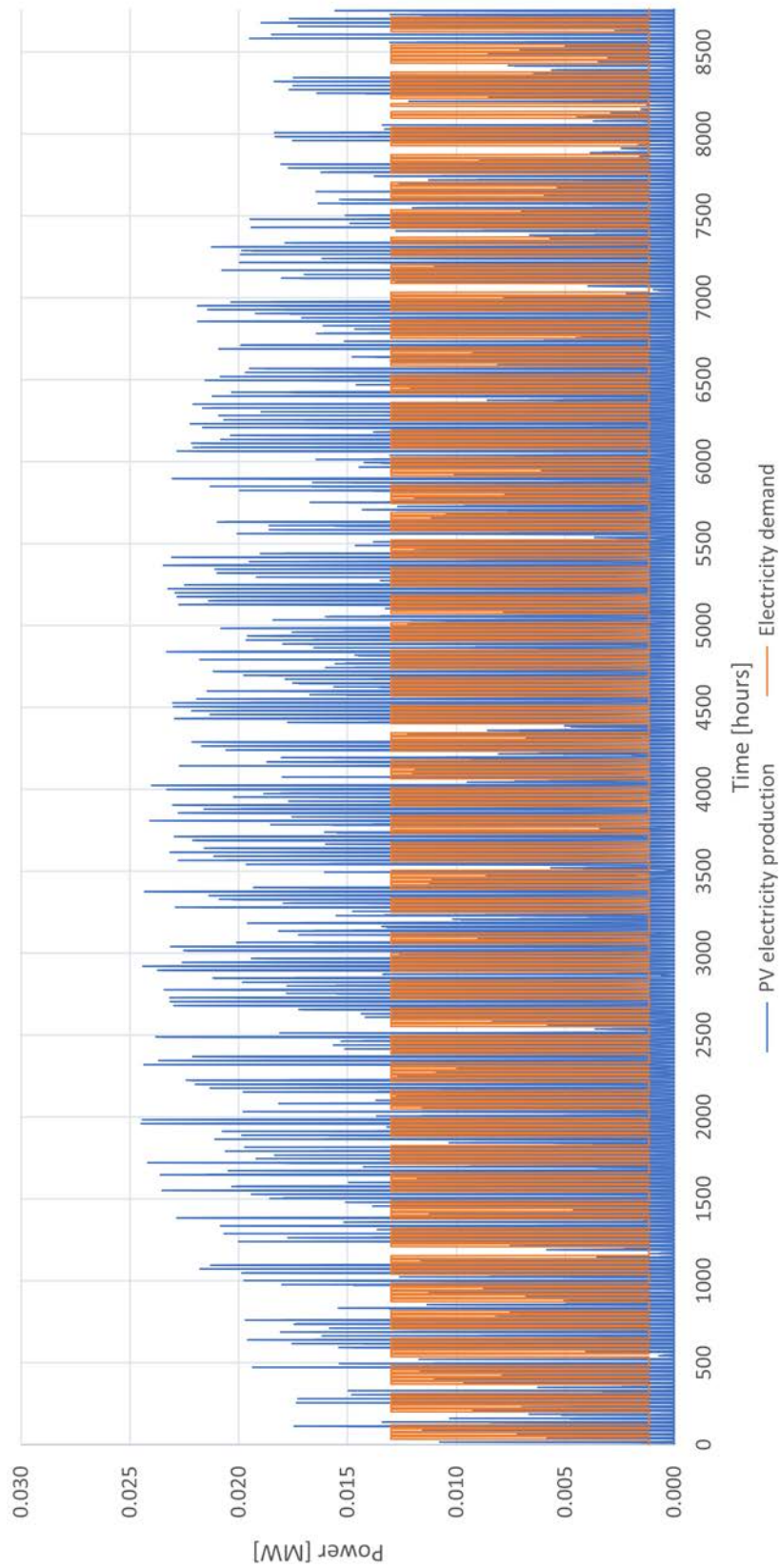


Figure 9: Electricity demand profile and electricity output from PV plant in Ispaster case.

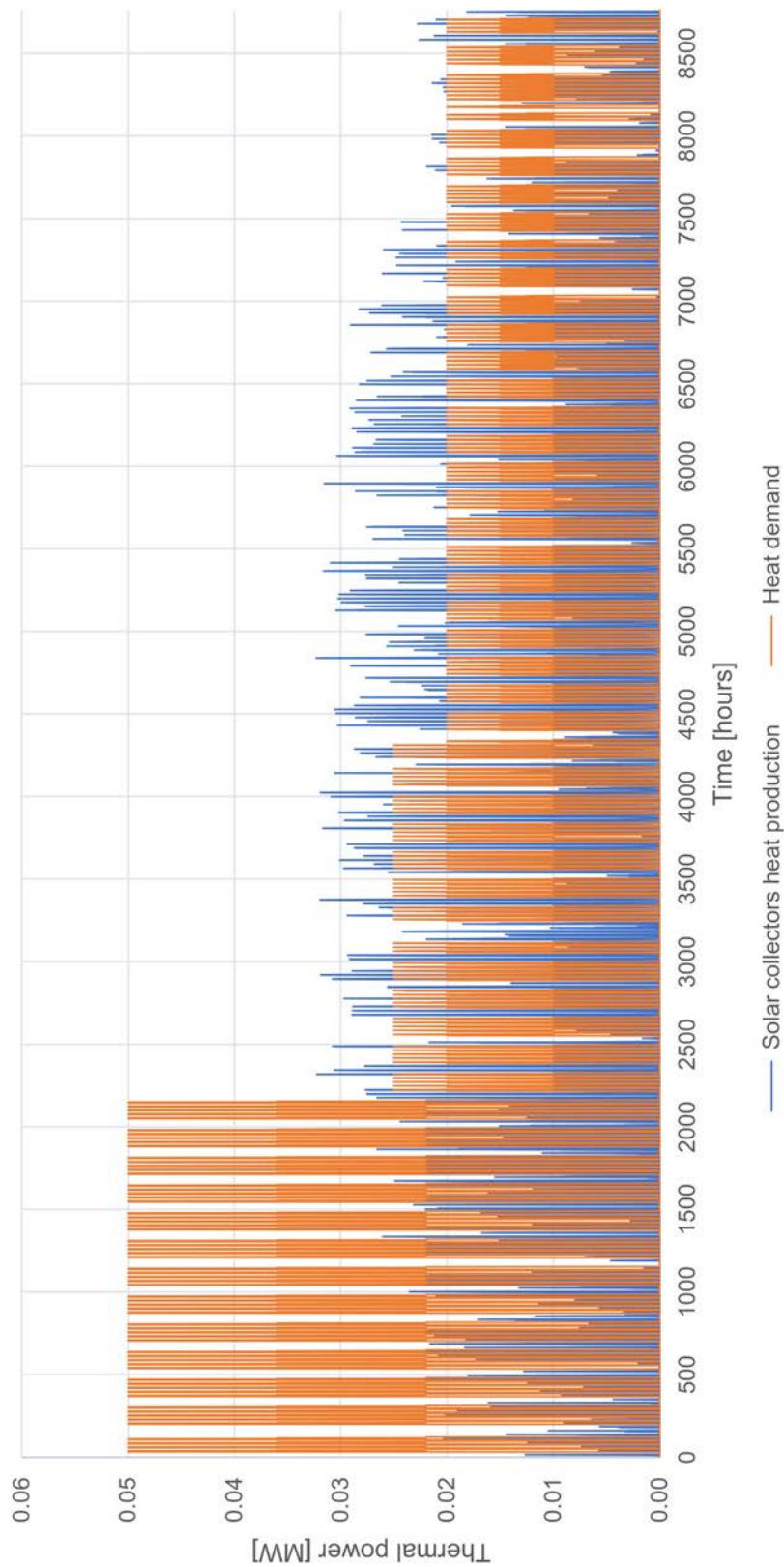


Figure 10: Profiles of the DH heat load and heat output from the solar collectors in the scenario without the CHEST system in Ispaster case.

2.2.3. Case Study #4: Barcelona, Spain

In the case study of Barcelona unfortunately, no profiles for the local RES electricity production and the local electricity demand are available. Therefore, consumption and production profiles from the pumped hydro plants on a national level (whole of Spain) are used and scaled down reasonably. Consumption of a pumped hydro plant means that the pumped hydro takes excess electricity from the electricity grid while production of a pumped hydro plant means that electricity is fed into the grid.

As RES heat, a part of the heat generated by the boiler of the waste to energy (WtE) plant is used. The nominal power output of the boiler (40 MW) is used and scaled down reasonably. As heat demand, the available profile for the load of the DH network is used. For the DH supply and return temperatures no profiles are available, so constant values of 90 °C and 60 °C, respectively, are used. Therewith, the resulting TRNSYS model used to simulate Barcelona case is shown in Figure 11.

The following inputs are used as input files to the TRNSYS model:

- *RES-el*: the electricity consumption of pumped hydro plants for all of Spain for 2017 is used. This is made available as a time series with a time step of 1 hour. A scaling factor of 0.02 is applied (see below for the explanation). The RES electricity production profile used in the TRNSYS model is shown in Figure 13.
- *El-demand*: the electricity production of pumped hydro plants for the whole of Spain for 2017 is used. This is made available as a time series with a time step of 1 hour. A scaling factor of 0.02 is applied (see below for the explanation). The electricity demand profile used in the TRNSYS model is shown in Figure 13.
- *RES-heat*: the nominal power output of the boiler (40 MW) of the WtE plant is used. This constant value is scaled with a factor of 0.14 (see below for the explanation), so the RES heat accounted for a constant value of 5.6 MW.
- *Heat-demand*: the load profile from Barcelona DH network is used. No scaling is applied. The DH heat demand profile used in the TRNSYS model is shown in Figure 14.
- *DH-T-fwd*: a constant supply temperature of 90 °C for the DH network is used.
- *DH-T-rtn*: a constant return temperature of 60 °C for the DH network is used.
- *Cond_T_ambient*: two different scenarios are investigated in this case study: on the one hand, the ambient air temperatures of Barcelona (available as hourly values) and on the other hand, the linear interpolation of the monthly-average temperatures of the sea water in Barcelona is used. The resulting profiles used in the TRNSYS model are shown in Figure 12.

On the left side of the TRNSYS model in Figure 11, the weather data reader supplies the ambient air temperature to the equation block *Condensation*. The weather file of Barcelona, available in the TRNSYS weather library, is used here. Above the weather data reader, the forcing function *Sea water* contains the monthly-average values of the sea water temperatures in Barcelona (Figure 12). In case of simulations with condensation to sea water, this forcing function is connected to the equation block *Condensation* instead of the weather data reader.

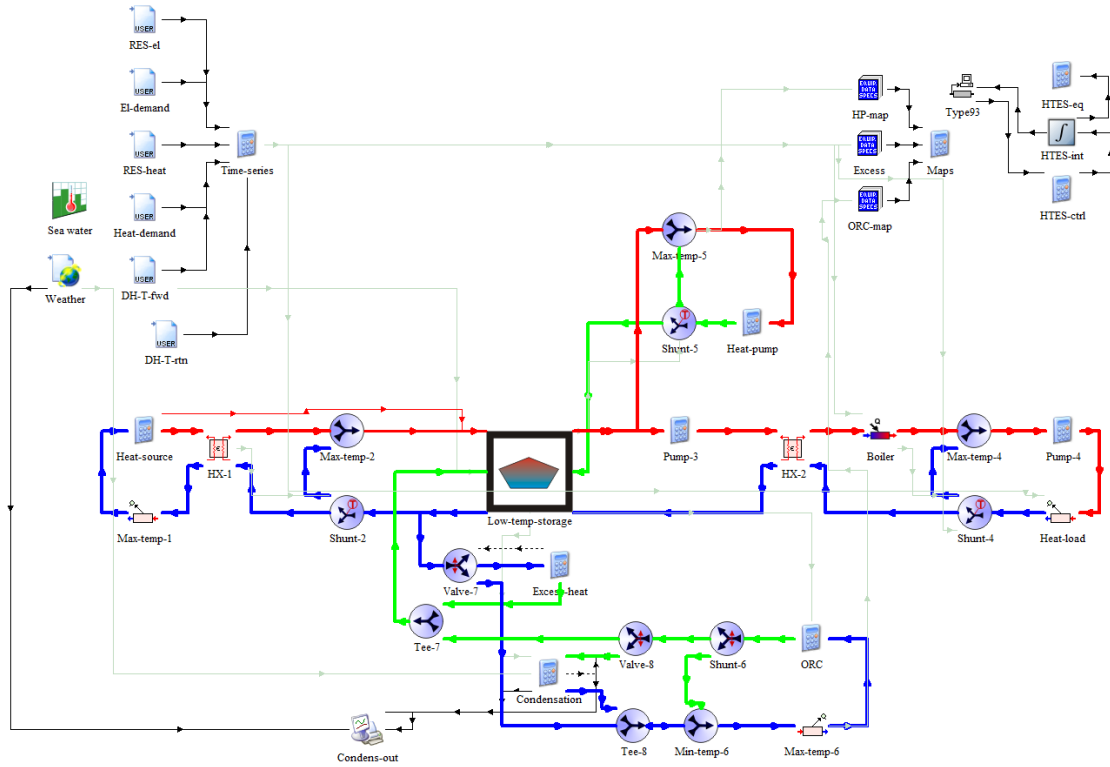


Figure 11: TRNSYS model used for Barcelona case study.

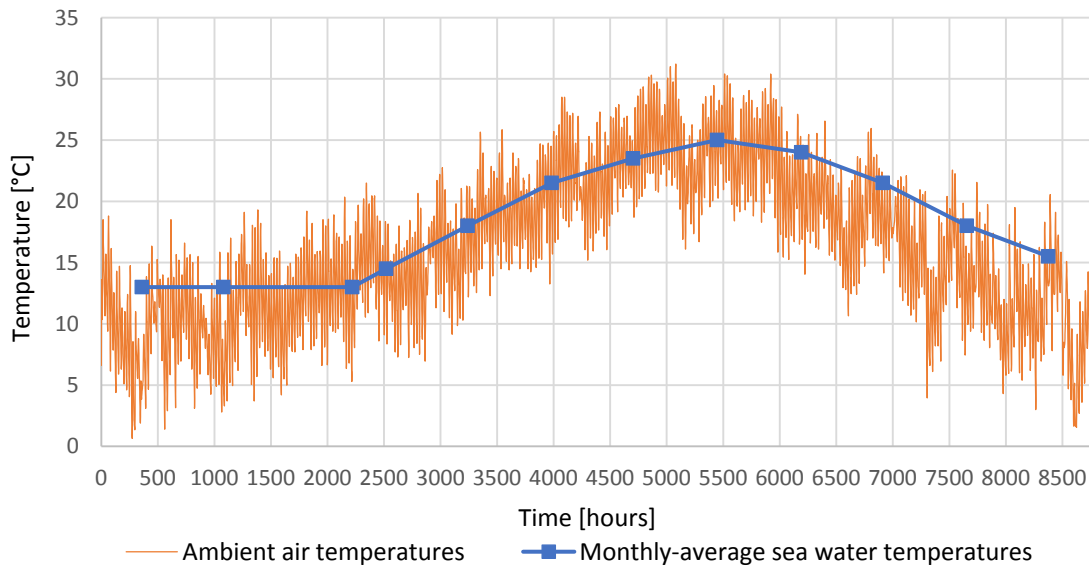


Figure 12: Ambient air temperatures of Barcelona and monthly-average temperatures of the sea water in Barcelona during the year.

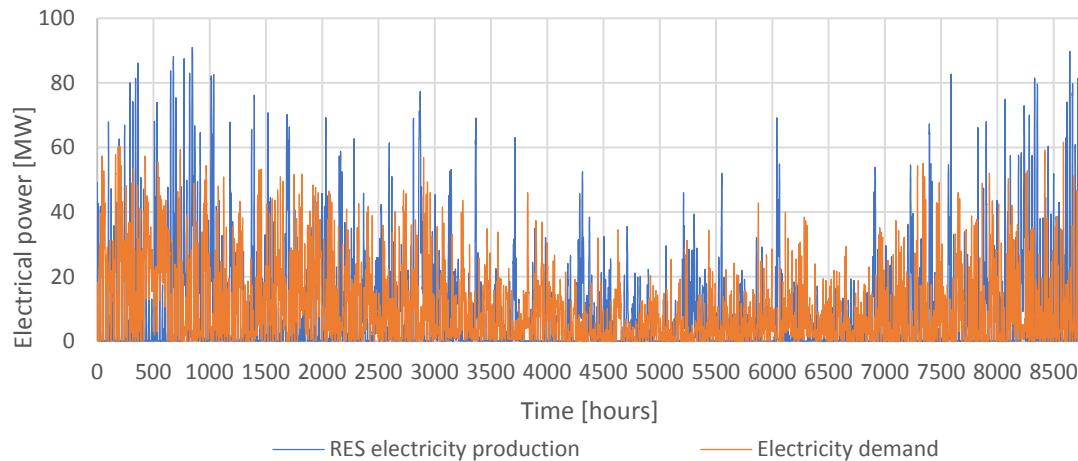


Figure 13: Profiles of the RES electricity production and the electricity demand used in Barcelona case.

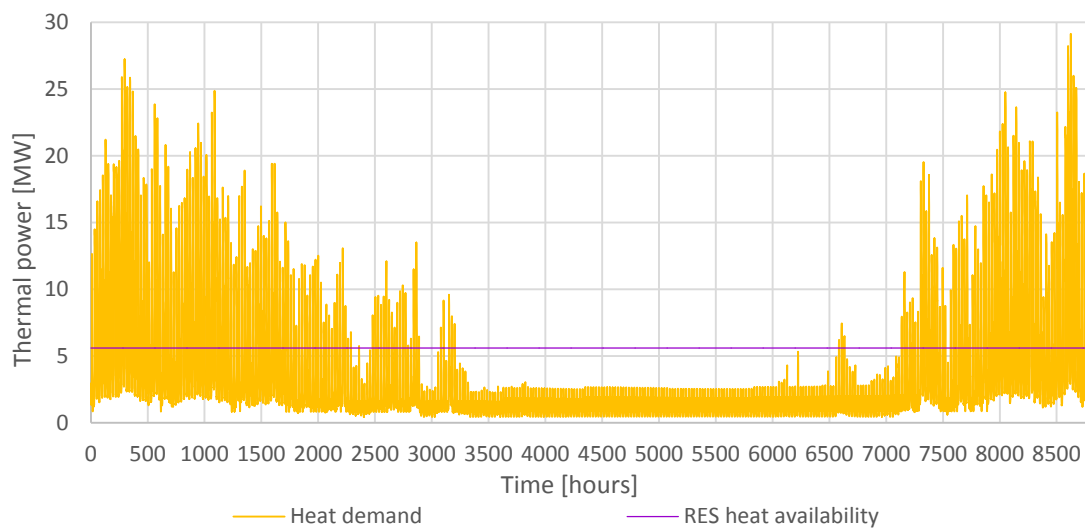


Figure 14: Profiles of the DH heat demand and RES heat availability used in Barcelona case.

Regarding the set point temperatures $Cond_T_limit_min$ and $Cond_T_limit_max$ of the ORC condensation mode (see Section 2.1.1), the values of 50 °C and 55 °C are used in all simulations, except for some simulations in Section 3.3.3. The above-mentioned values result in either ambient condensation or in partial condensation, depending on the CHEST size.

Concerning the choice of the above-mentioned scaling factors, the following considerations are made. The collected pumped hydro profiles refer to the national level, thus it is not reasonable that a single system could deal with such an amount of electricity unbalances. Besides, if the original profiles had been used, they would have likely created numerical problems in the simulations even at moderate CHEST sizes, unless the LT-TES had enormous dimensions. Moreover, in the Barcelona case study there is currently no LT-TES. As explained in the CHESTER deliverable D2.1, a large LT-TES would not necessarily be required, unless in case of a significant increase of the DH network in the future. So, the intention for the simulations of the Barcelona case study are to dimension the LT-TES as small as possible. Based on the intended range of simulations for the CHEST size between 1 MW and 60 MW (see Section 3.1.3), a scaling factor of 0.02 is applied to both the RES electricity production profile and the electricity demand profile, because this gives a maximum electricity surplus and deficit of about 90 MW and 60 MW respectively, which fits the maximum size of the CHEST system.

Also, the RES heat production is scaled down, because it is not reasonable to assume that the entire thermal power from the WtE plant is used to run the HT-HP of the CHEST system. If this was the case, the boiler would rather directly charge the HT-TES. Furthermore, taking the complete heat of the boiler as RES heat would result in a surplus of the annual RES heat production that is more than 10 times higher than the annual load of the DH network. This is not realistic and would also lead to numerical problems of energy balance when simulating the LT-TES, because of too large flows flowing through the LT-TES over a time step. Therefore, a scaling factor of 0.14 is applied. This led to an annual amount of RES heat available which is 1.69 times larger than the heat demand.

Concerning the RES heat temperatures, the following settings are applied in all simulations presented here:

- *RES_heat_T_out_C*: the expected outlet temperature from the RES heat source is set to 105 °C. The heat from the boiler is, in principle, available at even higher temperatures. However, the maximum heat source temperature of the HT-HP is 100 °C according to the utilized performance maps. Assuming a 5 K temperature difference across the heat exchangers, an outlet temperature of 105 °C seems a reasonable choice.
- *PTES_T_in_C_max*: given the above-mentioned outlet temperature from the RES heat source of 105 °C and the DH supply temperature of 90 °C, the maximum temperature allowed at the inlet of the LT-TES is set to 98 °C.
- *RES_heat_T_in_C_max*: the maximum temperature allowed at the inlet of the RES heat source component is set to 75 °C, necessarily higher than the DH return temperature (60 °C), due to a needed temperature difference across the heat exchanger.

As mentioned above, the aim is to make the size of the LT-TES as small as possible but avoiding possible numerical problems with respect to the energy balance that, may occur, in the simulation if the size of the LT-TES is too small compared to exchanged flows. After some preliminary simulations, a LT-TES size of 400,000 m³ is chosen for all simulations with HT-HP capacities up to the maximum value of 60 MW, as it does not cause numerical problems with the energy balance of the LT-TES. For most of the simulations, carried out with HT-HP capacities of only 1 and 10 MW, respectively, a much smaller LT-TES size of 70,000m³ is chosen. Besides, butene is assumed as the working fluid in all the presented scenarios, except for some simulations in Section 3.4, which used R1233zd(E).

As a reference scenario, a TRNSYS simulation is performed without the CHEST system to identify the performance of the DH system itself.

Under the above-mentioned boundary conditions and energy profiles, the parameters listed in Table 5 are common to all simulations referring to Barcelona case, unless otherwise specified.

Table 5: General parameters for Barcelona case during the 2nd year of operation (on an annual basis).

	Energy [MWh]
RES electricity production	7.42E+04
Electricity demand	7.91E+04
RES heat available	4.91E+04
DH heat demand	2.90E+04

Electricity surplus	6.42E+04
Electricity deficit	6.91E+04
RES electricity directly used	1.00E+04
WITHOUT CHEST SYSTEM:	
Boiler heat production (LT-TES = 400,000 m ³)	0.00E+04
Boiler heat production (LT-TES = 70,000 m ³)	0.17E+04

As seen in Table 5, the share of RES electricity directly used is very low. In fact, as the electricity profiles are those of the pumped hydro plants on a national level and pumped hydro plants compensate the imbalances of the electricity grid, they will generally operate “in phase”, i.e. either in upward (electricity production) or downward (electricity consumption, through pumping) regulation. So, in principle, from the electricity point of view, the installation of a CHEST system in this case study can be seen as a replacement of a part of the pumped hydro capacity in Spain.

Table 5 also shows that there is much more RES heat available compared to the DH heat demand. It would be expected that, in presence of a LT-TES and a RES-heat supply temperature higher than the DH forward temperature, there would not be any boiler operation. However, as seen in Table 5, about 1.7 GWh of boiler heat are needed in the scenarios with the LT-TES size of 70,000 m³. This is due to the fact that with the smaller LT-TES more RES heat is blown off in summer, which therefore could not cover the whole DH heat load.

The large excess of RES heat compared to the DH heat demand is advantageous for the CHEST system, as this entails that there is plenty of heat which can be used by the HT-HP. Additionally, this heat is at the high temperature (105 °C), which results in high COPs of the HT-HP. On the contrary, if this heat surplus heated up the entire LT-TES, it would penalize the efficiency of the ORC in pure blow-off operation mode (which however is not treated in the analysis) and somehow in partial condensation operation, because the efficiency decreases at higher heat-sink temperatures.

An overview of the parameters varied in the parametric analyses is presented in Table 6.

Table 6: Overview of the main parameters varied in the different parametric analyses presented in the following sections of this deliverable.

Section number		3.1.3	3.2.3	3.3.3
Scaling factor for RES heat	[-]	0.14	0.14	0.14
Scaling factor for RES electricity	[-]	0.02	0.02	0.02
Scaling factor for electricity demand	[-]	0.02	0.02	0.02
Capacity of HT-TES, Δt	[h]	Infinite	6, 12	12
Latent-to-sensible ratio of HT-TES	[-]	-	0.74	0.74
Fluid		Butene	Butene	Butene
HP capacity	[MW]	1 - 60	1, 10	1 - 60
ORC capacity / HP capacity	[-]	0.20 - 1.20	0.20 - 0.50	0.50

LT-TES size	[m ³]	400,000		70,000	400,000
ORC condensation		Partial		Partial	Blow-off, Partial (ambient: air, sea water)
Section number		3.4		3.5.3	
RES heat / Heat demand	[-]	0.14		0.14	
Scaling factor for RES electricity	[-]	0.02		0.01, 0.02, 0.03	
Scaling factor for electricity demand	[-]	0.02		0.02	
Capacity of HT-TES, Δt	[h]	6, 12		12	
Latent-to-sensible ratio of HT-TES	[-]	0.74	1.14	0.74	
Fluid		Butene	R1233zd(E)	Butene	
HP capacity	[MW]	1, 10		1, 10	
ORC capacity / HP capacity	[-]	0.20 - 0.50		0.20 - 0.50	
LT-TES size	[m ³]	70,000		70,000	
ORC condensation		Partial		Partial	

3. Simulation results

3.1. Variable HT-HP and ORC capacities with infinite HT-TES

3.1.1. Case Study #1: Turin

The analysis of the electricity surplus has been developed considering the Moncalieri GT3 Plant, since this unit shows the largest amount of unbalances among the other plants in Torino (Moncalieri GT2 and Torino Nord).

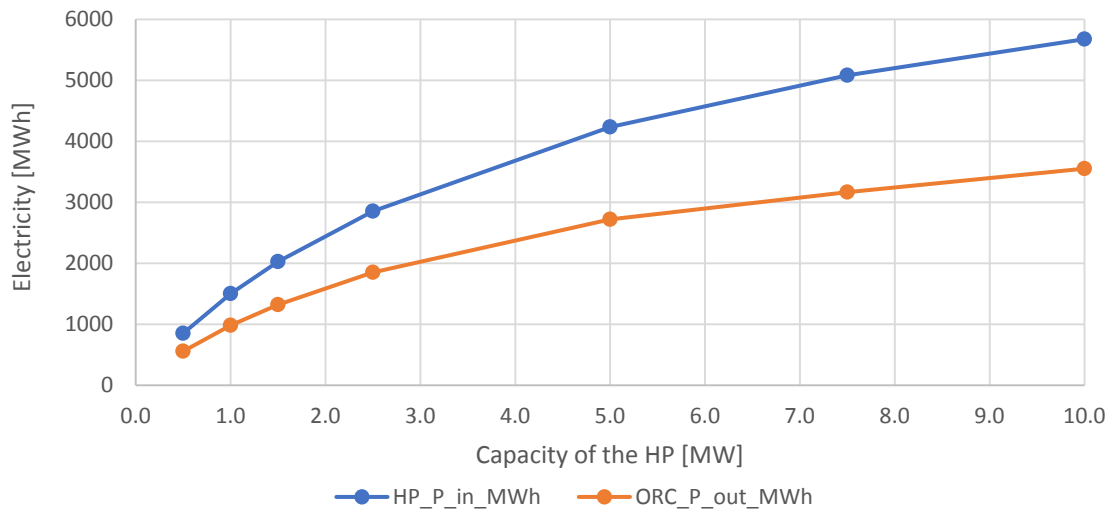


Figure 15: Electricity absorbed by the HT-HP and produced by the ORC as function of the HT-HP capacity for a fixed ORC relative capacity of 0.4 (infinite HT-TES size).

Figure 15 shows that increasing the capacity of the HT-HP and of the ORC, the electricity absorbed by the HT-HP and that produced by the ORC increases. The increase of the electricity absorbed by the HT-HP is quite proportional to the electricity produced by the ORC, varying the respectively installed capacities. The ratio between these two parameters is quite constant, settled to a value around 1.5. An asymptotic trend in the amount of absorbed/produced electricity with respect to the HT-HP capacity cannot be appreciated within the chosen range of HT-HP capacities, due to the small capacities of HT-HP and ORC considered. Choosing larger machines would have dramatically reduced their number of full-load hours, due to particular profiles of the electricity production and demand (Figure 2).

Analysing the electricity production as a function of the ORC relative capacity for different capacities of the HT-HP (Figure 15) two different behaviours can be observed:

- For capacities of the HT-HP equal or lower than 1.5 MW, the graph shows a benefit to increasing the relative size of the ORC to 0.3 with respect to the HT-HP capacity. Larger ORC does not increase the electricity production.
- For capacities of the HT-HP higher than 1.5 MW, the graph shows that an ORC with relative capacity of 0.2 is enough, as an increase of its capacity did not entail an increase of the electricity production.

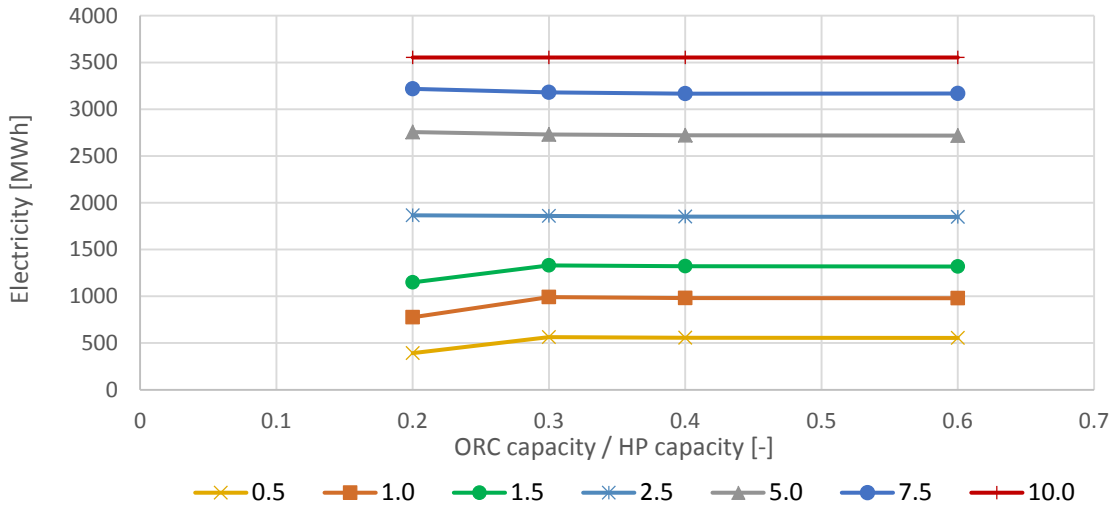


Figure 16: Electricity production of the ORC as a function of the ORC relative capacity for different sizes of HT-HP (legend entries, in MW) and infinite HT-TES size.

This behaviour can explain by the amount of electricity surplus given to CHEST by the plant for small sizes. An increase of the size of the HT-HP allows a higher electricity recovery and, thus, a higher heat production exploitable by the ORC. Once the energy stored in HT-TES is exploited, the maximum amount of electricity produced by the ORC is reached and an increase in the ORC size does not produce any benefit.

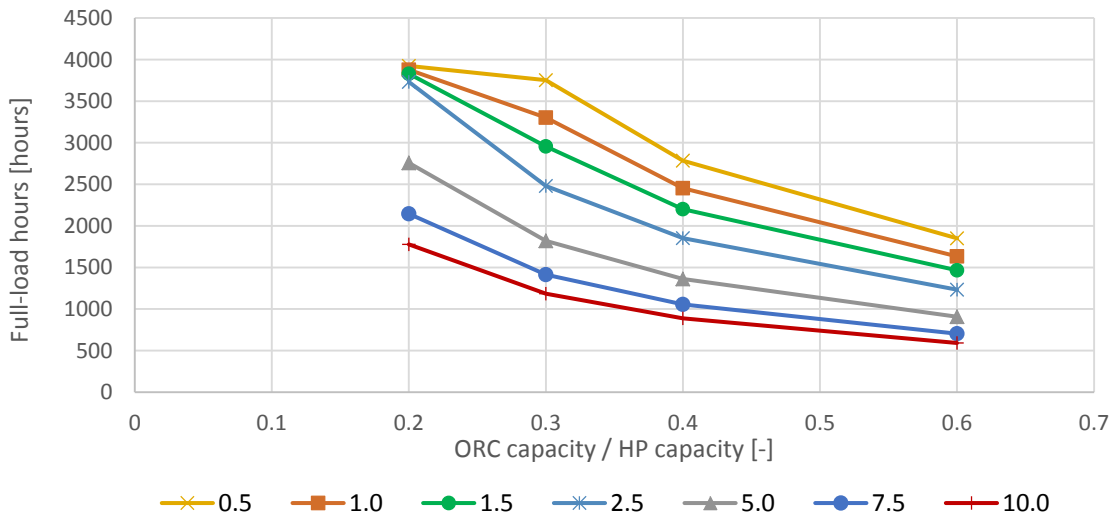


Figure 17: Full-load hours of the ORC as function of the ORC relative capacity for different sizes of HT-HP (legend entries, in MW) and infinite HT-TES size.

From the number of full-load hours of the ORC (Figure 17) can be observed that:

- for HT-HP capacities equal or lower than 2.5 MW, the figure shows the most utilization in terms of hours of the ORC and, in particular, considering a ratio between capacity of the ORC and HT-HP in the range of 0.2-0.3;
- for HT-HP capacities higher than 2.5 MW, even at low value of ratio, the figure shows a certain decrease on the hours of ORC utilization.

Smaller size of HT-HP and a small size of ORC allows a better exploitation of both units, with a consequently higher number of full-load hours. Being the surplus of electricity defined, the increase of the size the HT-HP and ORC means a decrease in the number of full-load hours of the HT-HP and of the ORC.

Due to the limited influence of the ORC relative capacity in case of infinite HT-TES, the following performance indicators of the CHEST system are shown as function of the HT-HP capacity for a fixed ORC relative capacity of 0.4. However, this can be considered valid for all other ORC relative capacities, except for the cases of the smallest HP-ORC combinations, as seen in Figure 16.

COP of the HT-HP, the efficiency of the ORC and the P2P ratio of the CHEST system respectively are shown in Figure 18 and Figure 19. The COP is not strongly affected by the size of the HT-HP, as its value remains in the range 4.53–4.63. This is due to the fact that the HT-HP draws heat from the top layer of the LT-TES, whose content is continuously renovated by the part of the return flow of the DH network (at 70 °C). Consequently, the inlet temperature to the evaporator is roughly constant and close to 70 °C, determining an almost constant COP of the HT-HP. The slight decrease of the COP for larger HT-HP is produced by the fact that the higher thermal power extracted by the HT-HP from the LT-TES causes a decrease in the temperature at the top of the LT-TES, so decreasing the inlet temperature to the HT-HP's evaporator and consequently its efficiency.

As the ORC operates in ambient-condensation mode, its efficiency is roughly constant in all scenarios, ranging from 14.3 % to 14.5 % (decreasing for larger HT-HP capacities), therefore is not shown graphically.

As a result, the P2P ratio of the CHEST system (Figure 19) follows roughly the same trend as the COP (and of the ORC), slightly decreasing with the HT-HP capacity from about 65.5 % to 61.6 %.

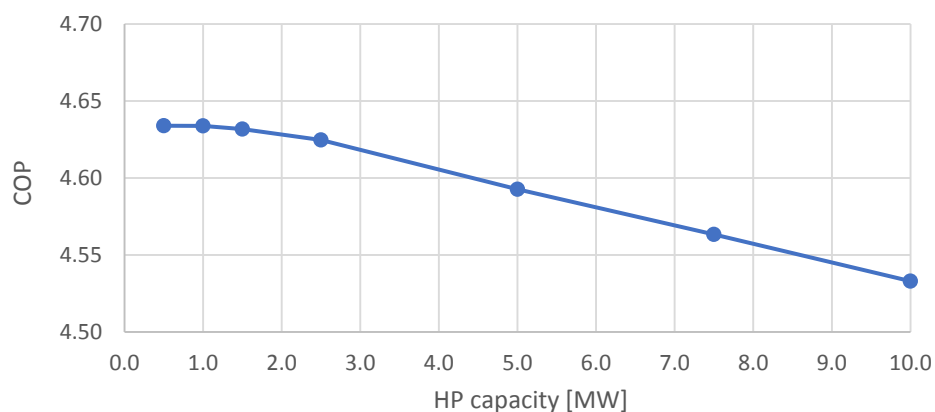


Figure 18: COP of the HT-HP as a function of the HT-HP capacity for a fixed ORC relative capacity of 0.4 (infinite HT-TES size).

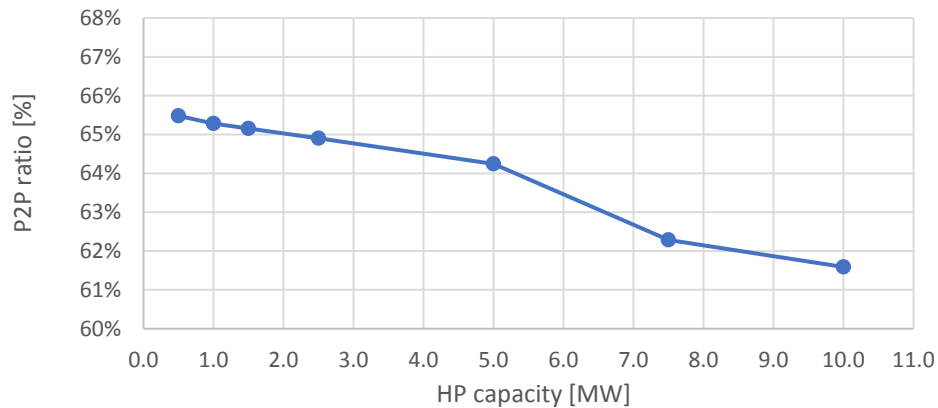


Figure 19: P2P ratio of the CHEST system as a function of the HT-HP capacity for a fixed ORC relative capacity of 0.4 (infinite HT-TES size).

The possibility of utilizing high-temperature heat from the *Boiler* component for preheating the inlet flow to the HT-HP's evaporator from 70 °C (DH return temperature) to 80 °C is also investigated. The reason is that an evaporator inlet temperature of 70 °C entails that a fairly large amount of excess heat produced by the HT-HP (about 8 % compared to the useful high-temperature heat transferred to the HT-TES). Due to its low temperature, most of this excess heat cannot be reinserted in the system and is dissipated to the environment. Besides, when the inlet temperature was 80 °C, the amount of excess heat decreases to about 1 % of the heat transferred to the HT-TES.

Therefore, simulations using preheating are carried out under the same boundary conditions as those used for the simulations just presented in this section, with the only difference being the maximum HT-HP's capacity investigated, which is 5 MW instead of 10 MW.

The lower amount of dissipated excess heat and the lower temperature lift provided by the HT-HP, increases the yearly-averaged COP from about 4.59-4.63 (scenarios without preheat, see Figure 18) to 5.47. Consequently, more energy is stored in the HT-TES, which increases the electricity production of the ORC and therefore the P2P ratio, which rose from 64 %-65.5 % (scenarios without preheat) to about 76 %-78 %, in those scenarios where the ORC is sufficiently large not to be a limiting factor for the electricity production. The heat output from the boiler also increases by about 13 %-16 % to provide the necessary preheating heat.

An electric efficiency of the CHEST system is defined as the ratio between the electricity production of the ORC (i.e., the useful output of the CHEST system) and the additional heat output of the boiler compared to the scenario without CHEST (i.e., the additional required input). The so-defined efficiency is in the range 16.4 %-16.7 % when preheating is not used, while it slightly increases to 17.2 %-17.5 % in case of preheating. Because of the minor efficiency gain achieved at the expenses of gas-produced and high-temperature heat, the preheat strategy is no further investigated in the later simulations.

3.1.2. Case Study #3: Ispaster

The range of installed capacities for the HT-HP and ORC used in the simulations is chosen based on the highest value of electricity surplus profile and that of the electricity deficit profile, shown in Figure 20.

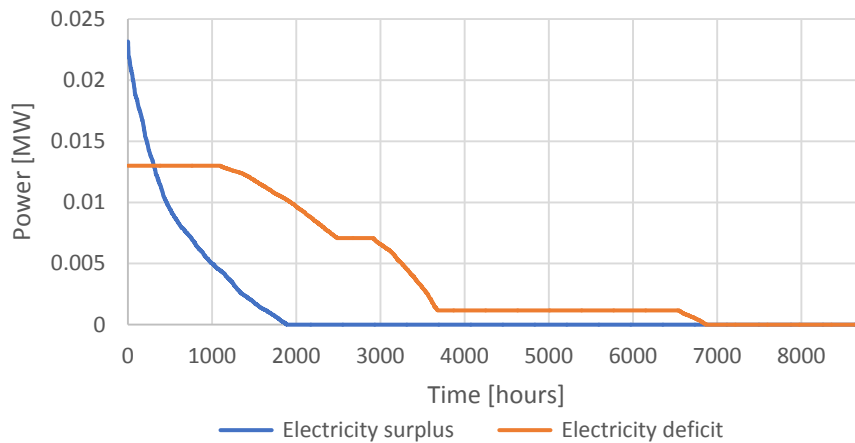


Figure 20: Distribution of electric surplus and electric deficit in Ispaster case during the year (8760 hours).

The highest electricity surplus is about 23 kW, which hence represents the largest size of the HT-HP which could be reasonable to assume. As minimum HT-HP, capacity a value of 1 kW is chosen. The highest electricity deficit is 13 kW, which hence represents the largest size of the ORC which is reasonable to assume. The relative capacity of the ORC is varied between 0.25 and 1.

Preliminary simulations show that at the highest HT-HP capacities, both the HT-HP and the ORC are highly underused, due to limited number of hours where the power of electricity surplus is high (>10 kW). Additionally, the current size of the solar collector array (and hence the availability of RES heat to be used by the HT-HP) is not enough to sustain the operation of the HT-HP. When the HT-HP draws from the LT-TES more heat than that produced by the solar thermal collectors, the temperature at the top of the storage falls below the collector setpoint temperature of 80 °C, so decreasing the COP of the HT-HP. In fact, the electricity produced by the ORC increases by only +11 %, when shifting from a 9 kW ORC to a 13 kW ORC (+44 % in capacity). Moreover, there is a nearly +30 % increase, when shifting from a 5 kW ORC to a 7 kW ORC (+40 % in capacity).

Consequently, a second round of simulation is carried out, this time varying the HT-HP capacity between 1 kW and 9 kW, while the ORC relative capacity is varied again in the range 0.25-1.00 for each size of the HT-HP. The ORC operated in ambient-condensation mode.

In presence of an infinite HT-TES, the ORC relative capacity has a negligible impact on the performance of the HT-HP. The capacity of the ORC does not have an impact on the electricity produced by the ORC, which means that the ORC relative capacity could be even smaller than 0.25. As the ORC electricity production is independent of the ORC size, the number of full-load hours of the ORC decreases inverse-proportionally with the ORC capacity, as seen in Figure 21.

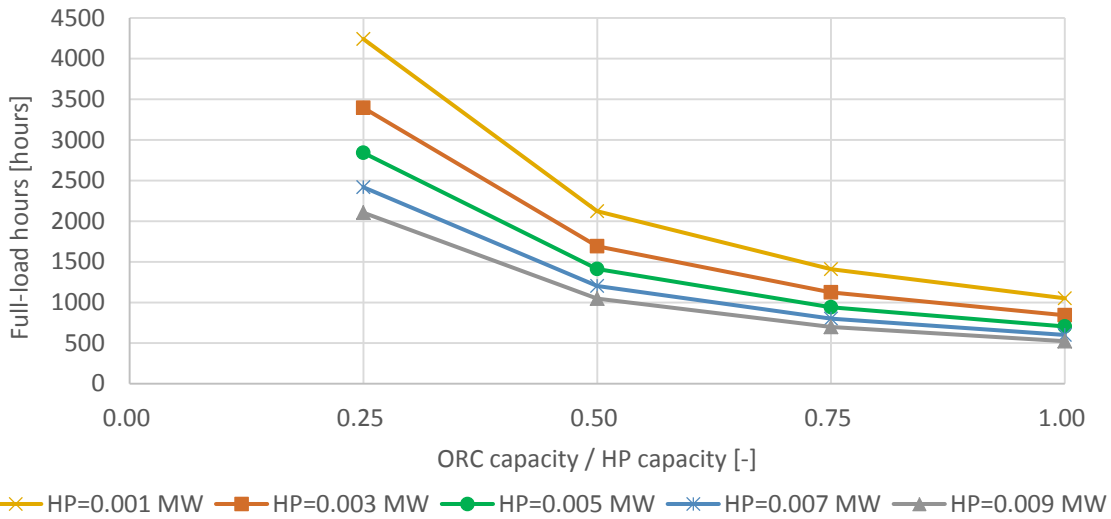


Figure 21: Full-load hours of the ORC as a function of its relative capacity for different sizes of the HT-HP (infinite HT-TES size).

Because the other performance indicators of the CHEST system do not depend on the size of the ORC, the following diagrams are shown as function of the HT-HP capacity, and not of the ORC capacity.

Figure 22 shows how both the electricity consumption of the HT-HP and the electricity production of the ORC increases at larger HT-HP capacities. Both curves present an asymptotic behaviour due to the lower amount of surplus electricity which is progressively available at higher capacities (Figure 20).

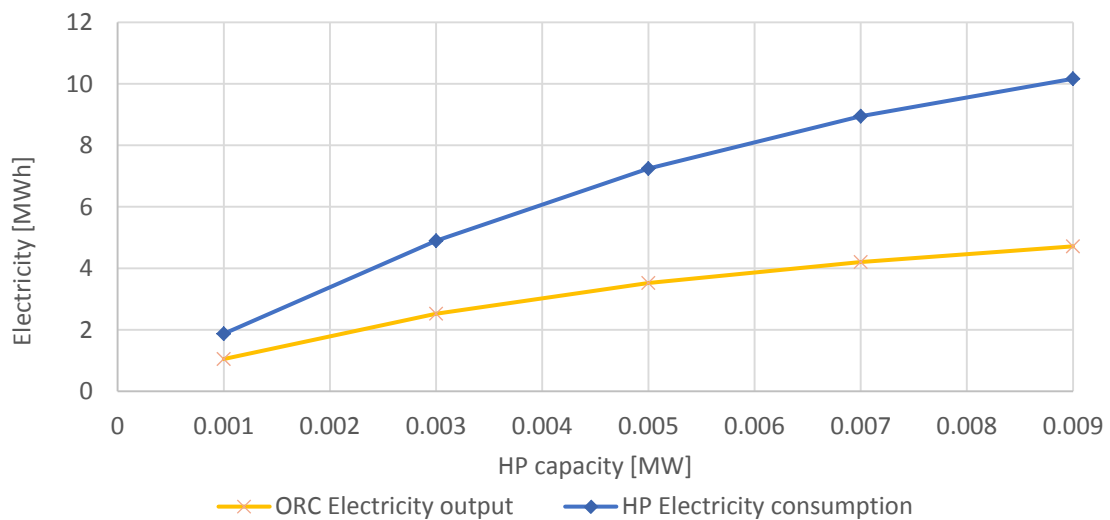


Figure 22: HT-HP electricity consumption and ORC electricity output as a function of the HT-HP capacity (infinite HT-TES size).

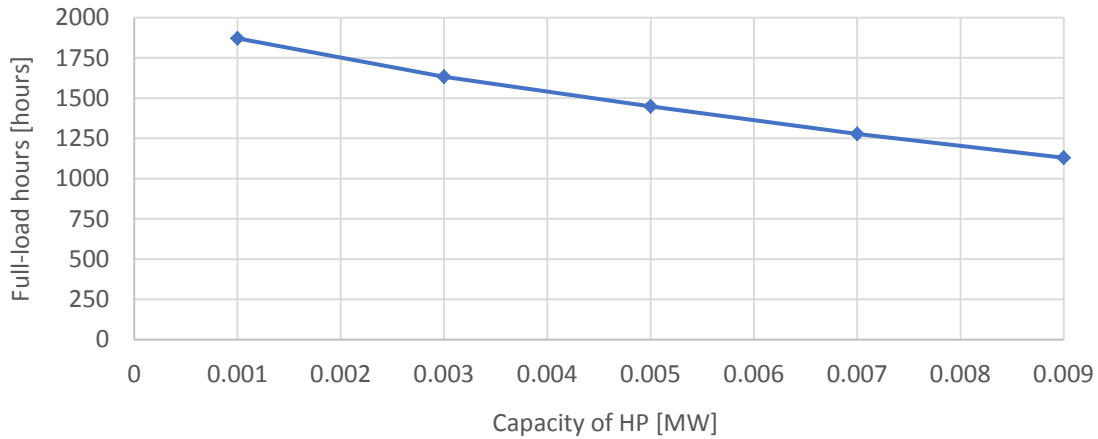


Figure 23: Full-load hours of the HT-HP as a function of its capacity (infinite HT-TES size).

The number of full-load hours of the HT-HP decreases proportionally to the capacity of the HT-HP. This is a consequence of the distribution of electricity surplus (Figure 20) as the operation of the HT-HP is only possible at the time of available excess electricity. Thus, the smaller size of the HT-HP is, the longer hours it can run during the year.

Figure 24 shows the COP of the HT-HP, the efficiency of the ORC and the P2P ratio as function of the HT-HP capacity. The COP of the HT-HP decreases for larger sizes of the HT-HP, because the progressively lower temperatures at the inlet of the evaporator of the HT-HP, while the efficiency of the ORC is basically constant and around 13.5 %. As all the simulations treated in this section assume ambient condensation (i.e. the entire condensation heat from the ORC is entirely dissipated to the environment), the DH boiler needs to compensate for this and increases its output to meet the DH demand (Figure 25). The reason why the boiler output increases less than the amount of condensation heat is that, through the clean-up procedure and the excess heat, part of the high-temperature heat from the HT-TES is supplied to the LT-TES. As this high-temperature heat includes a portion of energy coming from the electricity surplus, the PV electricity is indirectly used in the DH network (which on the other hand does not happen in the reference case without CHEST), so contributing to cover the DH heat demand and reducing the additional operation of the DH boiler.

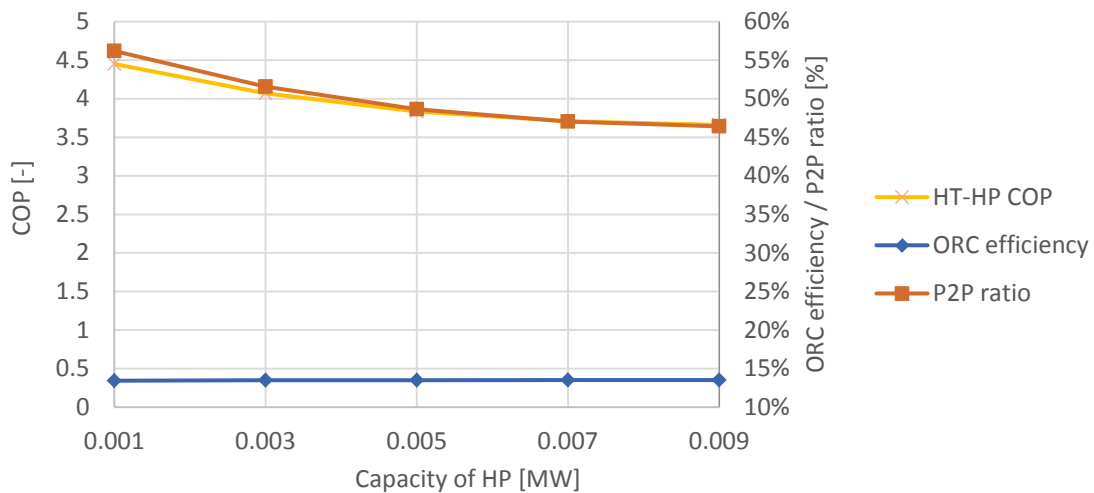


Figure 24: COP of the HT-HP, the efficiency of the ORC and P2P ratio as a function of the HT-HP capacity (infinite HT-TES size).

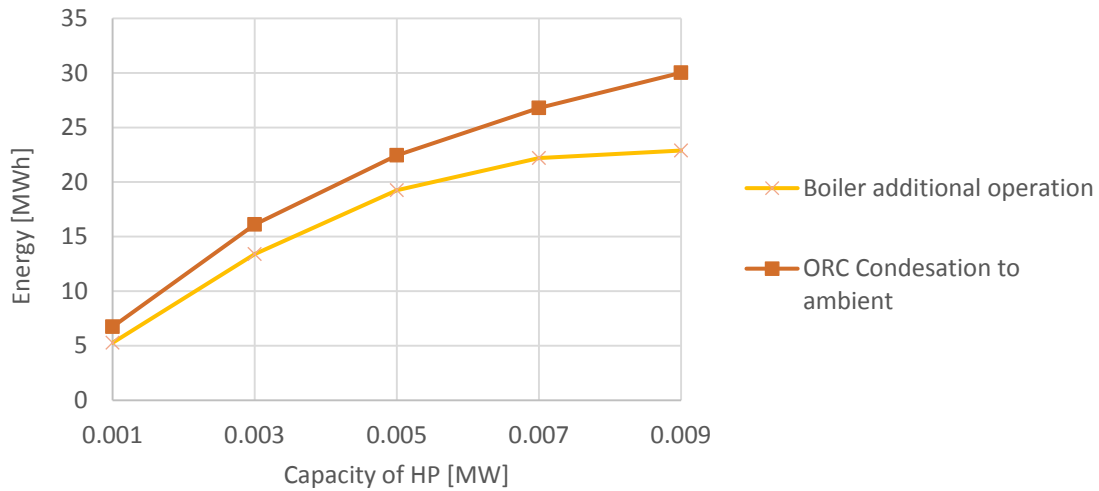


Figure 25: Additional heat production from the DH boiler with respect to the case without CHEST and condensing heat dissipated to the environment.

3.1.3. Case Study #4: Barcelona

The distribution of the electricity surplus and electricity deficit for the Barcelona case study are shown in Figure 26. The maximum electricity surplus is about 90 MW, while the maximum electricity deficit is about 60 MW. As the amount of electricity surplus available at a power higher than 60 MW is very limited, the HT-HP capacity is varied in the range 1 MW-60 MW.

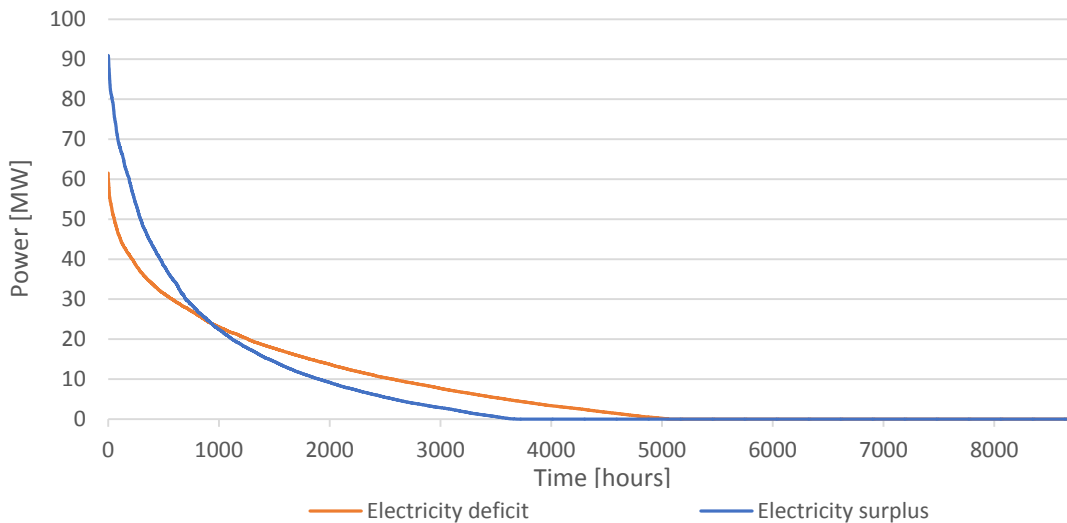


Figure 26: Distribution of the electricity surplus and the electricity deficit in the Barcelona case study during a year (8760 hours).

In these sets of simulations, the size of the HT-TES is assumed to be infinite. The ORC relative capacity is varied between 0.25 and 1.20. Figure 27 and Figure 28 show the electricity absorbed by the HT-HP and produced by the ORC respectively, as a function of the ORC relative capacity for different HT-HP capacities.

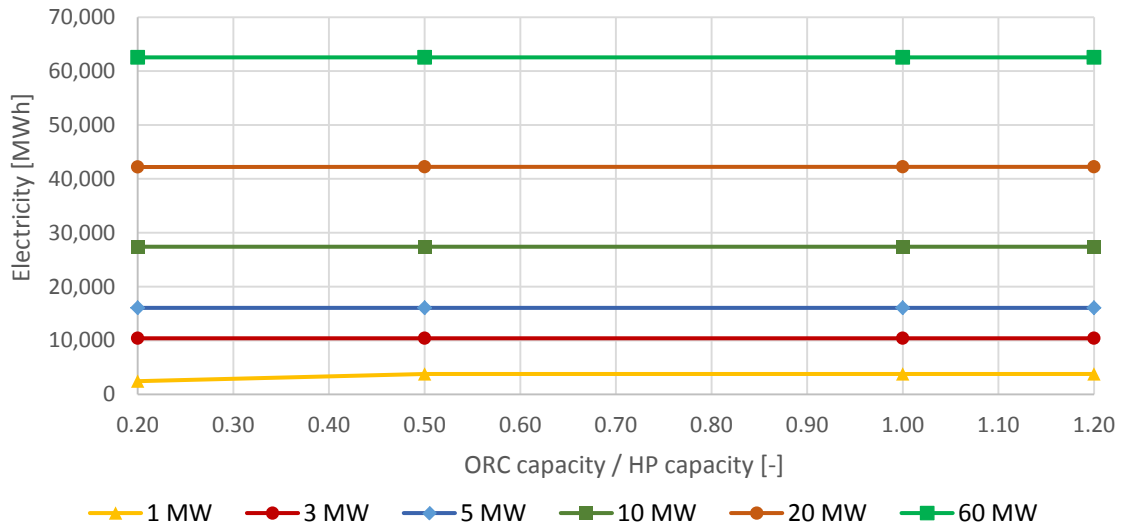


Figure 27: Electricity absorbed by the HT-HP as a function of the ORC relative capacity for different HT-HP capacities (infinite HT-TES size).

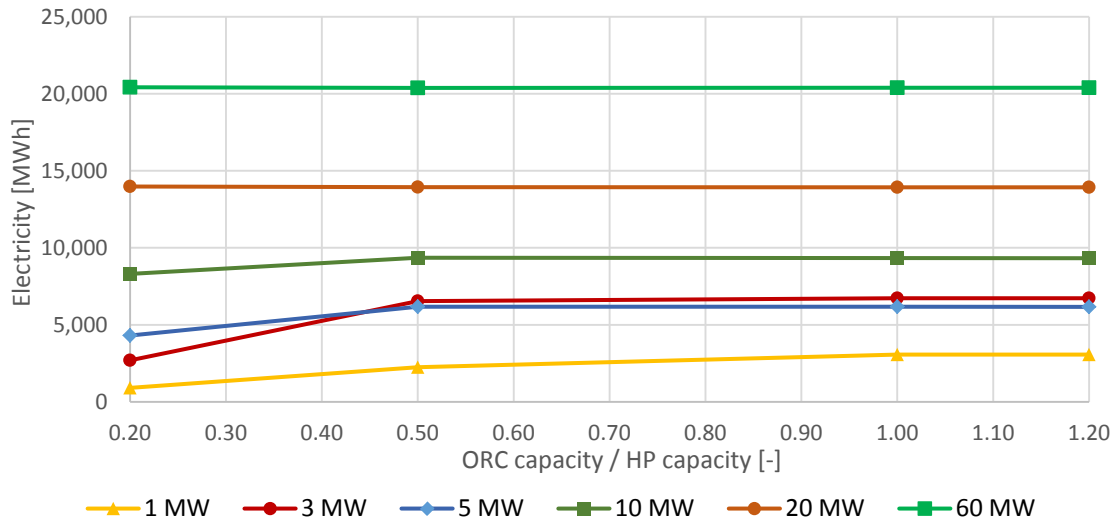


Figure 28: Electricity produced by the ORC as a function of the ORC relative capacity for different HT-HP capacities (infinite HT-TES size).

With an infinite HT-TES size, there is almost no influence of the ORC relative capacity on the amount of electricity absorbed and produced respectively. Only for small HT-HP capacities and small ORC relative capacities, there is a small decrease in the electricity production. In this case, the ORC is so small that it could not make use of the energy available in the HT-TES.

Also, the other performance parameters of the CHEST system, i.e. COP, ORC efficiency, P2P ratio as well as the boiler output, show nearly no dependence on the ORC relative capacity. Therefore, the results are shown as a function of the HT-HP capacity in the following diagrams. Figure 29 shows that an increase of the HT-HP capacity leads to an increase of both the electricity absorbed by the HT-HP and produced by the ORC. This increase, however, gets progressively smaller with increasing HT-HP capacity.

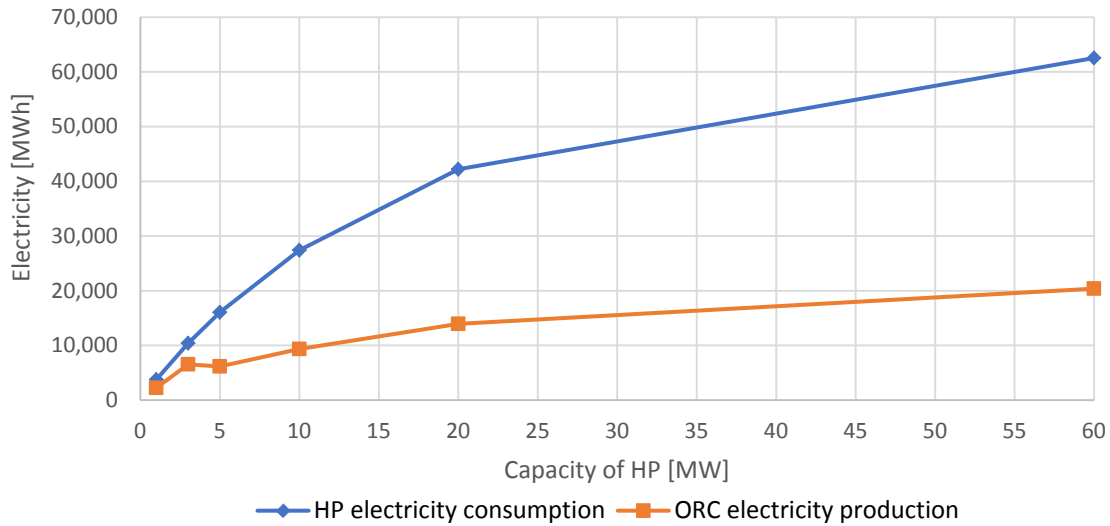


Figure 29: Electricity absorbed by the HT-HP and produced by the ORC as a function of the HT-HP capacity, for an ORC relative capacity of 0.50 (infinite HT-TES size).

Figure 30 shows the COP, the ORC efficiency and the P2P ratio as function of the HT-HP capacity. The COP decreases with increasing HT-HP capacity to reach a nearly constant value of 3.8 for HT-HP capacities larger than 10 MW. Regarding the ORC efficiency, this decreases when moving from a 3 MW HT-HP to a 5 MW HT-HP. This is due to fact that HT-HPs of 1 MW and 3 MW operate in full ambient-condensation mode, resulting in ORC efficiencies of about 13.8%. On the other hand, for HT-HP capacities equal to or larger than 5 MW, the condensation mode is increasingly more shifted toward partial condensation, characterized by higher condensing temperatures than ambient condensation, therefore lower ORC efficiencies.

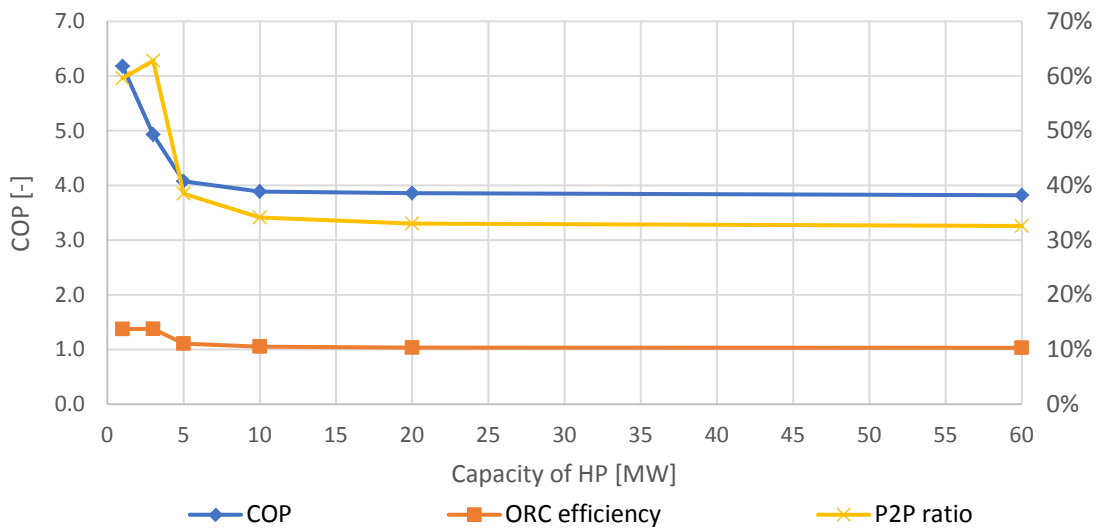


Figure 30: COP, ORC efficiency and P2P ratio as a function of the HT-HP capacity, for an ORC relative capacity of 0.50 (infinite HT-TES size).

At first glance, it might seem strange that the P2P ratio for the HT-HP of 3 MW is higher than for the HT-HP of 1 MW, even though the COP is lower (4.9 compared to 6.2) and the ORC efficiency is basically the same (13.8%). This is due to the fact that, in case of a HT-HP capacity of 1 MW and an ORC relative capacity of 0.5, a considerable amount of heat is accumulated in the HT-TES, which cannot be discharged by the ORC, due to its limited size (cf. Figure 28).

Moreover, the same ORC relative capacity of 0.5 results in a larger ORC in the case of a 3 MW HT-HP, which could better discharge the HT-TES, resulting in a higher electricity production, hence higher P2P ratio.

3.1.4. General discussion

On the one hand, in the three analysed case studies, the simulations results prove that, in presence of an infinite HT-TES, the ORC relative capacity has almost no effect on the performance of the HT-HP, such as in terms of electricity consumption, COP, heat exchanged between the HT-HP and the other components. This is explained by the fact that the most direct interaction between the ORC and the HT-HP is through the HT-TES, but in these simulations the HT-TES capacity is assumed infinite.

On the other hand, if HT-TES storage capacity is limited, it may occur that an undersized ORC limits the operation of the HT-HP. In this case, the reduced discharging rate of the HT-TES given by the ORC may prevent the HT-TES to be sufficiently discharged, therefore reducing the available storage capacity that the HT-HP can feed into.

For this reason, in the above scenarios it is found that the ORC capacity can always be much smaller than the HT-HP capacity with no negative effects on the performance of the CHEST system. However, the ORC capacity should not be so small to limit its own electricity production (e.g. as seen at the lower HT-HP's and ORC's capacities in Figure 16), because this would reduce the P2P ratio as well. Depending of the specific case study considered, feasible ORC relative capacities are between 0.25 and 0.50.

In the case that the ORC operates in blow-off operation mode, the ORC can affect the operation of HT-HP in a second way, and this is through the LT-TES. By condensing in the LT-TES, the ORC affects the temperature in the lower layers of the LT-TES. As the lower layers progressively move upwards, their temperature can have a relatively relevant impact on the temperature at the top of the LT-TES, where the HT-HP draws heat from.

As the ORC relative capacity has limited effect, the main performance indicators of the CHEST system could be expressed as a function of HT-HP capacity. Increasingly larger HT-HP capacities generally entails:

- **progressively lower COP** (e.g. cf. Figure 18)
 The more electricity is absorbed by the HT-HP, the higher the flow rate drawn from the top of the LT-TES. In presence of a limited amount of RES heat at a certain temperature feeding into the top of the LT-TES, the temperature at the inlet of the HT-HP's evaporator will be roughly the RES-heat temperature as long as the flow drawn by the HT-HP's evaporator is not higher than the flow supplied by the RES-heat source (for simplicity, we neglect the volume of water which may have been charged in the LT-TES in the time period before the activation of the HT-HP). If the flow drawn by the evaporator of the HT-HP is larger, the HT-HP will continue draw the necessary flow but at progressively lower temperatures, so reducing its COP. If it is desired that the HT-HP operates only at high efficiency, the control could be modified by increasing the value of minimum temperature which is required at the inlet of the HT-HP's evaporator (see the definition of the parameter PLF_{temp} in the CHESTER deliverable D2.2). This would increase the COP, but likely decrease the number of full-load hours of the HT-HP;

- ***progressively smaller increase in the amount of electricity absorbed by the HT-HP*** (e.g. cf. Figure 15)

Because of the profile of the curve of the electricity surplus, larger HT-HP determine larger amount of absorbed electricity, but with increases progressively smaller. This means that the electricity consumption of the HT-HP increases less than proportionally with respect to the HT-HP capacity, often according to a quadratic relationship of the type:

$$Electricity_{HP} = -Capacity_{HP} \cdot (Capacity_{HP} - const.)$$

Therefore, by definition of full-load hours, the number of full-load hours generally decreases linearly with the HT-HP capacity (see Figure 23).

- ***progressively smaller increase in the amount of electricity produced by the ORC*** (e.g. cf. Figure 15)

As the ORC uses the energy stored in the HT-TES by the HT-HP, it is straightforward that the electricity production of the ORC will generally have a similar trend as that of the electricity consumption of the HT-HP.

Because the efficiency of the ORC is found to be largely independent of all varied parameters (as it depends either on the heat sink temperature in ambient-condensation mode or on the LT-TES bottom temperature in blow-off operation mode, which are both little affected by the system sizing), the P2P ratio generally follows the same trend as the COP, unless in the case that the ORC capacity is so small that it limited the ORC electricity production (e.g. as seen for the smaller HT-HPs and ORCs in Figure 16).

3.2. Variable HT-HP and ORC capacities with finite HT-TES

3.2.1. Case Study #1: Turin

The influence of the size of the HT-TES on the electricity consumption of the HT-HP is shown in Figure 31. For all the cases analysed, the increase of the size of the HT-TES has an appreciable effect until a storage capacity of 5 hours. Storage capacities higher than 5 hours do not entail a relevant increase in the amount of electricity. The isolated markers on the far-right side of Figure 31 represent the electricity consumption for an infinite HT-TES capacity and confirm this behaviour.

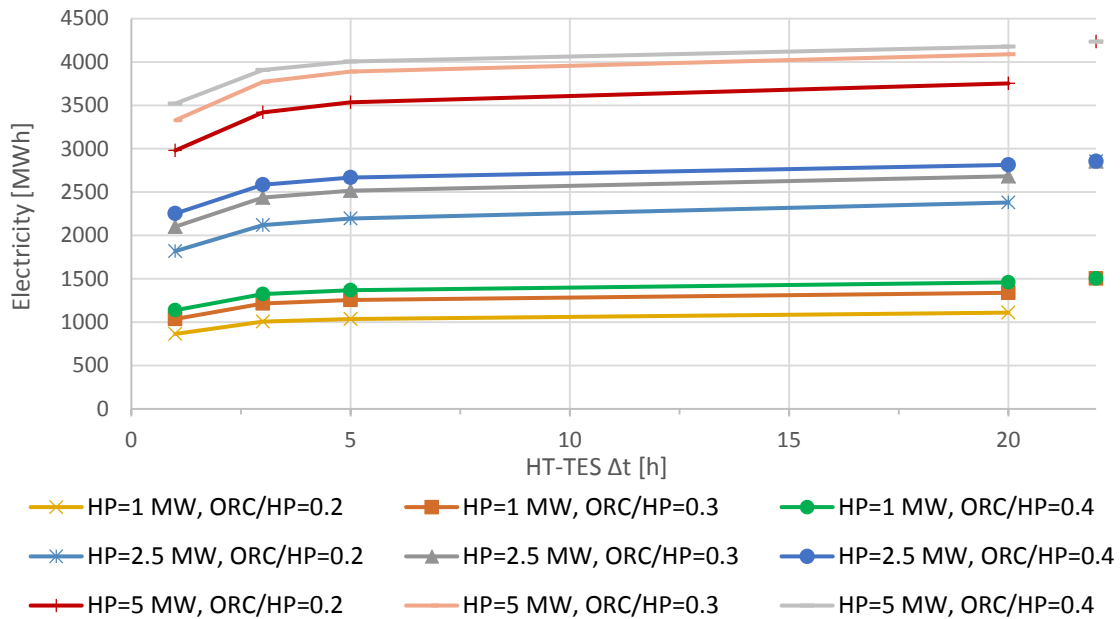


Figure 31: Electricity absorbed by the HT-HP as a function of the HT-TES capacity for different HT-HP capacities and ORC relative capacities.

Figure 32 and Figure 33 show the number of full-load hours of the ORC and the HT-HP as well. This is a confirmation of the optimum size of the HT TES (almost 5 hours), considering these ranges in capacity of ORC and HT-HP.

Regarding the COP and P2P ratio, these parameters are roughly constant in all investigated scenarios (HT-HP-s COP = 4.60-4.63 and P2P ratio = 64 %-66 %) and in agreement with those found presented in Section 3.1.1.

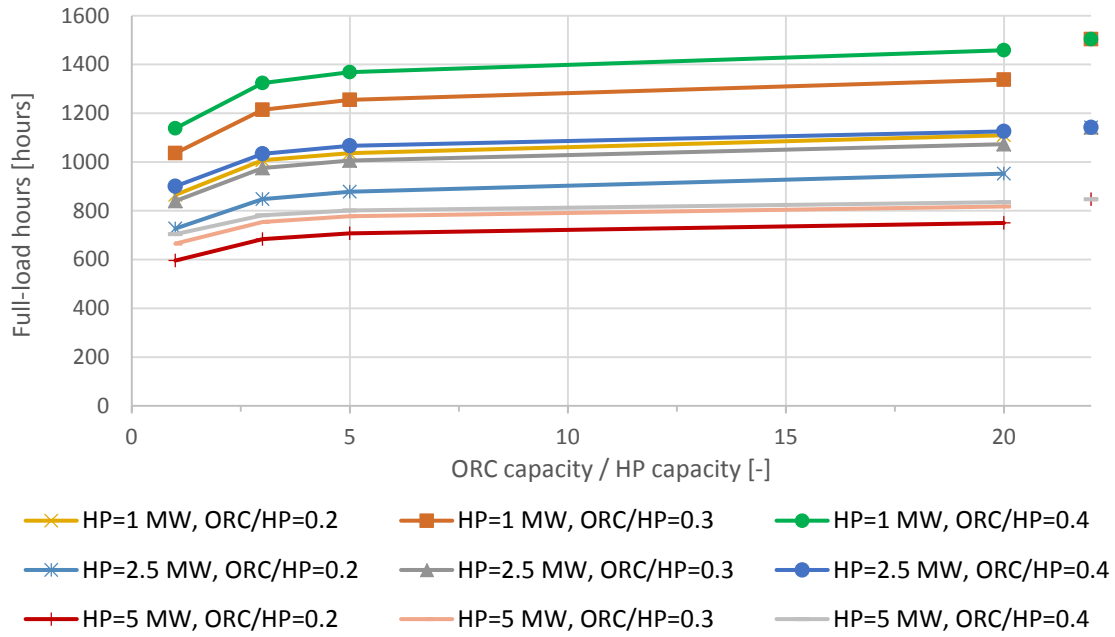


Figure 32: Full-load hours of the HT-HP as a function of the HT-TES capacity for different HT-HP capacities and ORC relative capacities.

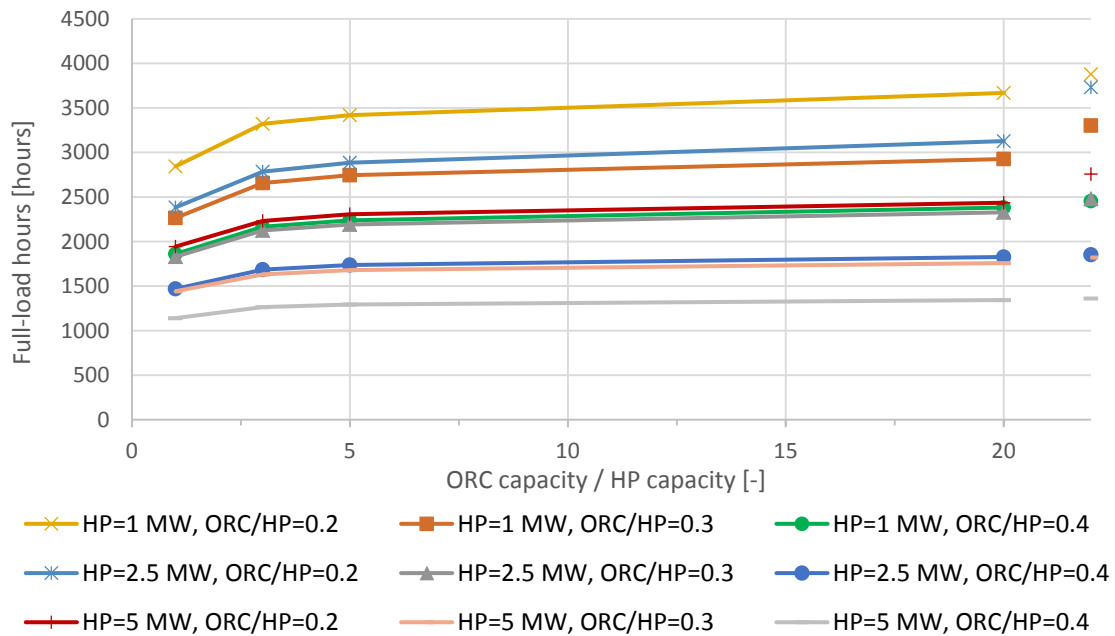


Figure 33: Full-load hours of the ORC as a function of the HT-TES capacity for different HT-HP capacities and ORC relative capacities.

3.2.2. Case Study #3: Ispaster

The combined effect of the HT-HP capacity, the ORC relative capacity and the HT-TES size is analysed in this section. First, a wider range of HT-TES sizes is considered, to later identify a narrower range, more tailored on the Ispaster case. Then the HT-HP capacity and the ORC relative capacity are varied for different HT-TES sizes.

In the first round of simulations, the size of the HT-TES is varied between 2 h and 24 h. The ratio between the storage capacity of the latent part of the HT-TES and that of the sensible

part is 0.74, as this is the average latent-to-sensible ratio at which the HT-HP works at, given by the inlet temperature to the HT-HP’s evaporator. The HT-HP capacity is varied between 1 kW and 9 kW, while the ORC relative capacity is constant and equal to 1.

The operation outputs of the HT-HP and the ORC increases with the HT-TES size. However, for storage periods higher than 12 h, the increase in operation is negligible. This can be seen in the following figures, showing the number of full-load hours of the units and the HT-HP’s COP.

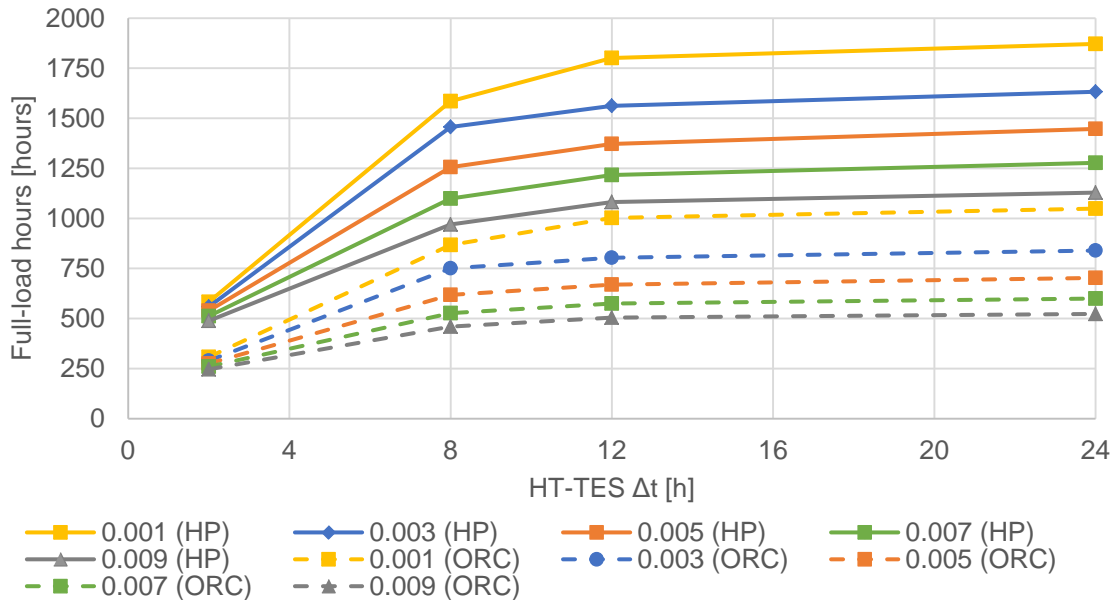


Figure 34: Full-load hours of the HT-HP (solid lines) and the ORC (dashed lines) as a function of the HT-TES capacity. The legend entries denote the capacity of the HT-HP (ORC relative capacity = 1).

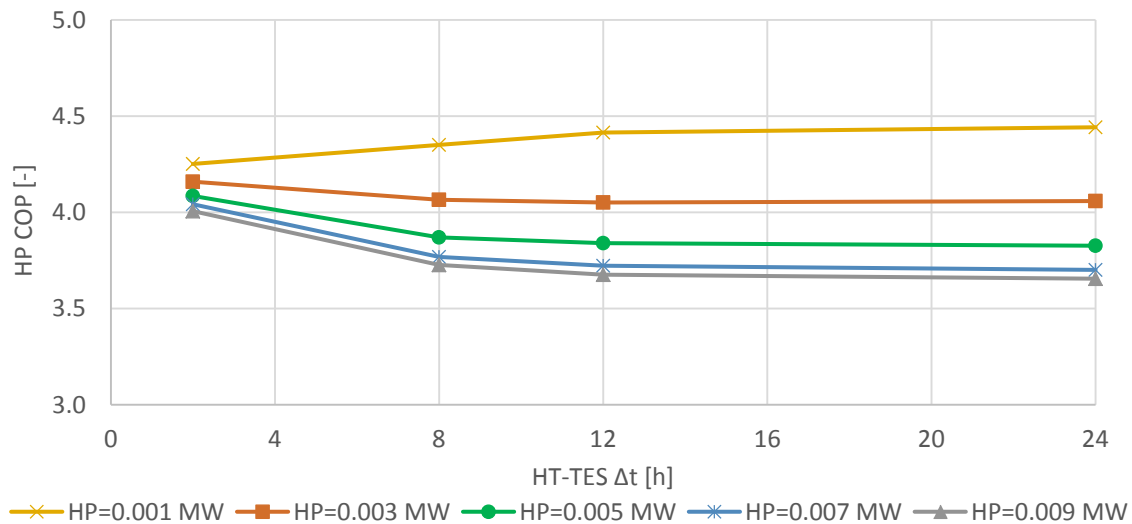


Figure 35: COP of the HT-HP as a function of the HT-TES capacity. The legend entries denote the capacity of the HT-HP (ORC relative capacity = 1).

Figure 34 shows that the better compromise between the performance of CHEST system in terms of full-load hours of the HT-HP (and of the ORC) and the size of the HT-TES is found for capacities of the HT-TES between 8 h and 12 h.

The smallest HT-HP of 1 kW increases its COP for larger HT-TES capacities (Figure 24), unlike the larger HT-HPs. The reason for this is that the COP of the HT-HP decreases at larger HT-HP capacities due to lower inlet temperatures at the evaporator of the HT-HP, due to the current area of the solar thermal collectors, while the ORC efficiency is relatively constant in all scenarios, ranging from 13.3 % to 13.6 %.

As the most extreme cases, two sizes of the HT-HP (1 kW and 9 kW) are selected for the detailed analysis with the variable ORC relative capacity. The considered sizes of HT-TES are 8 h and 12 h. Regarding the size of the ORC, the results in Section 3.1.2 show that ORC relative capacities in the range 0.50-1.0 are oversized. Therefore, here smaller ORCs are considered, with relative capacities down to 0.1. For each combination of HT-HP capacity and HT-TES's Δt , the value of COP_{ref} used to size the HT-TES is derived from previous simulations (Figure 35). The identified values of COP_{ref} are about 4.4 and 3.7 for the HT-HP of 1 kW and 9 kW respectively.

Figure 36 shows the number of full-load hours of the HT-HP as a function of the ORC relative capacity in the four investigated scenarios. As for the infinite HT-TES, the operation of the 9 kW HT-HP is not influenced by the ORC size, except for a relative capacity of 0.1. For the 1 kW HT-HP, ORC relative capacities smaller than 0.5 progressively reduce the amount of electricity absorbed by the HT-HP (although not shown, ORC relative capacities up to 1.0 are simulated, but they perform as well as a relative capacity of 0.5 in terms of operation of the HT-HP).

The fact that smaller ORC limits the operation of the HT-HP is caused by the fact that, in case of a finite HT-TES size, the slower discharging rate of the HT-TES given by smaller ORC units reduce the available storage capacity, which consequently limited the HT-HP operation.

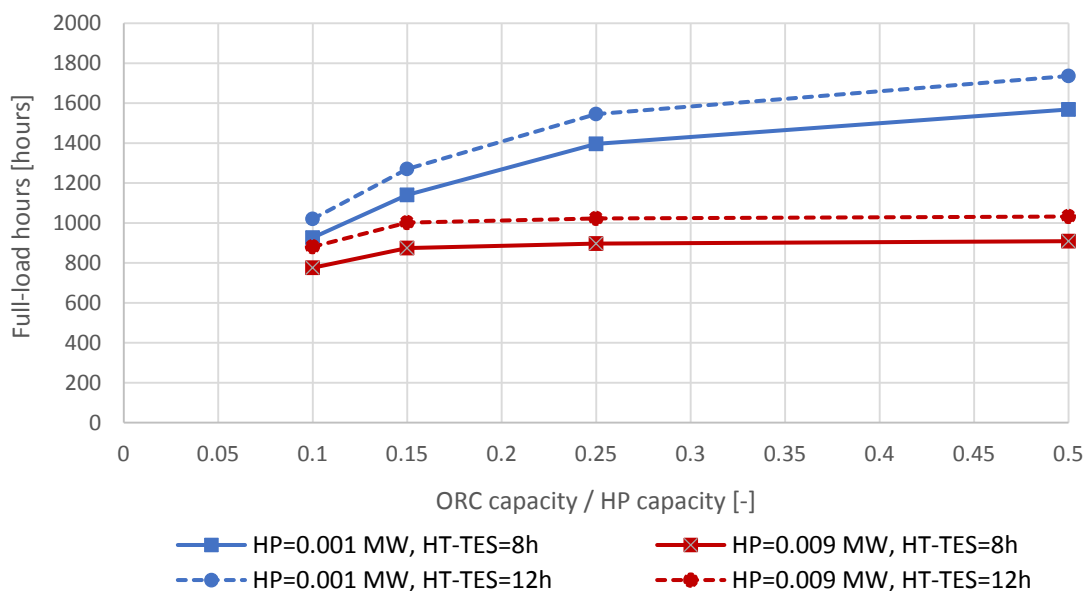


Figure 36: Full-load hours of the HT-HP as a function of the ORC relative capacity for 1 kW and 9 kW HT-HP, and an 8 h and 12 h HT-TES.

The same trend described above on the effect of the ORC relative capacity on the HT-HP operation is found also in Figure 35, which shows the ORC electricity production. Above a certain value of ORC relative capacity, the energy available in the HT-TES is the limiting factor for the ORC operation, so that larger ORC sizes do not entail a higher electricity production.

Moreover, ORC units sized below the same value are limited in their electricity production by their small size.

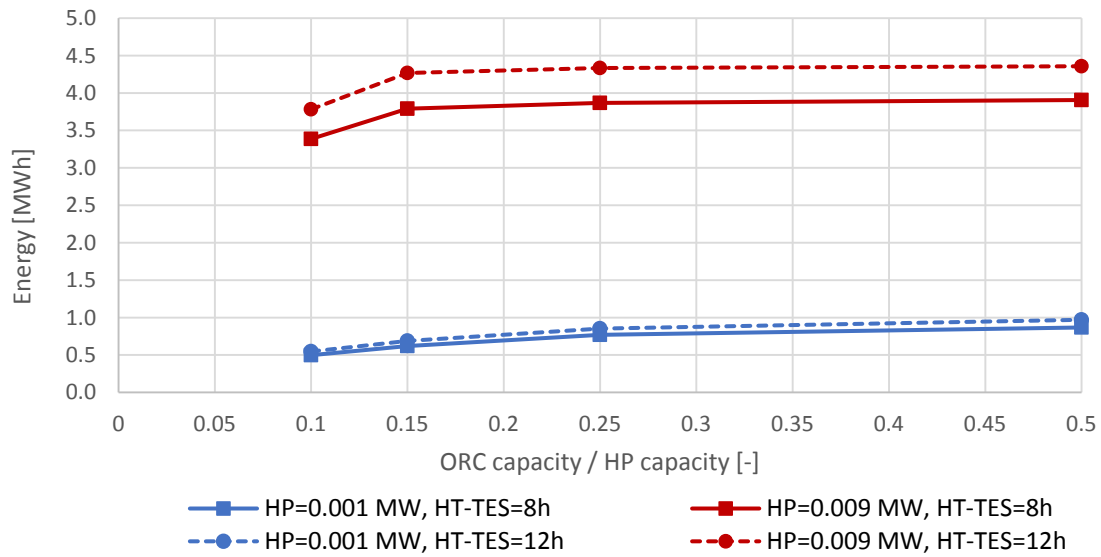


Figure 37: ORC electricity production as a function of the ORC relative capacity for 1 kW and 9 kW HT-HP, and an 8 h and a 12 h HT-TES.

As expected, the COPs of the two sizes of HT-HP are fairly constant with respect to the ORC relative capacity and close to the values found in the previous simulations: between 4.2 and 4.4 for 1 kW HT-HP and between 3.7 and 3.8 for 9 kW HT-HP. The ORC efficiency is, as well, fairly constant (13.5 %-13.7 %) in the four considered scenarios, in agreement with the previous results.

The heat absorbed by the HT-HP affects the operation of the DH boiler, determining an additional heat output compared to reference scenario without CHEST (Figure 38).

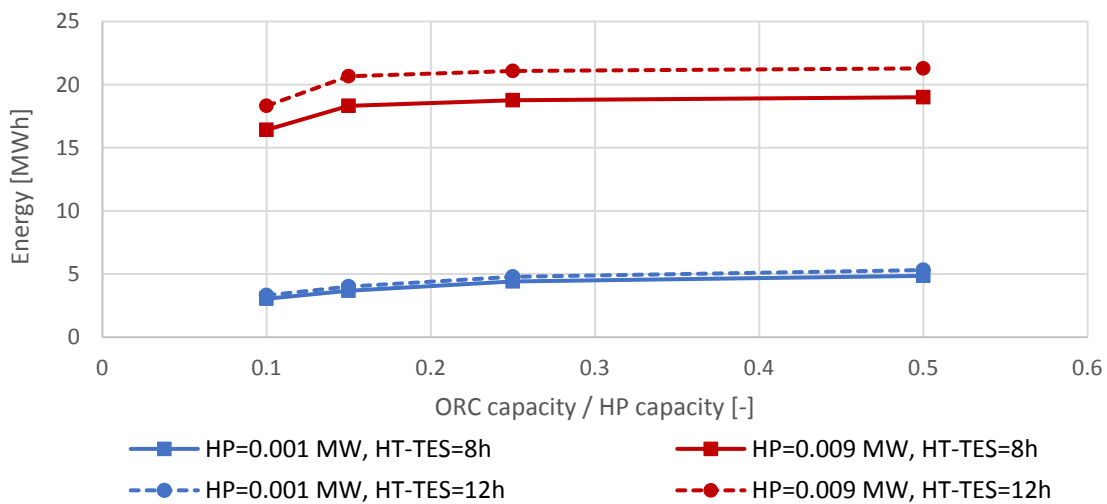


Figure 38: Additional heat output from the boiler compared to reference scenario without CHEST as function of the ORC relative capacity for 1 kW and 9 kW HT-HP, and an 8 h and 12 h HT-TES.

3.2.3. Case Study #4: Barcelona

Before carrying out simulations with varying ORC relative capacity for a finite HT-TES, the effect of the size of the HT-TES on the performance of the CHEST system is analysed for an ORC relative capacity equal to 0.5. Simulations with different HT-HP capacities (1 MW, 10 MW and 60 MW) are carried out while varying the HT-TES size from 1 h to 48 h. The ratio between the latent and the sensible part of the HT-TES is 0.74, as in every simulation using butene as working fluid.

As shown in Figure 39, Figure 40 and Figure 41, HT-TES sizes larger than 12 h have a minor influence on the electricity absorbed by the HT-HP, the electricity produced by the ORC and the P2P ratio. Therefore, HT-TES sizes larger than 12 h are no more investigated in later simulations.

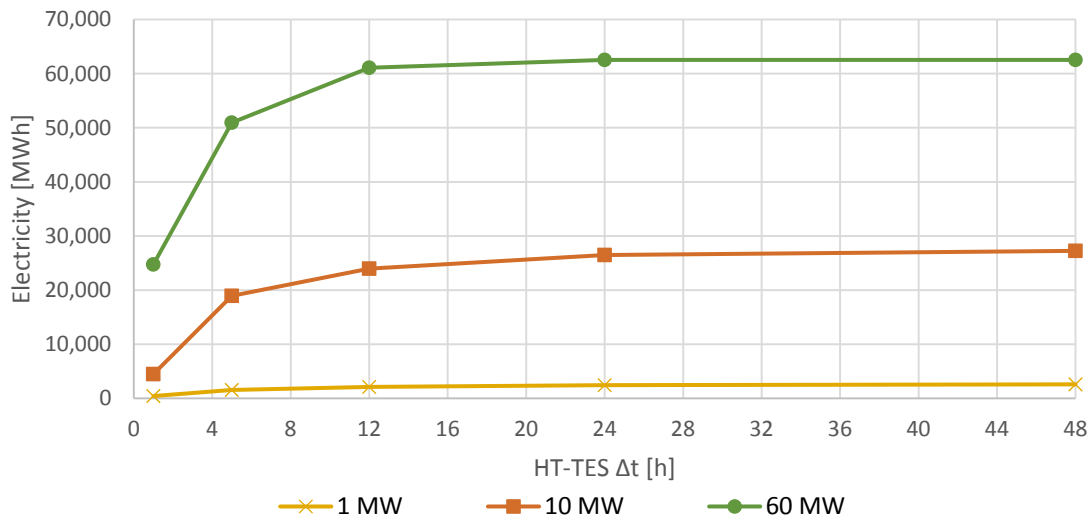


Figure 39: Electricity absorbed by the HT-HP as a function of the HT-TES size for different HT-HP capacities (ORC relative capacity = 1).

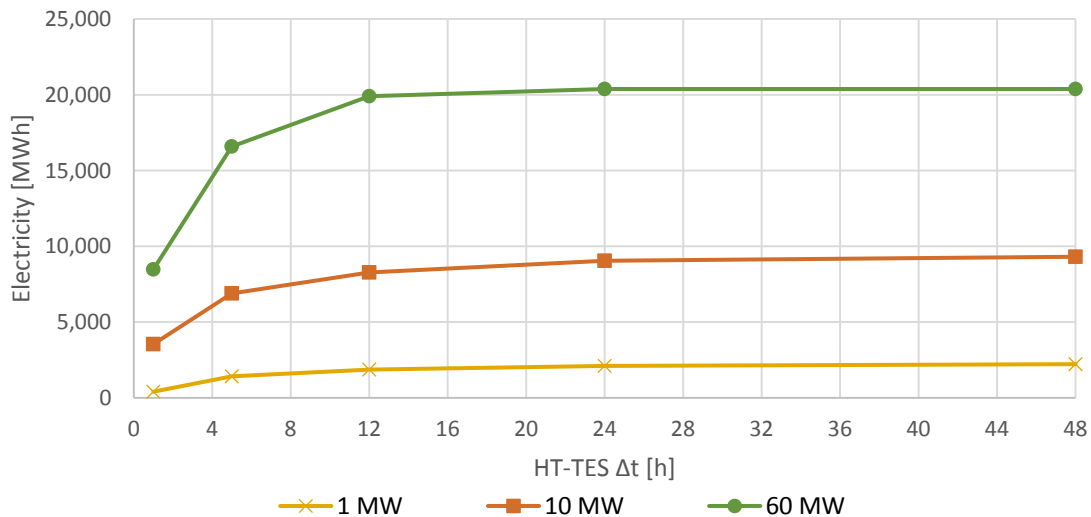


Figure 40: Electricity produced by the ORC as a function of the HT-TES size for different HT-HP capacities (ORC relative capacity = 1).

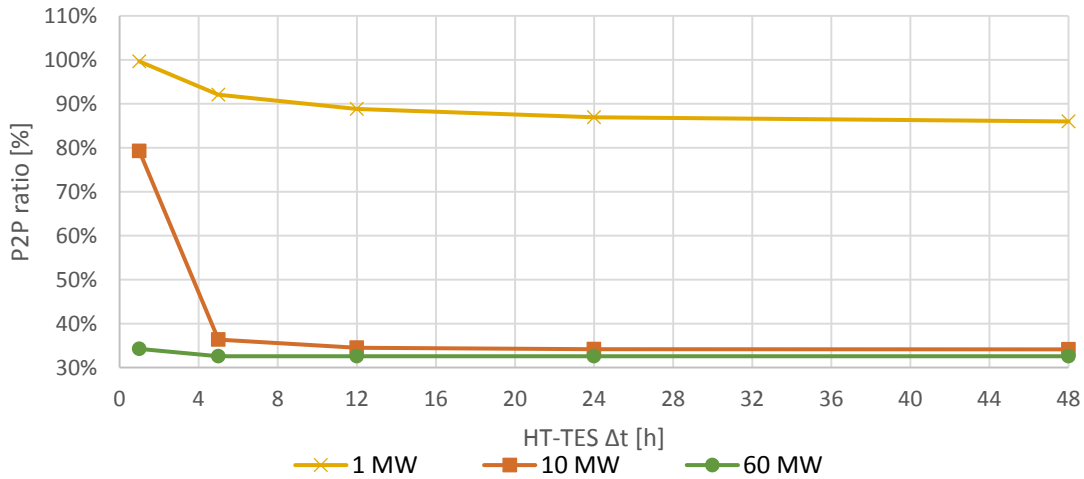


Figure 41: P2P ratio as a function of the HT-TES size for different HT-HP capacities (ORC relative capacity = 1).

Based on the results presented above, later simulations are performed for HT-HP capacities of 1 MW and 10 MW and for HT-TES sizes of 6 h and 12 h, while varying the ORC relative capacity between 0.20 and 0.50.

Figure 42 and Figure 43 show the electricity absorbed by the HT-HP and the electricity produced by the ORC respectively. A larger ORC capacity (at a constant HT-HP capacity) entails a faster discharge of the HT-TES, thereby the time period when the HT-HP operation is inhibited by a fully charged HT-TES is reduced. Therefore, a larger ORC results in higher amounts of the electricity absorbed by the HT-HP, and consequently in an increase of the ORC electricity production. However, the influence of the ORC size is smaller at larger ORC capacities, and for ORC relative capacities larger than 0.50 no influence occurs. It can be concluded that, in case of a finite HT-TES, the ORC capacity can be half the size of the HT-HP, with a negligible reduction in the amount of electricity absorbed by the HT-HP and produced by the ORC. Another result is that the amount of electricity absorbed by the HT-HP and produced by the ORC increase with increasing HT-HP capacities and increasing HT-TES sizes.

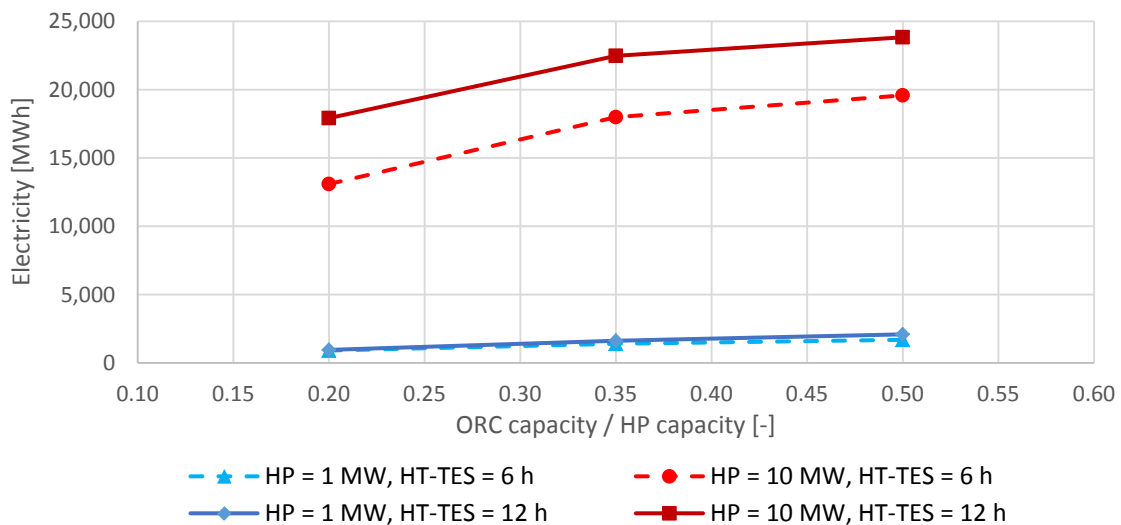


Figure 42: Electricity absorbed by the HT-HP as a function of the ORC relative capacity for different HT-HP capacities and different HT-TES sizes.

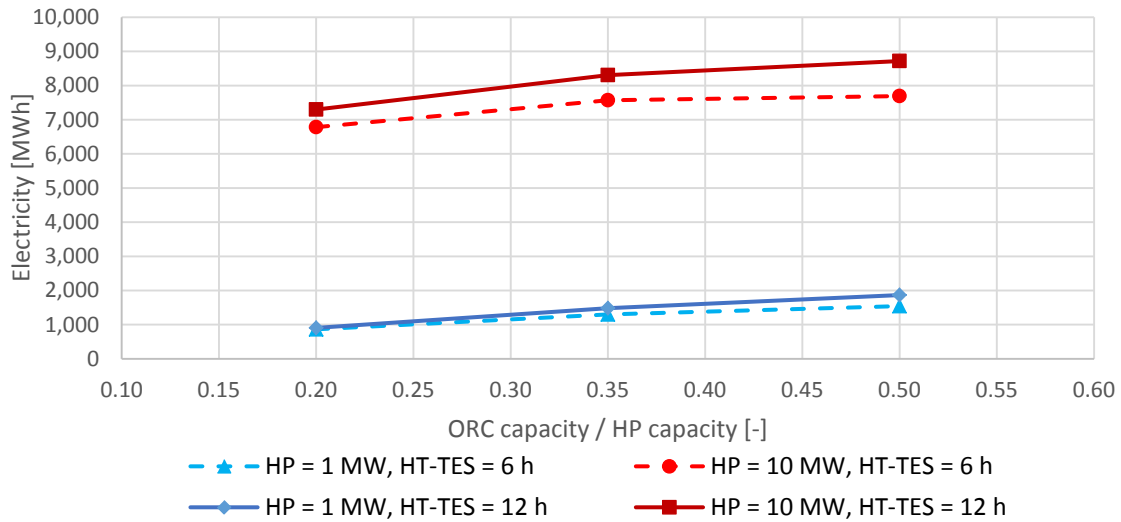


Figure 43: Electricity produced by the ORC as a function of the ORC relative capacity for different HT-HP capacities and different HT-TES sizes.

Figure 44, Figure 45 and Figure 46 show the COP of the HT-HP, the ORC efficiency and the P2P ratio of the CHEST system respectively in the four investigated scenarios. An increase of the HT-HP capacity and/or an increase of the HT-TES size leads to lower COP, because the increased amount of electricity absorbed by the HT-HP (cf. Figure 41) entails that more heat is drawn from the LT-TES, which reduces the temperature at the top of the LT-TES, therefore at the inlet of the HT-HP evaporator.

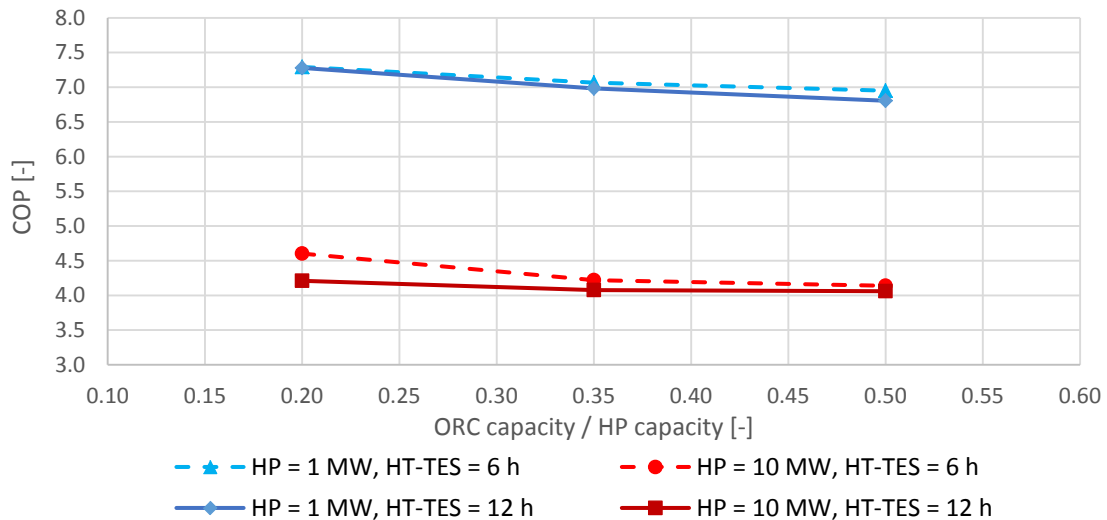


Figure 44: COP of the HT-HP as a function of the ORC relative capacity for different HT-HP capacities and different HT-TES sizes.

The ORC efficiency is found to be independent of the ORC relative capacity for a 1 MW HT-HP, because in this case full ambient condensation takes place, which means that the ORC efficiency is not affected by the rest of the system, but only by the ambient temperature used at the condenser, while, for the 10 MW HT-HP, warmer water from the LT-TES is partially used as inlet flow to the ORC condenser. The ORC efficiency is, therefore, lower compared to ambient condensation and it is no longer independent of the ORC capacity.

The P2P ratio follows the trend of the COP for the 1 MW HT-HP because of the constant ORC efficiency. For the 10 MW HT-HP, there is a similar trend of all the three performance parameters (COP, ORC efficiency and P2P ratio).

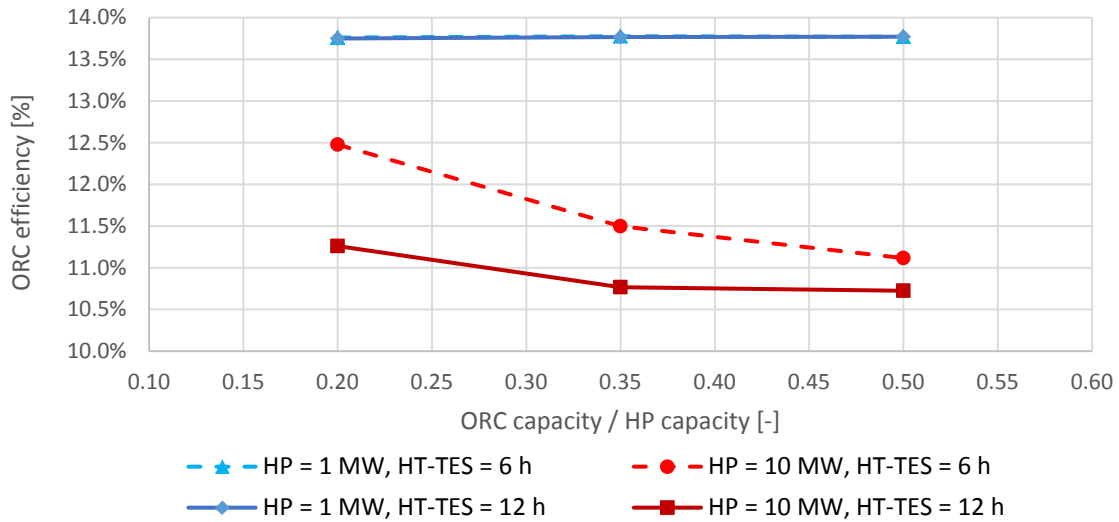


Figure 45: ORC efficiency as a function of the ORC relative capacity for different HT-HP capacities and different HT-TES sizes.

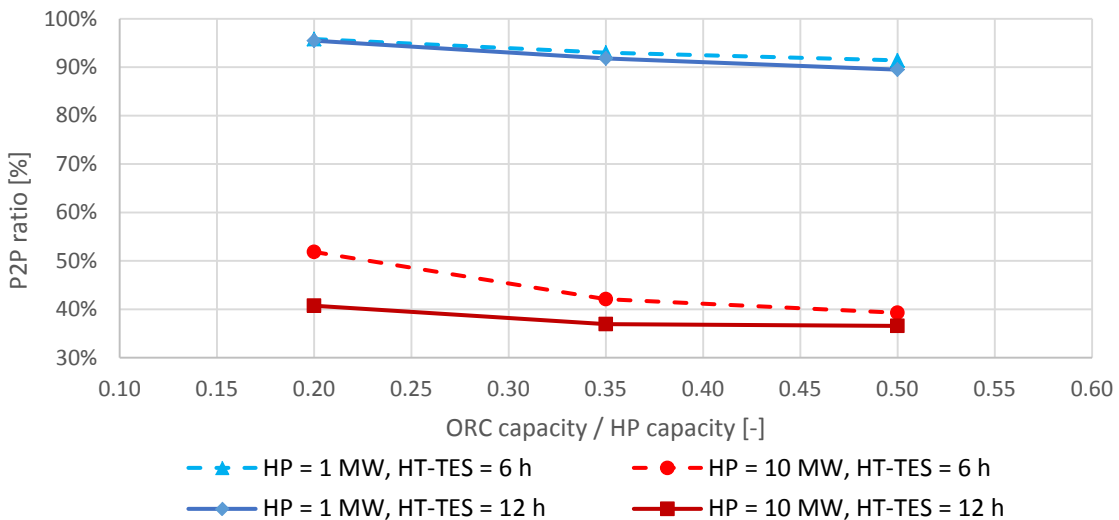


Figure 46: P2P ratio as a function of the ORC relative capacity for different HT-HP capacities and different HT-TES sizes.

The energy output of the boiler is shown in Figure 47. For the 10 MW HT-HP and the 12 h HT-TES, no difference with varying ORC relative capacity is visible, because already for an ORC relative capacity of 0.20, the maximum possible value of about 29 GWh is reached. A boiler output of 29 GWh means that the complete DH heat demand is covered by the boiler (cf. Table 5). For the other scenarios, a slight increase of the boiler output with increasing ORC relative capacity is visible.

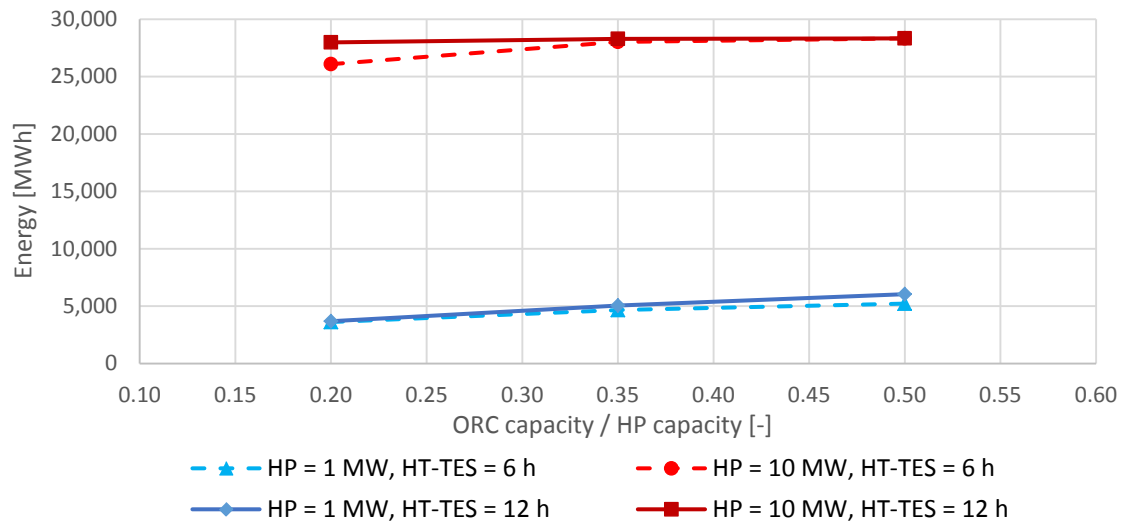


Figure 47: Boiler output as a function of the ORC relative capacity for different HT-HP capacities and 2 different HT-TES sizes.

3.2.4. General discussion

A finite size of the HT-TES has a relevant influence on the performance of the CHEST system. The size of the HT-TES should be large enough not to constrain the operation of the HT-HP. Nevertheless, the HT-TES should not be excessively large, because a part of the storage capacity would never be used, or it would be used for such a limited number of times that its economic feasibility would be questionable. It should be clarified that an upper limit on the HT-TES is not strictly relevant for the model, as it will not negatively affect the performance of the CHEST system. However, in real-world applications a larger size will entail higher cost as well as higher thermal losses (which are not considered for the HT-TES at the current stage of the TRNSYS model).

Performance indicators such as the number of full-load hours of the HT-HP or that of the ORC (or similarly the electricity consumption/production) will typically present an increasing trend for larger HT-TES sizes, but this increase will become progressively smaller, until it stops above a certain size.

The more suitable size of the HT-TES depends strongly on the application and, more precisely on the distribution of the profiles of electricity surplus and electricity deficit, which are directly calculated from the RES electricity production profile and the electricity demand profile (e.g. Figure 9). For instance, if the RES electricity production comes from a PV array and the corresponding electricity surplus during daytime is consumed overnight, the Δt for sizing the HT-TES could be around 6 hours, somehow closer to the number of full-load hours of the PV array.

In the case study of Ispaster, values of Δt in the range 8-12 hours are found to be more suitable. In fact, in Ispaster the electricity demand comes mainly from public buildings, which are closed during the weekends and holidays. In these periods the very low electricity demand entails a large amount of electricity surplus during the daytime. Therefore, the HT-TES system is better sized to be able to store about two days (i.e. weekend days) of PV production, around 12 hours.

In the Turin case study, the electricity surplus and electricity deficit came from non-optimised control of the gas turbine. As periods of electricity surplus and electricity deficit alternated

often, HT-TES having a Δt of 3 hours are sufficient in recovering a good fraction of the surplus electricity.

In the case studies analysed in the CHESTER deliverable D2.2, where the surplus electricity came from wind turbines, larger HT-TES ($\Delta t \geq 24$ h) were feasible.

Similarly to what explained in Section 3.1.4, on the decrease of the COP for larger HT-HP, also the increase of the HT-TES would generally entail a decrease of the COP, due to longer operation of the HT-HP.

Regarding the effect of the ORC size on the performance of the CHEST system, similar considerations as those presented in Section 3.1.4 hold true, and ORC relative capacities in the range 0.25-0.50 prove to be enough to reach almost the same performance as much larger ORC. Similar results were also found for the Aalborg case and the Alpha Ventus case in the CHESTER deliverable D2.2.

The fact that the ORC can be sized to be 0.25-0.50 times the size of the HT-HP should not be taken as a general rule-of-thumb of every CHEST system, but it depended on the profiles of the electricity production/demand assumed in the different case studies. It is simple to imagine profiles which would require the ORC to have the same (or even larger) capacity as the HT-HP capacity. Assuming a scenario with a periodic daily cycle, with a 23-hours long electricity surplus at a power of 1 MW and 1-hour long electricity deficit at a power of at least 23 MW. Additionally, it is assumed for simplicity that the P2P ratio of the CHEST system is 100 %. If the HT-TES is large enough to store the entire condensing heat of the HT-HP over a cycle, then it would be reasonable to install a 1 kW HT-HP and a 23 kW ORC, corresponding to an ORC relative capacity of 23.

3.3. Blow-off operation against condensation to the environment

3.3.1. Case Study #1: Turin

Due to the high return temperature of the DH network (70 °C) in Turin, the ORC always condenses to the environment, using the water of the Po river as heat sink. If the ORC condenses into the DH network (after lowering the DH return temperature through the auxiliary cooling device *Max-temp-6*), it would supply water at 60 °C to the bottom of the LT-TES, which is lower than the DH return temperature. Therefore, this operation mode, which does not offer any advantage compared to the ambient condensation mode, is neglected. Therefore, no comparison between blow-off operation and condensation to the environment is made.

3.3.2. Case Study #3: Ispaster

The DH network in Ispaster has a return temperature of 55 °C, which flows to the bottom of the LT-TES. Because the maximum temperature at the inlet of the condenser of the ORC is 50 °C, some heat has to be dissipated in case of blow-off operation. Therefore, it might be more efficient to dissipate heat to the environment by operating the ORC in ambient-condensation mode, because the resulting lower condensing temperature would improve the ORC efficiency.

The CHEST system for Ispaster is examined in the three condensation modes described in Section 2.1.1. In case of partial condensation, *Cond_T_limit_min* and *Cond_T_limit_max* are given the values of 56 °C and 60 °C respectively. The analysis is carried out considering an infinite HT-TES and an ORC relative capacity of 1.

As expected, the lower heat sink temperature in the ambient-condensation mode increases the efficiency of the ORC to about 13.5 %, while it is about 9.8 % in blow-off operation (Figure 48). Both efficiencies were constant with respect to the HT-HP size.

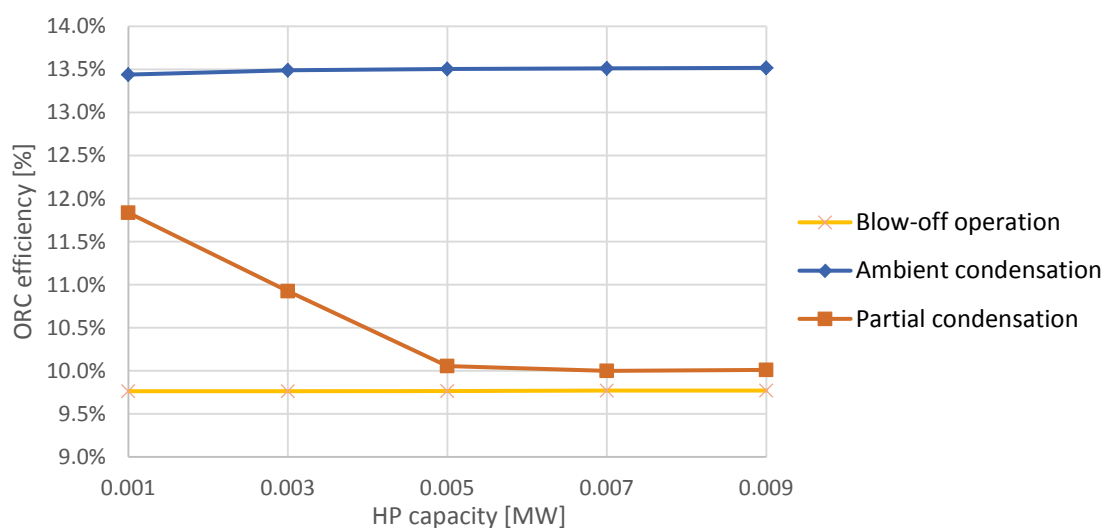


Figure 48: ORC efficiency in different condensation modes as a function of the HT-HP capacity.

In the scenario with the partial condensation, the ORC efficiency varies with the HT-HP capacity. It is highest for the 1 kW HT-HP, then decreases for larger HT-HP up to 5 kW capacity

and remains constant for even larger HT-HP. This trend is due to the progressively lower temperature at the bottom of LT-TES caused by the fact that progressively larger HT-HPs absorbs more heat than that supplied by the solar thermal collectors. The ambient-condensation (blue curve in Figure 48) occurs at temperatures at the bottom of the LT-TES higher than 60 °C, while at temperatures lower than 56 °C, the ORC condenses entirely to the LT-TES (yellow curve in Figure 48). When the temperature at the bottom of LT-TES is between 56 °C and 60 °C, the tee-junction *Valve-8* (Figure 7) is more open to the ambient-condenser (the *Condensation* equation block) when the LT-TES temperature is closer to 60 °C. HT-HPs with capacities equal to or larger than 5 kW cause the temperature at the bottom of the LT-TES to be lower than 60 °C, or even lower than 56 °C (Figure 49), entailing an ORC condensation shifted towards the blow-off operation mode, resulting in an ORC efficiency very close to the pure blow-off operation.

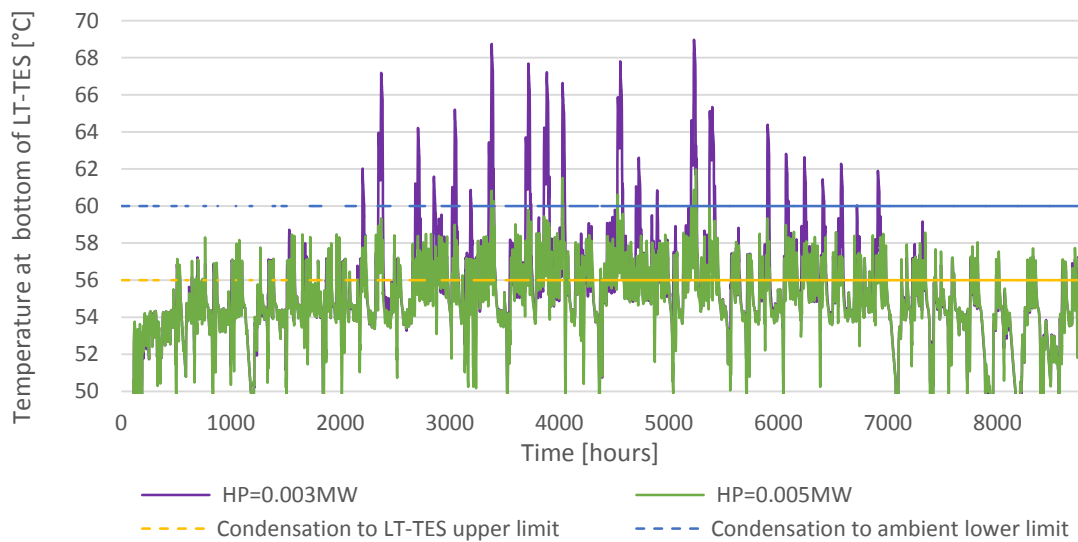


Figure 49: Temperature at the bottom of the LT-TES over a year for the operation of 3 kW and 5 kW HT-HP at partial condensation mode.

The heat dissipation from the system imposes higher heat production on the DH boiler. The annual boiler heat output along with the heat dissipated to the environment, either as condensation heat or blow-off heat (depending on the ORC condensation mode) are shown in the following diagrams.

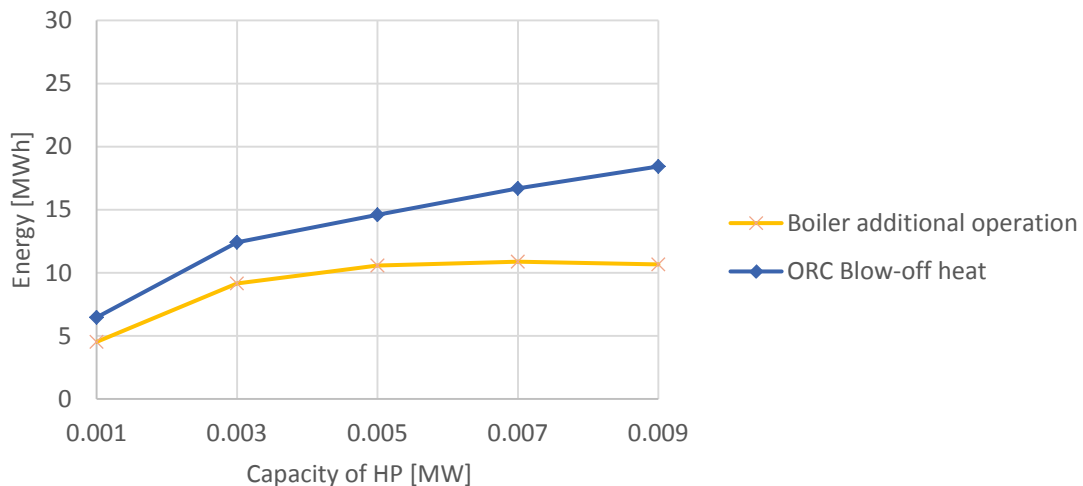


Figure 50: Heat production from the DH boiler and heat blown-off to the environment from the ORC loop.

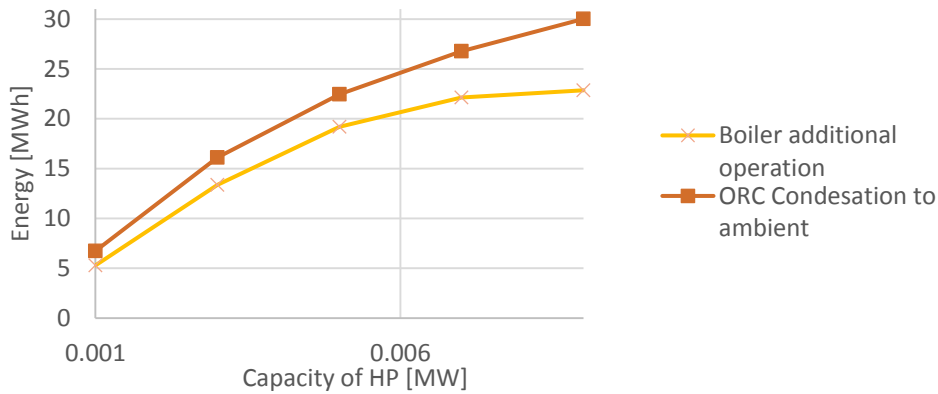


Figure 51: Heat production from the DH boiler and heat dissipated to the environment by the ambient condenser.

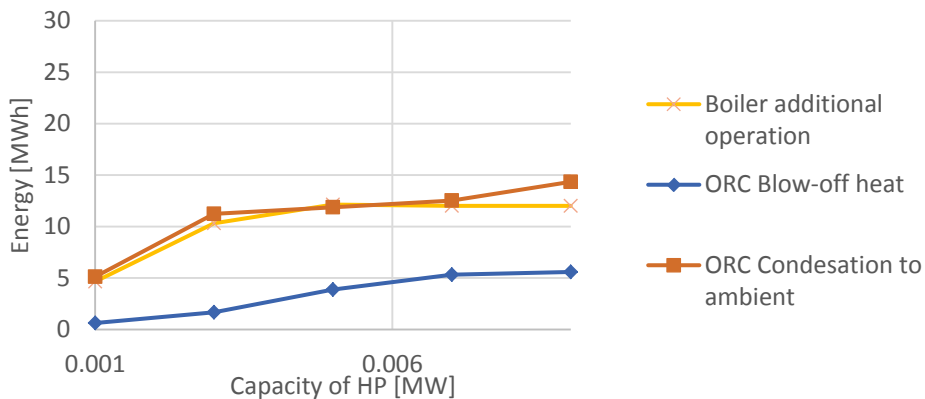


Figure 52: Heat production from the DH boiler, heat blown-off to the environment from the ORC loop and heat dissipated to the environment by the ambient condenser in partial condensation mode.

As in Section 3.1.1, considering the electric efficiency of the CHEST system as the ratio between the electricity production of the ORC and the additional heat output of the boiler compared to the scenario without CHEST. The so-defined efficiency varies for the different HT-HP capacities and the different condensation modes, as shown in Figure 53. This efficiency is highest in the blow-off operation for HT-HP capacities larger than 3 kW, while the ambient-condensation mode gives the best performance in presence of HT-HPs of 3 kW or smaller. These figures are not affected by the ORC relative capacity.

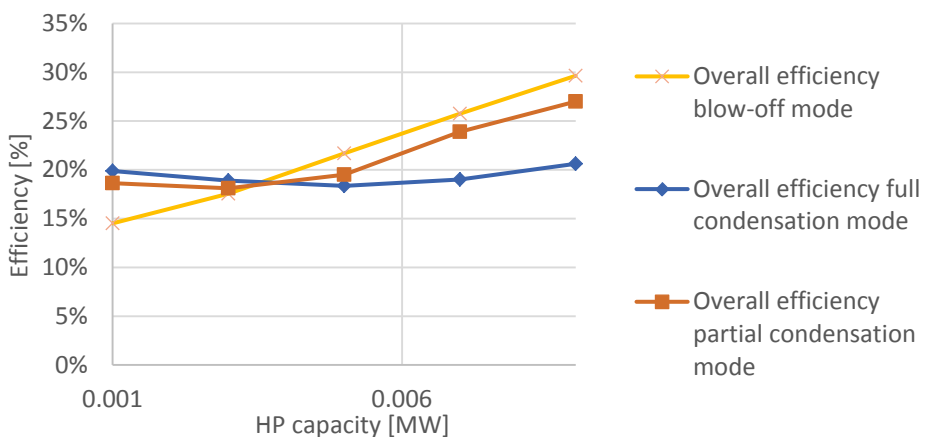


Figure 53: “Electric efficiency” of the CHEST system in three different ORC condensation modes.

In case of the condensation to the ambient air, a certain amount of electricity is required for the operation of the cooling fans. This is not included in the TRNSYS model, hence is not considered in the results shown above. However, in real-world application, this would entail a lower net electricity production from the CHEST system.

The performance of an air-based heat rejection system is estimated based on average seasonal values for the electricity consumption of heat rejection equipment (including fans and pumps), as listed in [Fugmann, 2015]. These values range between 0.018 kW_{el}/kW_{th} for open wet cooling towers and 0.045 kW_{el}/kW_{th} for dry heat rejection systems. Therefore, the electricity consumption of a wet cooling tower as function of the ORC electricity production is expressed by the following relation (6):

$$E_{el.,condenser} = \frac{0.018 E_{el.,ORC} (1 - \eta_{ORC})}{\eta_{ORC}} \quad (6)$$

where $E_{el.,condenser}$ is the electricity consumption of the air-based heat rejection system (in kWh);

$E_{el.,ORC}$ is the electricity production of the ORC (in kWh);

η_{ORC} is the efficiency of the ORC;

0.018 [kW_{el}/kW_{th}] is the performance of the heat rejection system.

As in ambient condensation the efficiency of the ORC is about 13.5 %, the equation above entails that for 1 kWh of electricity produced by the ORC; 0.115 kWh of electricity are consumed by the air-based heat rejection system. Therefore, the net electricity output of the CHEST system (and similarly the net ORC efficiency and the net P2P ratio) is 11.5 % lower compared to the results shown in connection to ambient-condensation.

3.3.3. Case Study #4: Barcelona

In these sets of simulations, the different condensation modes are investigated in order to quantify their impact on the performance of the CHEST system. Two different heat sinks are considered: ambient air and sea water. The difference between the condenser outlet temperature and the ambient temperature is set to 10 K in the case of ambient air and to 5 K in the case of sea water. The results for condensation to ambient air are not shown here, because these are very similar to those for condensation to sea water in terms of the CHEST performance parameters. Due to much more electricity is required by the fans in case of condensation with ambient air (cf. Section 3.3.2), sea water is regarded as the more suitable heat sink for this case study.

To reproduce the different condensation modes, three different settings for the setpoint temperatures $Cond_T_limit_min$ and $Cond_T_limit_max$ are applied. These temperatures are set to 10 °C and 15 °C respectively, when ambient condensation is aimed at. Setpoint temperatures of 50 °C and 55 °C respectively result in partial condensation mode (although as shown below, this setting results in ambient condensation at small HT-HP capacities). Finally, setpoint temperatures of 90 and 95 °C respectively result in blow-off operation. This is blow-off mode (see Section 2.1.1 for the description of the different condensation modes).

Figure 54 and Figure 55 show the electricity absorbed by the HT-HP and produced by the ORC respectively, in the different condensation modes. For the ambient condensation, HT-HP larger

than 10 MW entails no further increase in the electricity absorbed by the HT-HP (therefore no additional ORC electricity production). Due to the high capacity of the HT-HP (and no ORC condensing heat injected back into the LT-TES), the LT-TES is cooled down to 40 °C (the lowest temperature allowed at the inlet of the HT-HP’s evaporator), which very often prevents the further operation of the HT-HP and entails a very low COP (Figure 56). Besides, the ORC efficiency in the case of ambient condensation is higher (because the heat sink temperature is lower) and independent of the HT-HP capacity (because this does not affect the heat sink temperature) (Figure 57).

As seen from Figure 54-Figure 58, in case of HT-HP capacities smaller than 10 MW, all performance parameters are identical for ambient condensation mode and partial condensation. In fact, the small HT-HP does not cool the LT-TES as described above for the larger HT-HPs. Therefore, the partial condensation entails in practice ambient condensation, because the temperatures at the bottom the LT-TES are never lower than 55 °C (*Cond_T_limit_max*). Moreover, for HT-HP capacities equal to or larger than 10 MW, the partial condensation modes avoids the limitation of the HT-HP operation by transferring the ORC condensing heat back into the LT-TES. Thus, the amounts of electricity absorbed by the HT-HP and produced by the ORC increases with increasing HT-HP capacity. The COP is also higher, because of higher temperatures of the LT-TES. As the temperatures in the LT-TES are highest in blow-off mode, the COP and the amounts of electricity absorbed by the HT-HP and produced by the ORC are even higher in this mode.

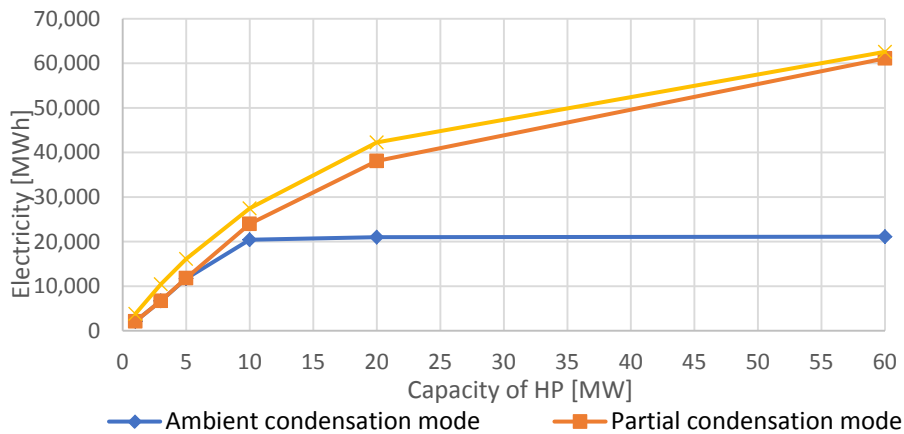


Figure 54: Electricity absorbed by the HT-HP as a function of the HT-HP capacity for a HT-TES of 12 h, an ORC relative capacity of 0.50 and different condensation modes.

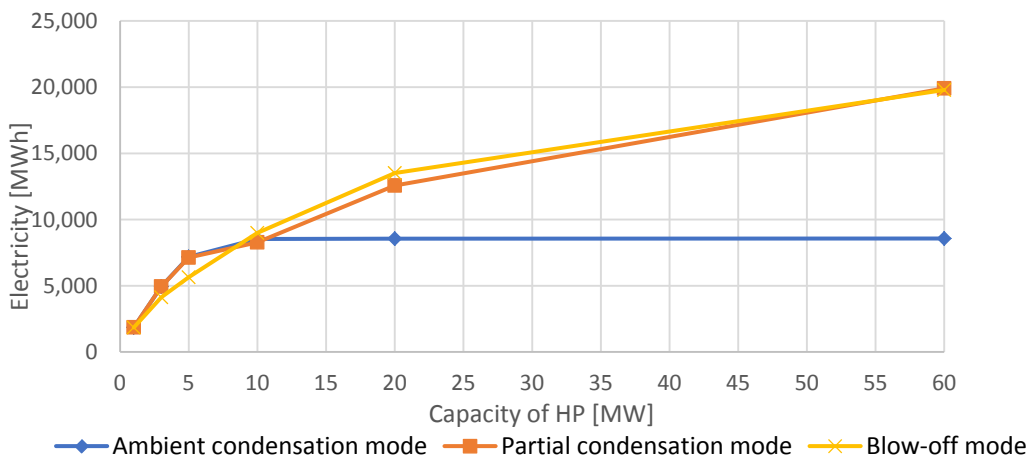


Figure 55: Electricity produced by the ORC as a function of the HT-HP capacity for a HT-TES of 12 h, an ORC relative capacity of 0.50 and different condensation modes.

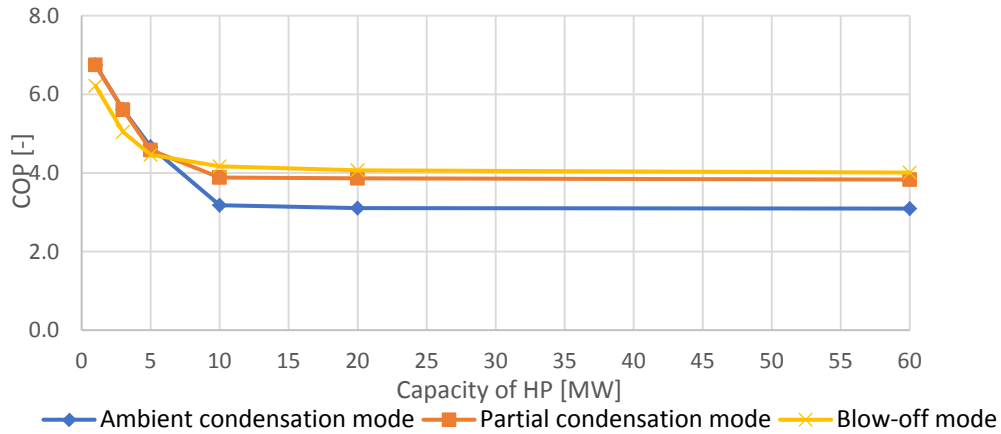


Figure 56: COP of the HT-HP as a function of the HT-HP capacity for a HT-TES of 12 h, an ORC relative capacity of 0.50 and different condensation modes.

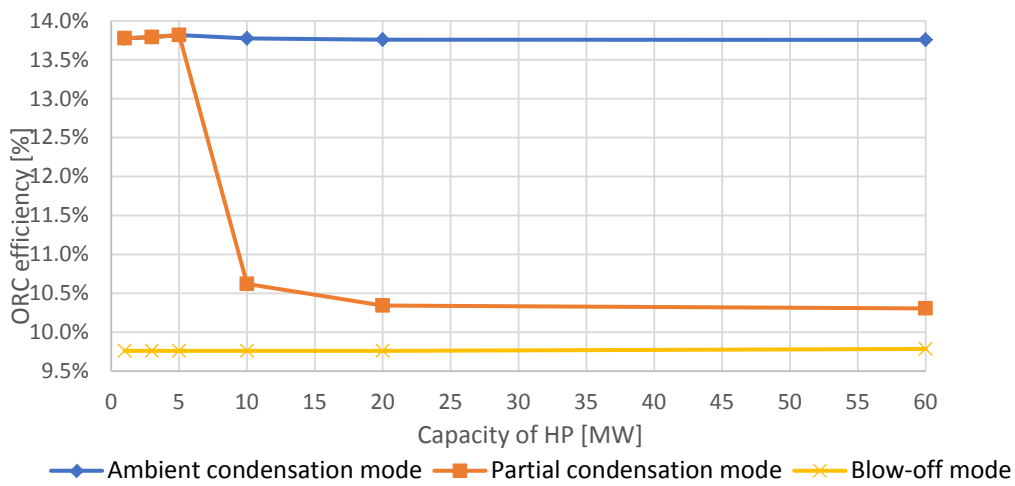


Figure 57: ORC efficiency as a function of the HT-HP capacity for a HT-TES of 12 h, an ORC relative capacity of 0.50 and different condensation modes.

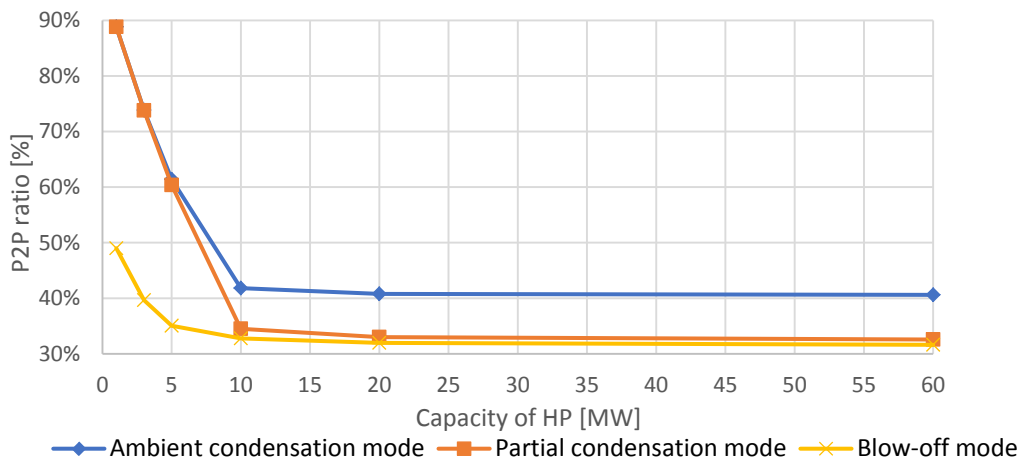


Figure 58: P2P ratio as a function of the HT-HP capacity for a HT-TES of 12 h, an ORC relative capacity of 0.50 and different condensation modes.

The energy output of the boiler is shown in Figure 59. For HT-HP capacities of 5 MW or larger, the entire DH heat demand of 29 GWh is delivered by the boiler. For HT-HPs smaller than 5 MW, the heat production from the boiler is higher for the blow-off mode compared to ambient condensation mode.

The “electric efficiency”, as defined in Section 3.3.2, is shown in Figure 60. Because the ORC electricity production does not increase for HT-HP larger than 10 MW, the electric efficiency is lowest for the ambient condensation mode for this range of HT-HP capacity. However, for HT-HP capacities lower than this value, the electric efficiency is higher compared to the blow-off operation mode.

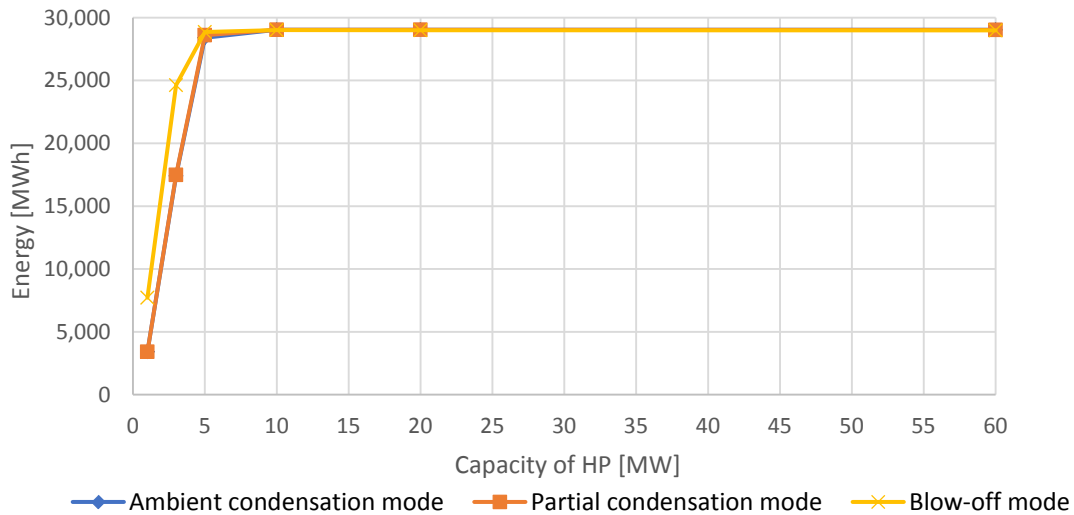


Figure 59: Boiler output as a function of the HT-HP capacity for a HT-TES of 12 h, an ORC relative capacity of 0.50 and different condensation modes.

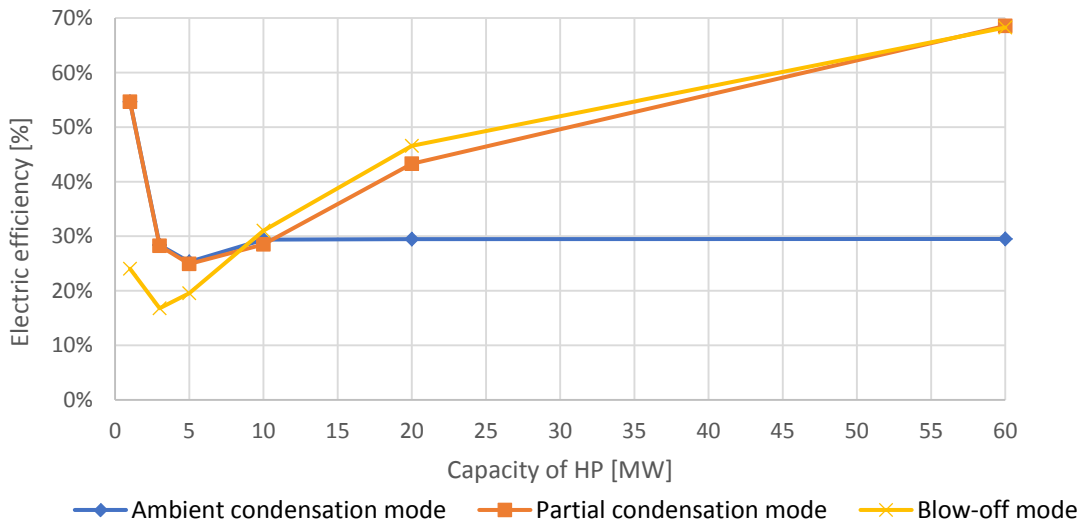


Figure 60: “Electric efficiency” as a function of the HT-HP capacity for a HT-TES of 12 h, an ORC relative capacity of 0.50 and different condensation modes.

As a conclusion of these results, partial condensation is found to be a better option than ambient condensation for HT-HP capacities larger than 10 MW. For HT-HP capacities smaller than 10 MW, ambient condensation shows considerably improved performance parameters compared to blow-off operation.

3.3.4. General discussion

From the perspective of the overall system, the DH+CHEST system reaches a higher energy performance, when as little energy as possible is dissipated to the environment. Therefore, the ORC should condense to the DH network (i.e. to the LT-TES) as much as possible. However, given the constraint of the maximum temperature which can be accepted at the inlet of the ORC (50 °C according to the performance maps, see CHESTER deliverable D2.2), it may not be possible for the ORC to condense directly into the DH network, but some heat may have to be preliminary blown off from the flow supplying the ORC condenser, so to decrease its temperature to at least 50 °C. According to the performance maps, the temperature of the cooling water at the outlet of the ORC's condenser is 60 °C, when the inlet temperature is 50 °C. Therefore, the blow-off operation mode is disadvantageous with respect to the ambient-condensation mode, if the temperature at the bottom of the LT-TES is higher than 60 °C. In this case in fact, the amount of blown-off heat is higher than the condensation heat, so that allowing the ORC to condense to the LT-TES will (in net terms) remove heat from LT-TES instead of adding it. Additionally, the high condensing temperature entails a lower ORC efficiency compared to the efficiency which could be achieved, if ambient-condensation was used.

From a purely energy point of view, the most efficient condensation mode is found to be the partial condensation, having setpoint temperatures *Cond_T_limit_min* and *Cond_T_limit_max* properly set close to the maximum temperature allowed at the inlet of the ORC's condenser (currently 50 °C). For example, a *Cond_T_limit_min* equal to 50 °C would ensure that no heat is blown-off, when this can be avoided. The value of *Cond_T_limit_max* should be a bit higher than *Cond_T_limit_min* (although *Cond_T_limit_min* = *Cond_T_limit_max* is also possible). The temperature difference between the two setpoints depends on how rapidly the transition between ambient condensation and blow-off operation should occur. In any case, using the performance maps from the CHESTER deliverable D2.2, *Cond_T_limit_max* should not be higher than 60 °C, as this would likely entail a net subtraction of heat from the LT-TES, even when the ORC partially condenses to the LT-TES.

In order to reduce the heat dissipated to the environment from the ORC loop, the ORC should condense at a higher temperature (nominally the DH return temperature) or alternatively the DH return temperature should be lowered to the highest condensing temperature of the ORC. There are organic fluids (e.g. cyclopentane, acetone) that could increase the ORC condensing temperature, however, their use would require significant changes in the composition of the CHEST system.

Another aspect which should be kept in mind is the electricity consumption of the ambient condenser, which is neglected in the presented calculations. While this may represent a small amount (therefore could be neglected) in case of condensation with river or sea water, it is more relevant in case of condensation with ambient air, due to the high electricity consumption of the fans. Based on a simple calculation method, it is estimated that, in case of pure ambient condensation, the electricity consumption of a wet cooling tower represents about 11 % of the electricity production of the ORC.

3.4. Working fluid: R1233zd(E) against Butene

In the CHESTER Deliverable D2.2, a comparison between the two working fluids butene and R1233zd(E) showed that R1233zd(E) had slightly better performance, due to the higher ORC efficiency. Conversely, the COP of the HT-HP was slightly better when butene was used.

Due to these preceding investigations it was decided to analyse the influence of the working fluid in the updated TRNSYS model, but only for the case study of Barcelona. Simulations have been carried out with HT-HP capacities of 1 MW and 10 MW and HT-TES sizes of 6 h and 12 h, while varying the ORC relative capacity between 0.20 and 0.50. In case of butene, a latent-to-sensible ratio of the HT-TES equal to 0.74 has been used for sizing the HT-TES, while for R1233zd(E) a ratio of 1.14 has been used.

Figure 58 and Figure 59 show the electricity absorbed by the HT-HP and the electricity produced by the ORC for the 1 MW HT-HP respectively. Both the electricity consumption and the electricity production ORC are slightly for R1233zd(E). In the case of a HT-HP capacity of 10 MW, however, there is almost no difference between the two working fluids.

The differences between the two fluids are more evident in the diagrams of the COP and of the ORC efficiency (Figure 60 and Figure 61 respectively). Butene gives a higher COP, whereas R1233zd(E) gives a higher ORC efficiency, as expected from the results of the deliverable D2.2. The ORC efficiency is independent of the ORC relative capacity and also of the HT-TES size for the 1 MW HT-HP, because there is always ambient condensation.

Regarding the P2P ratio (Figure 62), butene is found to be the better working fluid here. This result is different from the results presented in the CHESTER deliverable D2.2 where, the P2P ratio was found to be higher for R1233zd(E).

However, the results for the 10 MW HT-HP are different to that (Figure 66, Figure 67 and Figure 68).

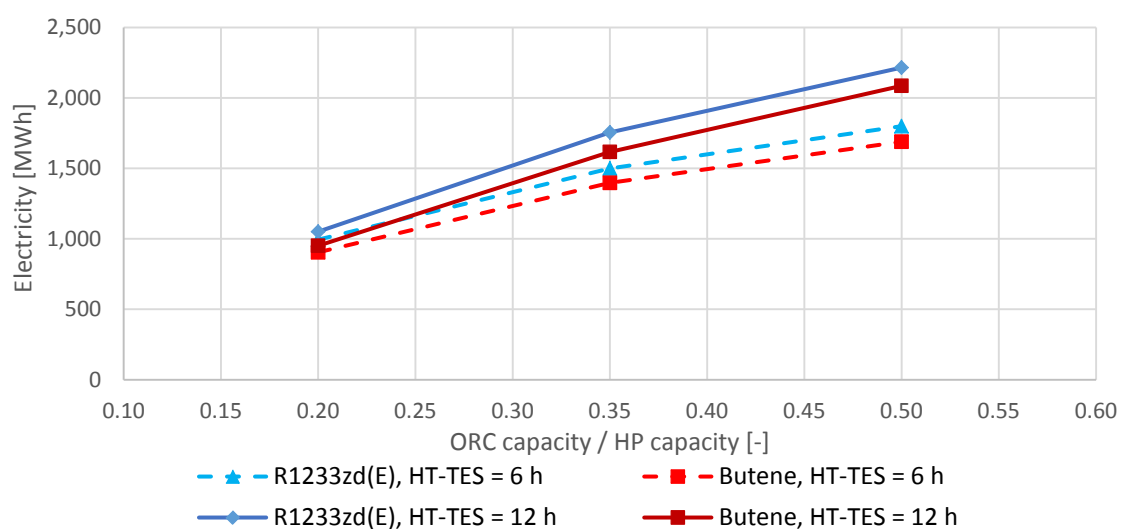


Figure 61: Electricity absorbed by the HT-HP as a function of the ORC relative capacity for different working fluids, a HT-HP capacity of 1 MW, HT-TES sizes of 6 and 12 h.

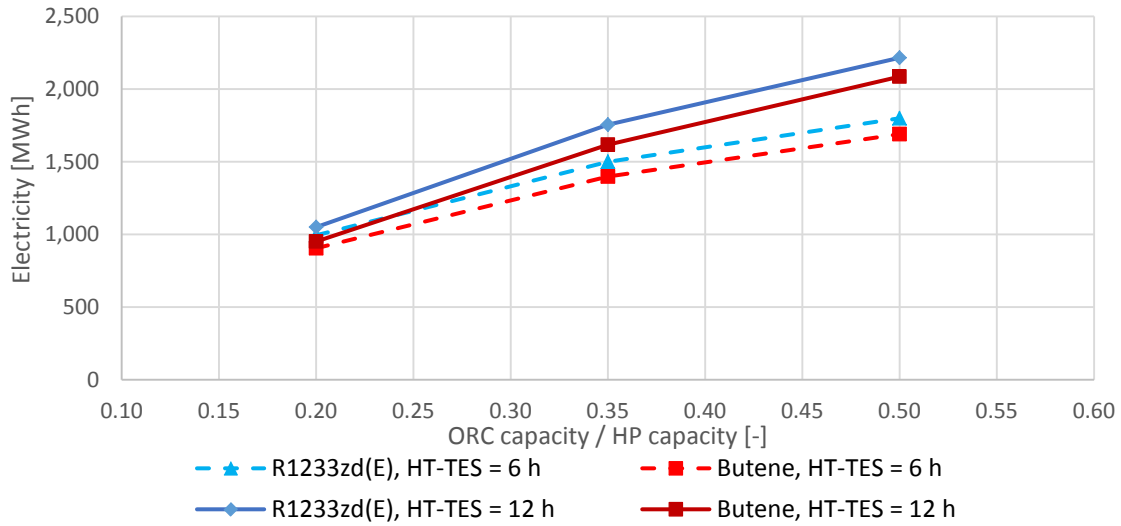


Figure 62: Electricity produced by the ORC as a function of the ORC relative capacity for different working fluids, a HT-HP capacity of 1 MW, HT-TES sizes of 6 and 12 h.

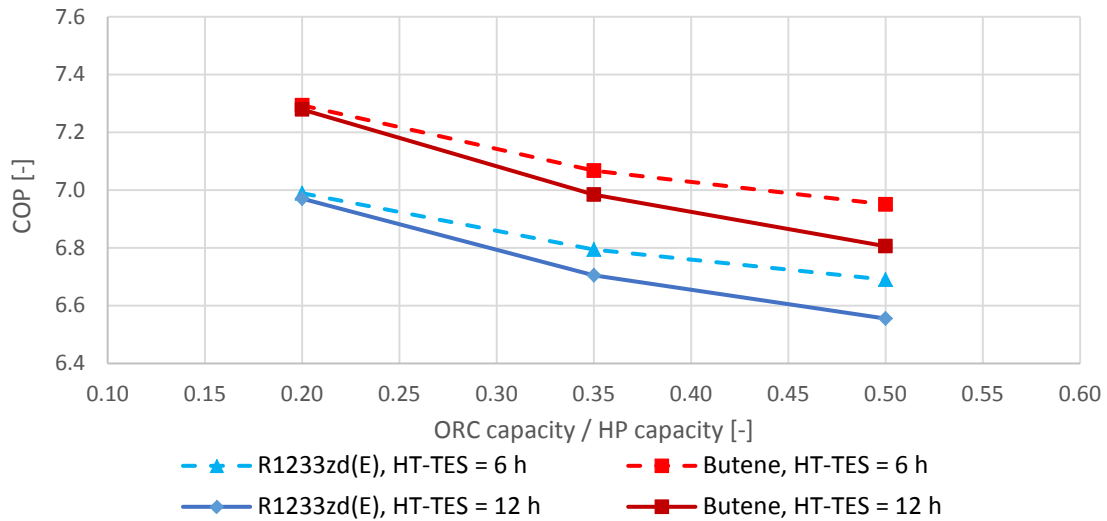


Figure 63: COP of the HT-HP as a function of the ORC relative capacity for different working fluids, a HT-HP capacity of 1 MW, HT-TES sizes of 6 and 12 h.

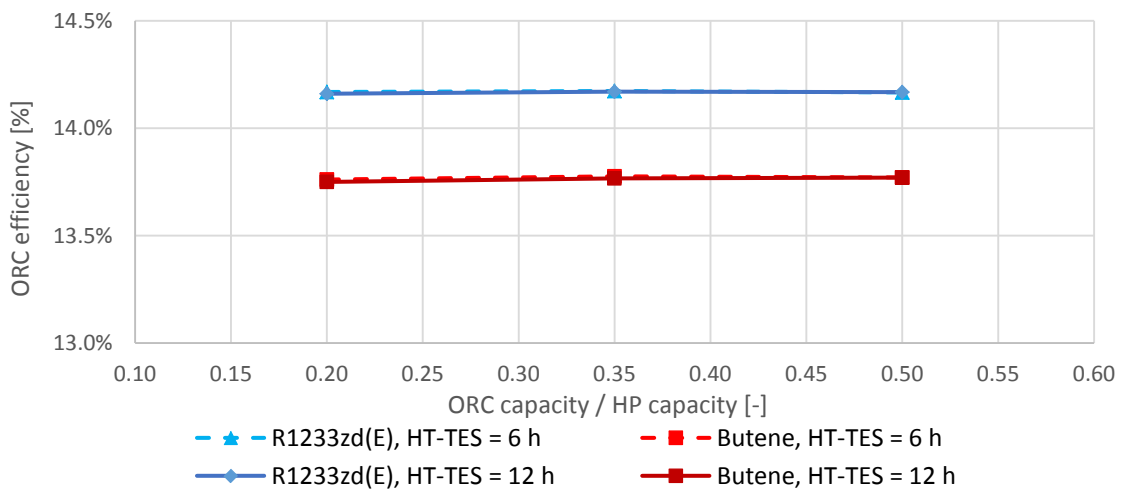


Figure 64: ORC efficiency as a function of the ORC relative capacity for different working fluids, a HT-HP capacity of 1 MW, HT-TES sizes of 6 and 12 h.

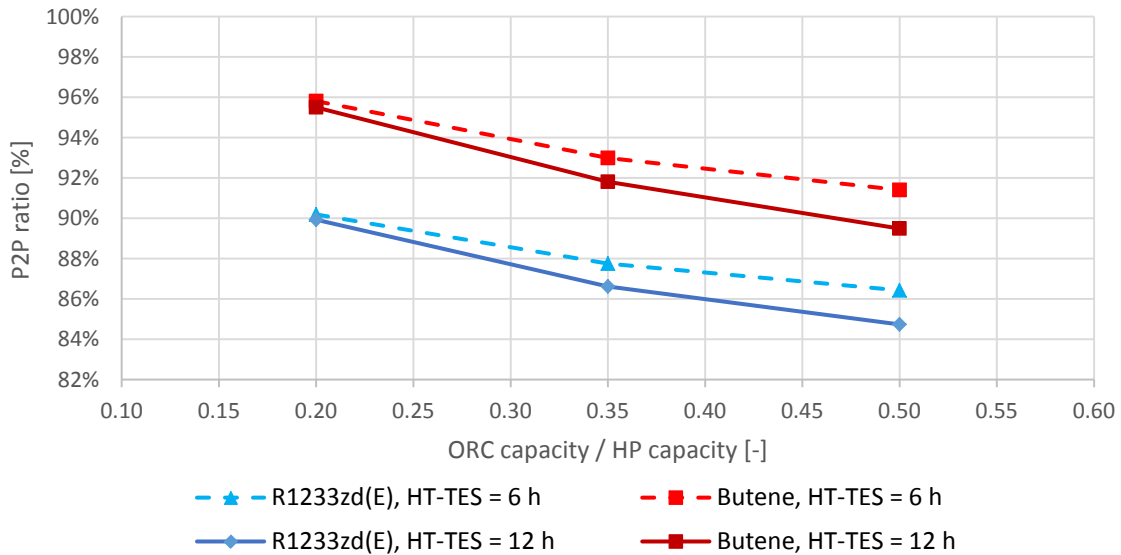


Figure 65: P2P ratio as a function of the ORC relative capacity for different working fluids, a HT-HP capacity of 1 MW, HT-TES sizes of 6 and 12 h.

For the 10 MW HT-HP, partial condensation occurs. Therefore, the ORC efficiency depends on the ORC (relative) capacity. As some of the heat from the condenser of the ORC is injected to the LT-TES, this also affects the COP of the HT-HP. Also, in this case, butene entails a better performance of the HT-HP, while R1233zd(E) gives a better performance of the ORC. However, in this case the P2P ratio is higher for R1233zd(E) as was found in CHESTER deliverable D2.2.

Obviously, butene is always the better working fluid for the HT-HP, while R1233zd(E) is always the better working fluid of the ORC, but regarding the P2P ratio, either fluid can be better, depending on the condensation mode.

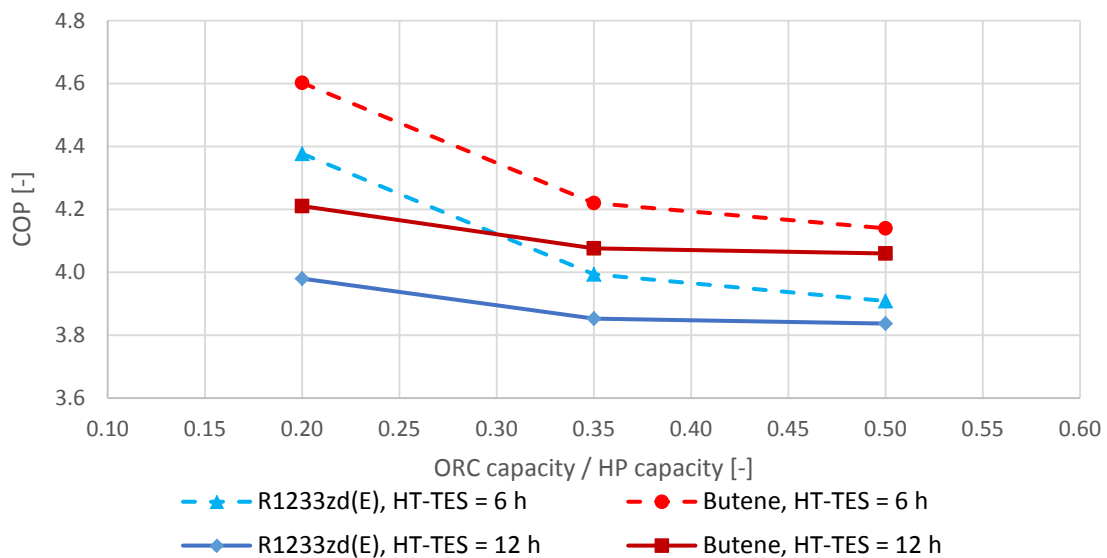


Figure 66: COP of the HT-HP as a function of the ORC relative capacity for 2 different working fluids, a HT-HP capacity of 1 MW, HT-TES sizes of 6 and 12 h.

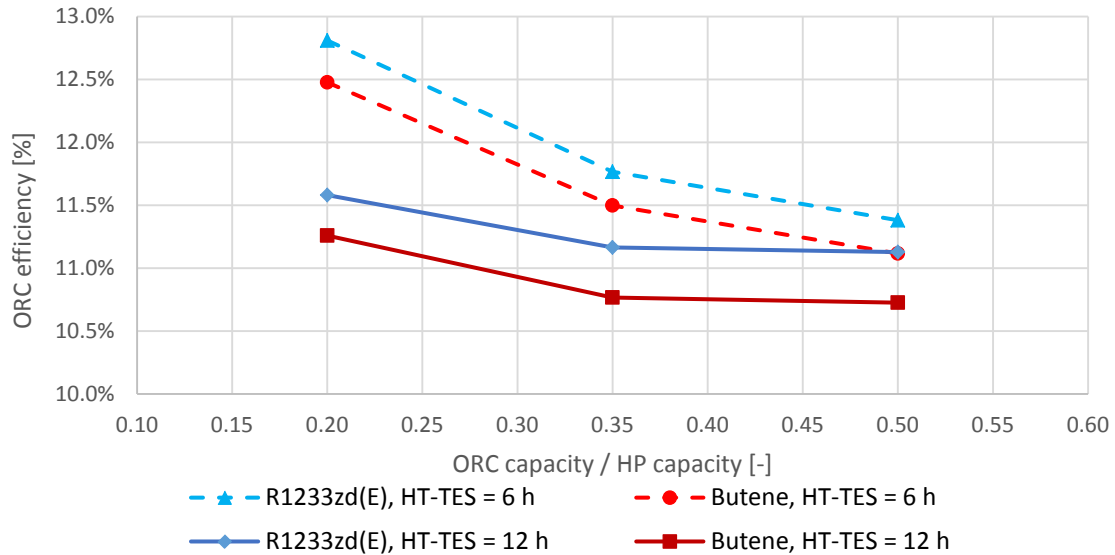


Figure 67: ORC efficiency as a function of the ORC relative capacity for 2 different working fluids, a HT-HP capacity of 1 MW, HT-TES sizes of 6 and 12 h.

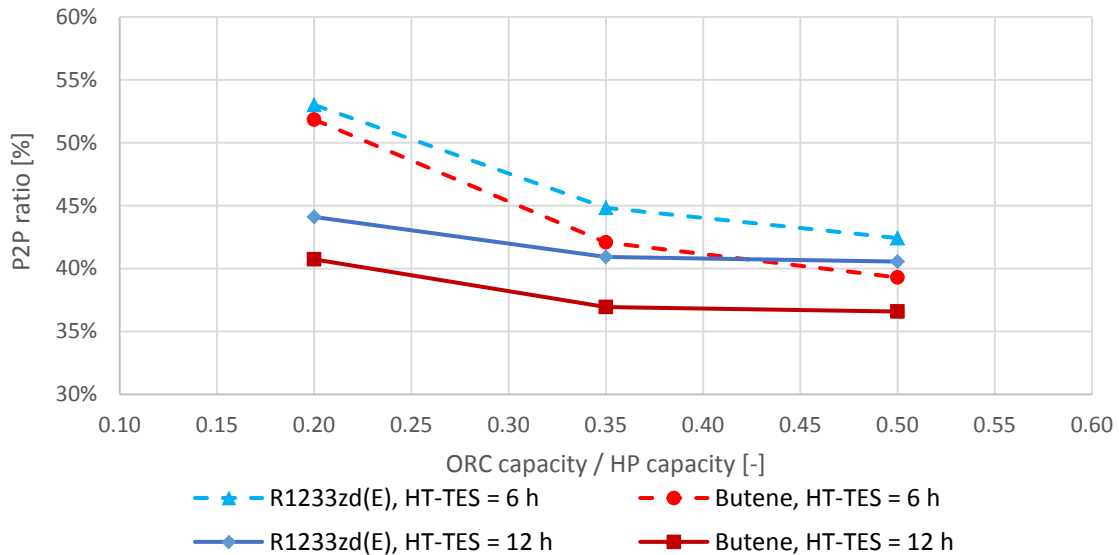


Figure 68: P2P ratio as a function of the ORC relative capacity for 2 different working fluids, a HT-HP capacity of 1 MW, HT-TES sizes of 6 and 12 h.

The fact that butene is advantageous for the HT-HP process and R1233zd(E) is advantageous for the ORC process could lead to the assumption that it would be the best to use butene for the HT-HP and R1233zd(E) for the ORC in the same CHEST system. However, this would not improve the overall performance of the CHEST system, because of the difference between the two thermodynamic cycles.

As seen from the performance maps of the HT-HP and of the ORC for the two working fluids (see CHESTER deliverable D2.2), the ratio between the exchanged latent-to-sensible heat for the two fluids is very different. When butene is used for the HT-HP, this ratio is about 0.74, nearly regardless of the heat source temperature. If R1233zd(E) is used for the ORC, the latent-to-sensible ratio would be in the range of 0.89-1.38, depending on the heat sink temperature (against a range of 0.74-1.11, in case Butene was used). So, a CHEST system using this combination of working fluids would see the HT-TES being charged with a latent-to-sensible

ratio always much lower than that at which it is discharged. This causes different state of charges of the latent and sensible part of the HT-TES, and the clean-up strategy would remove high-temperature excess energy from either part of the HT-TES and mix it with the lower-temperature heat-source heat. Similar considerations apply when inverting the use of the two fluids, with R1233zd(E) having a latent-to-sensible ratios of 1.14-1.18 when used in the HT-HP, while butene has ratios between 0.74 and 1.11 when used in the ORC (against a range of 0.89-1.38, in case R1233zd(E) was used). Hence, it is important that the latent-to-sensible ratios in charging and discharging mode are as close as possible to limit the operation of the clean-up procedure.

3.5. RES electricity production and electricity demand

3.5.1. Case Study #1: Turin

The electricity unbalance of the 3GT plant in Turin is mainly due to control problems, for which the gas turbine cannot be regulated to meet exactly the commitment. This causes differences between the actual electricity production and the expected one, the majority of which happens at low power (Figure 3). The current control of the gas turbine is more likely to improve over the time rather than get worse. Therefore, in this section, it is assumed that improved control allows to reduce the deviations between production and commitment (both positive and negative) by 50 %. The impact on the size and performance of the CHEST system is analysed.

Table 7: General parameters for Turin case (on an annual basis).

Scaling factor of the electricity unbalances	Energy [MWh]	
	1.0	0.5
GT3 electricity production	1.74E+06	1.74E+06
GT3 committed production	1.74E+06	1.74E+06
DH heat demand	2.31E+06	2.31E+06
Electricity surplus	1.51E+04	7.56E+03
Electricity deficit	2.04E+04	1.02E+04
RES electricity directly used	1.72E+06	8.61E+05

Figure 69 shows that the behaviour of the curves of the electricity absorbed by the HT-HP are similar to those in Figure 31, and that the values follow the same reduction as the scale factor of 0.5. In this way, the model underlines a certain proportionality between the scale factor and the results. The analysis of the performance of the HT-HP and ORC (respectively, COP and efficiency) shows that the scale factor does not affect these parameters. Therefore, in terms of efficiencies, the performance of the CHEST system is not influenced by the improved control of the gas turbine. Moreover, the absolute amount of exchanged energy and powers (by the HT-HP and ORC) varies proportionally to the scaling factor, so that also the CHEST components could downscale accordingly.

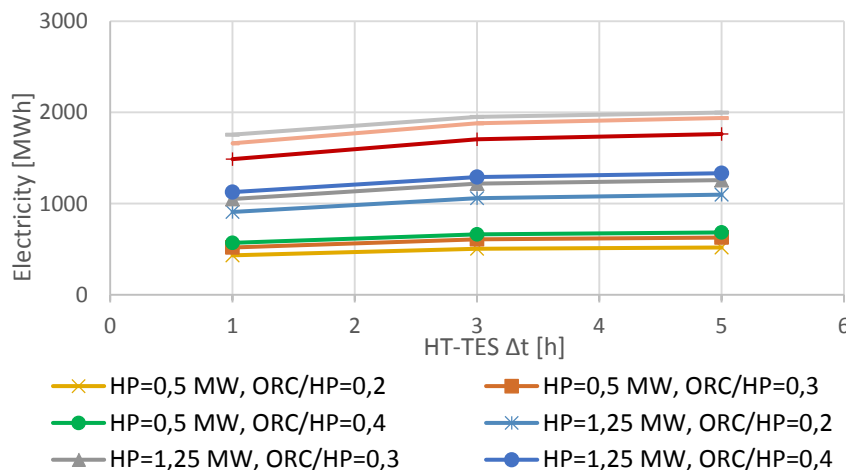


Figure 69: Electricity absorbed by the HT-HP as function of the HT-TES capacity.

3.5.2. Case Study #3: Ispaster

According to the energy strategy and development plans of the municipality (see CHESTER deliverable D2.1), both the local electricity microgrid and the DH systems are expected to be extended in the future. More local households would be connected to the DH system, while the municipality encourages the installation of individual solar installations among the new and the existing customers. The current PV array is expected to be increased by 3.3 kW_p, but this is meant mainly to cover the demand of the DH central plant (pumps, etc.).

The results presented in the previous sections show that the performance of the CHEST system is limited by the low availability of RES heat. Thus, a few scenarios with increased solar collector area are investigated, while the PV capacity is kept constant (25 kW_p).

Three groups of scenarios are investigated: one having the original solar collector area of 54 m² (referred to in the diagrams as S=100 %), a second one with a collector area of 108 m² (S=200 %) and a third one with a collector area of 162 m² (S=300 %). In each group of scenarios, three sizes of HT-HP are assumed (1 kW, 9 kW and 15 kW) and for each HT-HP capacity, the ORC relative capacity is varied between 0.10 and 0.25. The HT-TES is sized on a 12 h storage time in all cases. The values of COP_{ref} used to size the HT-TES are iterated for each combination of solar collector area and HT-HP capacity, until convergence between the values of the COP_{ref} and the actual yearly-averaged COP is reached (Figure 70). Blow-off operation is selected as ORC condensation mode.

The increase of RES heat production increases the COP of the HT-HP (Figure 70), due to the higher temperature at the top of the LT-TES. As explained in Section 3.1.4, the COP decreases for larger HT-HPs, while it is largely unaffected by the size of the ORC.

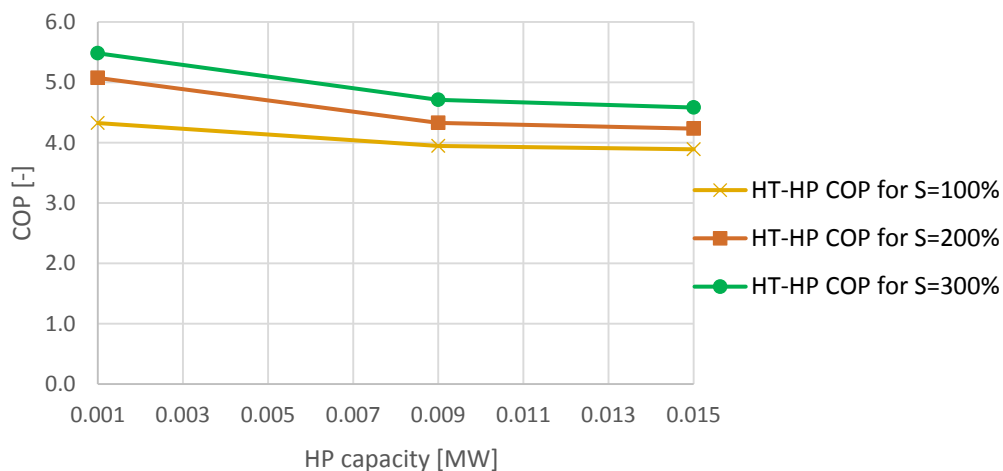


Figure 70: COP of the HT-HP for the different HT-HP capacities in for a solar collector area of 54 m² (S=100%), 108 m² (S=200%) and 162 m² (S=300%), and ORC relative capacity of 0.15.

The higher COP results in a larger amount of heat transferred to the HT-TES, which increases the ORC production (Figure 71). However, the ORC does not increase proportionally to the HT-HP's COP in all cases as might be expected. In case of the 1 kW HT-HP, especially when coupled with the ORC with relative capacity of 0.10, the impact of the improved COP has a minor effect on the ORC electricity production. In fact, a small ORC could not properly discharge the HT-TES: this results in the fact that, for the HT-HP of 1 kW (and for that of 9 kW), the electricity production decreases when moving from an ORC with relative capacity of 0.15 to 0.10. Even in

case of a large enough ORC (relative capacity of 0.25), the electricity production does not increase proportionally to the COP in case of the 1 kW HT-HP. The reason for this is that the HT-TES is sized assuming a COP_{ref} equal to the yearly-averaged COP of the HT-HP. Especially in summer when both the solar thermal production and the electricity surplus are highest, it can happen that the HT-HP operates for more consecutive hours and with a COP higher than COP_{ref} . Therefore, the HT-TES may get fully charged faster than the 12 hours expected, so interrupting the HT-HP operation. In fact, other simulations performed using a higher COP_{ref} ($COP_{ref} = 6$) (whose results are not reported here) show that the increase in the ORC electricity production is roughly proportional to the increase in the average COP.

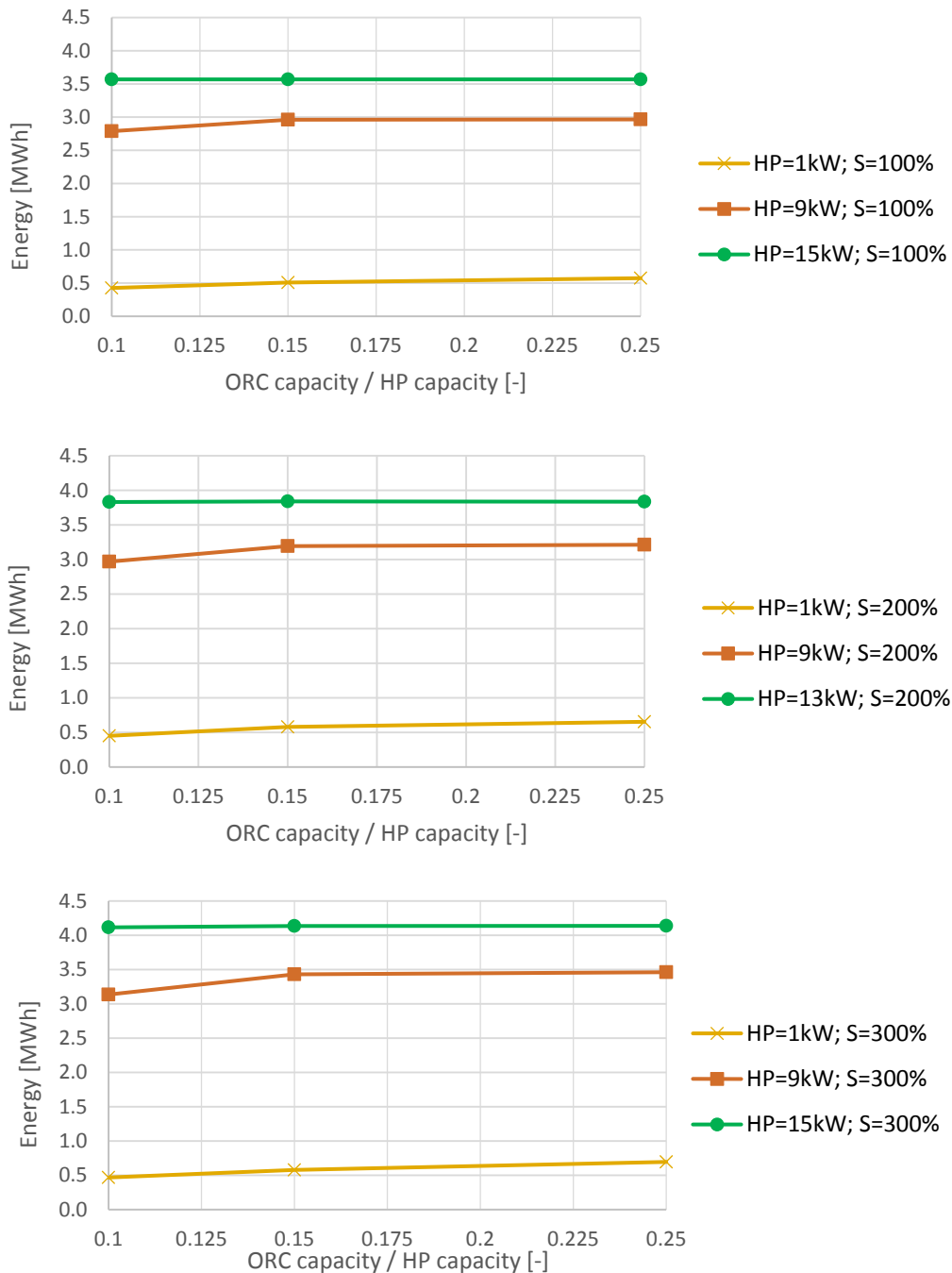


Figure 71: Electricity output from the ORC as function of the ORC relative capacity for the different HT-HP capacities for a solar collector area of 54 m² (S=100%, top graph), 108 m² (S=200%, middle graph) and 162 m² (S=300%, bottom graph).

The efficiency of the ORC is constant for all relative ORC (9.7 %) which reflects its performance in a blow-off operation investigated in Section 3.3.2.

Due to increased capacity of solar collectors and despite the operation of the CHEST system, the annual heat output from the DH boiler is lower than in the reference scenario without CHEST (57 MWh) (Figure 72).

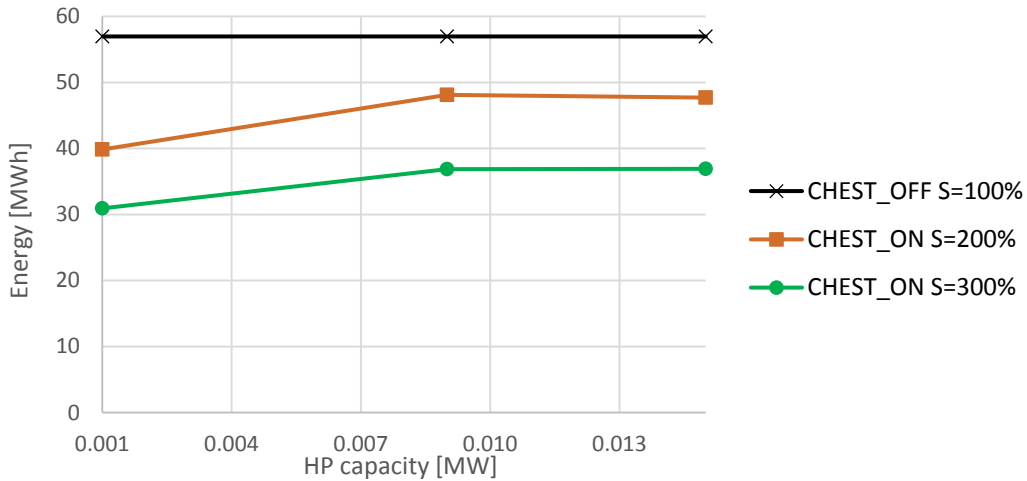


Figure 72: Annual heat production from the DH boiler as a function of the HT-HP capacity in the reference case (no CHEST and solar collector area of 54 m², S=100%), and for a solar collector area of 108 m² (S=200%) and 162 m² (S=300%) with the CHEST system in operation.

3.5.3. Case Study #4: Barcelona

The results presented in this section are obtained varying the scaling factor for the RES electricity production to 0.01, 0.02 and 0.03, while the scaling factor of the energy demand is kept constant at 0.02. Doing so, the ratio between the RES electricity production and the electricity demand is 0.47, 0.94 and 1.41 respectively. Simulations are carried out with HT-HP capacities of 1 MW and 10 MW, and a HT-TES of 12 h, while varying the ORC relative capacity between 0.25 and 0.50.

Figure 73 and Figure 74 show the amount of electricity absorbed by the HT-HP and the electricity produced by the ORC respectively.

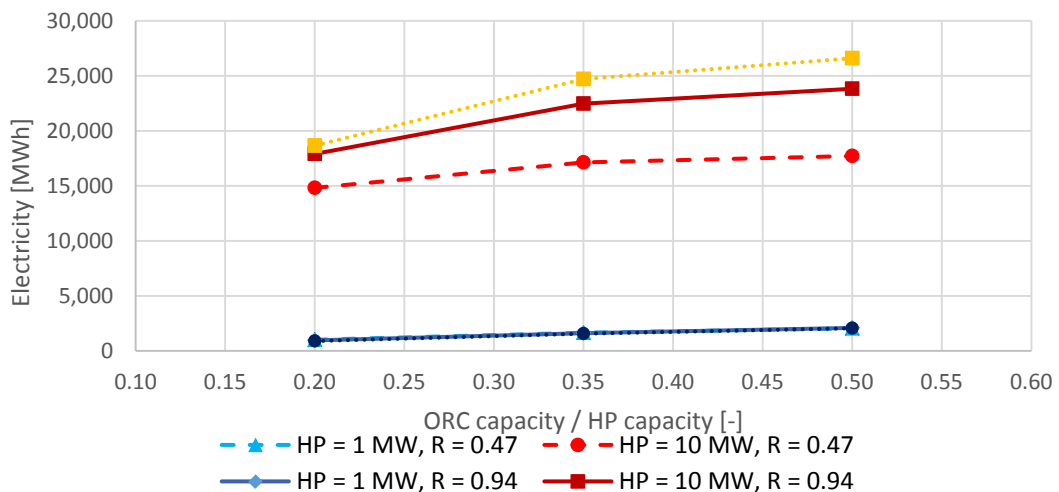


Figure 73: Electricity absorbed by the HT-HP as a function of the ORC relative capacity for different HT-HP capacities, a HT-TES of 12 h and 3 different ratios R of RES electricity production to electricity demand.

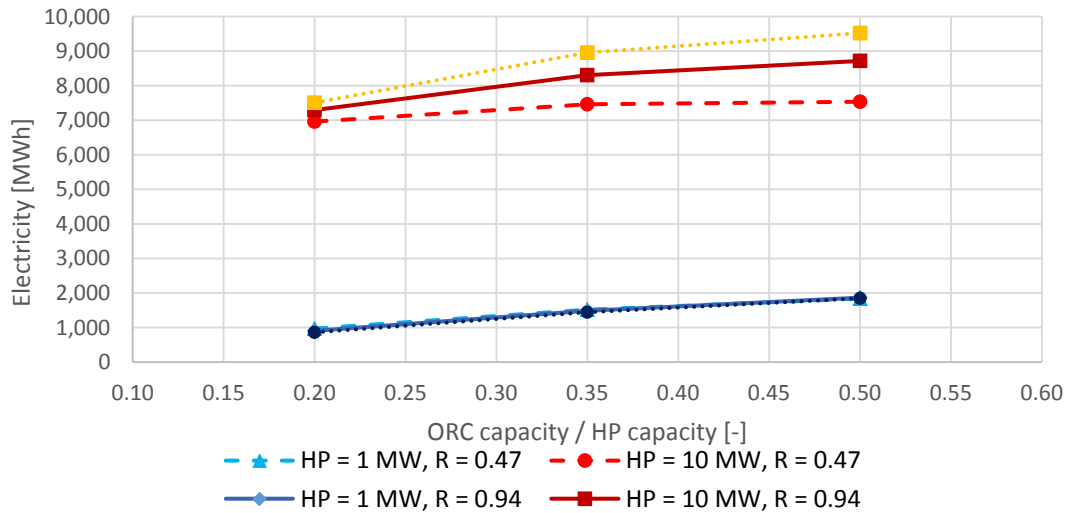


Figure 74: Electricity produced by the ORC as a function of the ORC relative capacity for different HT-HP capacities, a HT-TES of 12 h and 3 different ratios R of RES electricity production to electricity demand.

The two figures show that both the electricity absorbed by the heat pump and the electricity produced by the ORC increase with increasing ratio of RES electricity production to electricity demand for the 10 MW HT-HP. For the 1 MW HT-HP, the amounts of electricity are found to be independent of the ratio of RES electricity production to electricity demand. For the 1 MW HT-HP, this result is expected, because already in the reference scenario most of the electricity surplus is at power higher than 1 MW anyway, as seen from Figure 26.

Figure 75 shows how the COP decreases slightly at larger amount of RES electricity for the 10 MW HT-HP. This is due to the fact that higher RES electricity availabilities lead to higher amounts of electricity absorbed by the HT-HP (Figure 73), therefore to a larger amount of heat drawn from the LT-TES by the HT-HP. This leads to lower temperatures at the inlet of the HT-HP’s evaporator. For the 1 MW HT-HP, again no effect is visible.

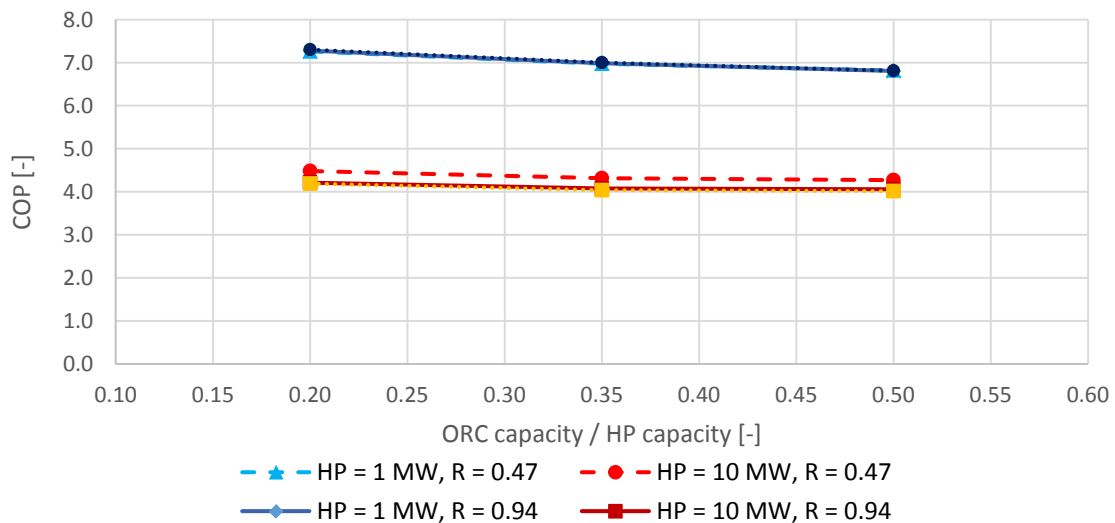


Figure 75: COP of the HT-HP as a function of the ORC relative capacity for different HT-HP capacities, a HT-TES of 12 h and 3 different ratios R of RES electricity production to electricity demand.

For the same reason the ORC efficiency (Figure 76) as well as the P2P ratio (not shown here) are independent of the ratio of RES electricity production to electricity demand for the HT-HP capacity of 1MW. For the HT-HP capacity of 10 MW the ORC efficiency is highest for the ratio $R = 0.47$ but does not show differences between the two higher ratios of 0.94 and 1.41. The diagram for the P2P ratio has the same appearance as the one for the ORC efficiency, therefore is not shown here.

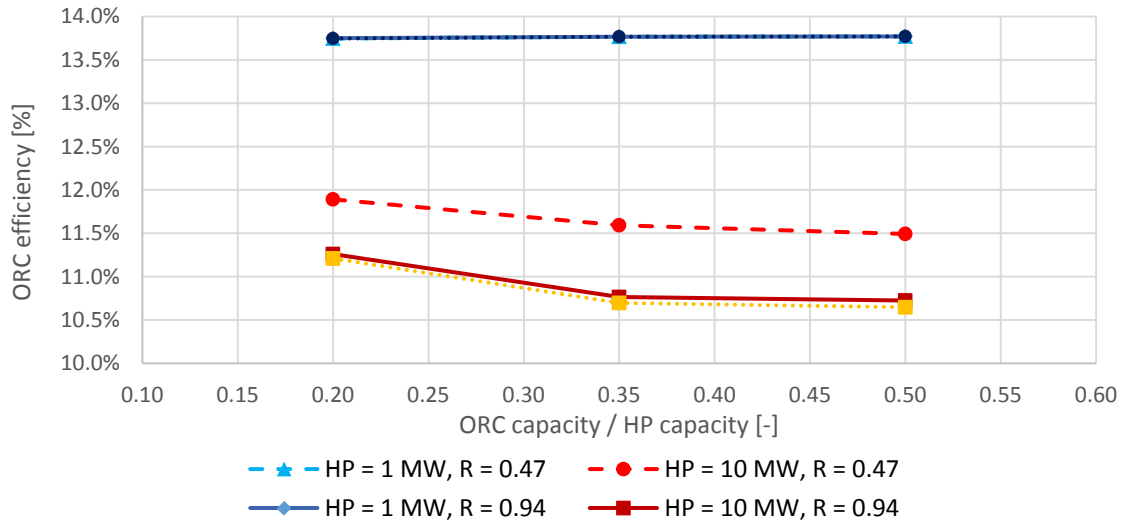


Figure 76: ORC efficiency as a function of the ORC relative capacity for different HT-HP capacities, a HT- TES of 12 h and 3 different ratios R of RES electricity production to electricity demand.

4. Conclusions

4.1.1. Case Study #1: Turin

Given the distribution of the energy unbalances, small HT-HP's capacities are better suited in the Turin case study. A HT-HP's capacity of 2.5 MW can be considered the right trade-off. This choice is characterized by a high COP (4.63), high number of full-load hours of the HT-HP and so the amount of heat produced and available for the ORC device.

As far as the ORC cycle, ORC relative capacities of 0.3 is found to be the best compromise between the number of full-load hours of ORC's operation and annual electricity production. While, regarding the HT-TES, a storage time period of 5 hours is suitable for the above-mentioned HT-HP and ORC sizes

Assuming a HT-HP capacity of 2.5 MW, an ORC relative capacity of 0.3 (i.e. ORC's capacity of 0.75 MW) and a HT-TES of 5 hours, the HT-HP absorbs about 2500 MWh of electricity surplus (about 1000 full-load hours), while the ORC produces about 1650 MWh (about 2200 full-load hours), resulting in a P2P ratio of around 65%. Besides, the heat output from the DH plant is 9900 MWh higher compared to the reference scenario without CHEST.

Given the very high temperature of the DH network, it is not reasonable to allow for the ORC condensation to the DH network. Therefore, only condensation to the environment (Po river) is considered.

In the case of a reduction of the electrical unbalances due to a better control of the GT3 plant, it is found that HT-HP and the ORC of the CHEST system could be proportionally scaled, achieving very basically the same performance (COP, ORC efficiency, P2P ratio) as in the original scenarios (without scaling).

4.1.2. Case Study #3: Ispaster

Based on the existing electricity surplus given by the local PV electricity production, the maximum size of the HT-HP could be 23 kW. Due to the limited number of hours where the power of the electricity surplus is high (>10 kW) and the limited amount of RES heat available (from the solar thermal collectors), HT-HPs larger than 9 kW would not be efficient, as they would draw heat from LT-TES at progressively lower temperature, decreasing their COP. Additionally, the increase in electricity output when moving from a 9 kW HT-HP to a 13 kW HT-HP (+44 % in installed capacity) is relatively just 11 %, compared to a nearly 30 % increase when shifting from a 5 kW HT-HP to a 7 kW HT-HP (+40 % capacity).

Although the maximum power of the electricity deficit is 13 kW, an ORC sized on this power would be strongly underused. Based on the sizing of the HT-HP and on the performance maps of the components, it is found that an ORC having a relative capacity of 0.25 would be enough.

The most efficient HT-TES storage is sized at 12 h as any further increase of the HT-TES does not improve the performance of the system.

The most efficient operation of the HT-HP is observed for the smallest unit of 1 kW. Moreover, in terms of absolute amount of produced electricity, the largest investigated HT-HP of 9 kW (and an ORC relative capacity of 0.25) gives the best performance.

Regarding the ORC condensation mode, the ambient-condensation mode is compared to the blow-off operation mode and to the partial condensation. The electric efficiency of the CHEST system, expressed as the ratio between the ORC electricity output and the additional heat output from the DH boiler, varies for different HT-HP capacities. This so-defined electric efficiency is higher in blow-off operation for HT-HP capacities larger than 3 kW, while is higher in ambient-condensation mode for HT-HP capacities of 3 kW or smaller.

Because of the large heat requirements from the CHEST system, an increase in solar thermal collector is recommended to improve the system performance. For example, doubling the installed solar collector area improves the COP of the HT-HP, but it also reduces the operation of the boiler operation compared to the reference scenario without CHEST system.

Comparing the performance of the CHEST system with the reference scenario (battery storage, no CHEST system, cf. Table 3), the CHEST system is not competitive with the battery storage from an energy point of view, as it requires a more intense operation of the DH boiler (hence higher fuel consumption) and delivers a lower amount of electricity back to the system, even when absorbing the same amount of electricity surplus, due to a P2P ratio (in the range of 40 %- 50 %) lower than the battery efficiency (70 %). The CHEST may still be competitive in terms of economic feasibility, if its investment cost is lower than that of battery storage.

4.1.3. Case study #4: Barcelona

Depending on the priority of either heat or electricity production, the conclusions for the dimensions of a CHEST system are different. If the focus lies on the supply of heat to the DH system, a CHEST system is not reasonable. Instead, only a LT-TES, for instance with a size of 70,000 m³, should be installed, because a CHEST system does not lead to advantages for the heat side. In fact, more backup heating than before is needed, as shown below.

If the focus, however, is on the electricity side, a CHEST system for the Barcelona case could be dimensioned as follows:

- HP capacity of 10 MW
- ORC capacity of 5 MW
- HT-TES size of 12 h
- LT-TES size of 70,000 m³
- condensation mode: partial condensation to sea water

In Table 8, a comparison of these two scenarios and of the original situation (current status without CHEST system and without LT-TES) is shown in order to illustrate the benefit of the CHEST system.

In the current situation of the Barcelona case study, despite the availability of 49.1 GWh of RES heat, there is still a demand of 8.3 GWh as backup heat, due to non-synchronicity between RES heat availability and heat demand (Figure 14). While in a scenario where a LT-TES of 70,000 m³ is installed, the need for backup heat is reduced by about 6.6 GWh to 1.7 GWh. On the electricity side, nothing changes.

Installing a CHEST system with the dimensions mentioned above results in a considerable increase of the backup heat, as the CHEST system needs a lot of high-temperature heat for its operation and wastes a lot of low-temperature heat through the ORC condensation through

ambient-condensation. The amount of low-temperature heat dissipated to the environment is so large that despite the massive RES heat availability, nearly the complete DH heat demand is covered by the boiler. On the other hand, there is now a benefit of 8.7 GWh electricity production from the ORC and thus a respective reduction of the electricity deficit.

Table 8: Overview of the amounts of heat and electricity in three different scenarios.

Scenario		Current situation	Only LT-TES	CHEST system with LT-TES
DH Heat demand	[GWh]	29.0	29.0	29.0
RES heat available	[GWh]	49.1	49.1	49.1
Heat deficit = Backup heating	[GWh]	8.3	1.7	28.3
Electricity deficit	[GWh]	69.1	69.1	60.4
Electricity surplus = Unused RES el.	[GWh]	64.2	64.2	40.4
Electricity absorbed by HP	[GWh]	-	-	23.8
Electricity produced by ORC	[GWh]	-	-	8.7
P2P ratio	[%]	-	-	36.6

The impact of the CHEST system on the Barcelona case is the following: the backup heat increases by 20 GWh, while the electricity deficit decreases by 8.7 GWh. In other words, 8.7 GWh of electricity are produced with the use of 20 GWh of heat, which gives an efficiency of 43.5 % for this electricity production.

4.1.4. General conclusions

Based on the results presented both in this deliverable and in the previous CHESTER deliverable D2.2, the following conclusions can be drawn.

In presence of a finite availability of RES-heat, increasingly larger HT-HP capacities generally entail:

- progressively lower COP, due to the lower temperature at the inlet of the HT-HP's evaporator,
- progressively smaller increase in the amount of electricity absorbed by the HT-HP, due to the shape of the profile of the electricity surplus,
- progressively smaller increase in the amount of electricity produced by the ORC, due to its correlation to the amount of absorbed electricity.

Unlike the COP of the HT-HP, the efficiency of the ORC, only function of the inlet temperature to the ORC's condenser, is found to be largely independent of the size of the components of the CHEST systems. Therefore, the P2P ratio, which as first approximation can be assumed to be proportional to the product of HT-HP's COP and ORC efficiency, generally follows the same trend as the HT-HP's COP.

Besides the size of the HT-HP, also larger HT-TES sizes generally entails a decrease of the COP, due to longer operation of the HT-HP. However, the more important effect of the size of the HT-TES is on performance indicators such as the number of full-load hours of the HT-HP or that

of the ORC (or similarly the electricity consumption/production). These parameters typically present an increasing trend for larger HT-TES sizes, but this increase is progressively smaller for larger HT-TES sizes. The more suitable size of the HT-TES depended strongly on the application and, more precisely on the distribution of the profiles of electricity surplus and electricity deficit. So, the storage time period of the HT-TES may vary between a couple of hours up to a couple of day, depending on the origin of the electricity surplus (imperfect control, PV, wind turbines, etc.). Especially in case of frequent on/off operation of the CHEST system, the ability of the CHEST components to have a fast-dynamic response should be verified, as this aspect is not considered in this analysis.

Unless the size of the ORC is particularly small (relative capacities <0.25), this component has a minor influence on the performance of the CHEST system in the investigated scenarios. Additionally, it is found that ORC having relative capacities in the range 0.25-0.50 are sufficient to reach almost the same performance as much larger ORC.

Regarding the condensation of the ORC, the overall DH+CHEST system reaches a higher energy performance, when as little energy as possible is dissipated to the environment. Therefore, the ORC should condense to the DH network (i.e. to the LT-TES) as much as possible. Currently, the CHEST system wastes a lot of low-temperature heat, which could be reduced in the case that

1. the ORC condenses at a higher temperature (nominally the DH return temperature)

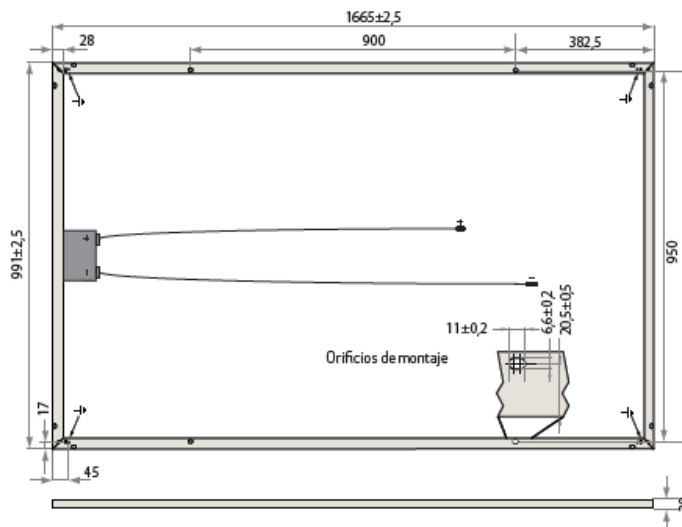
and/or

2. the DH return temperature is lowered to the highest condensing temperature allowed by the ORC.

If the above-mentioned options are not feasible, and in presence of DH return temperatures higher than the maximum ORC condensing temperature, having the ORC condensing to the environment is preferable both because of the higher efficiency of the overall system and because of the higher ORC efficiency

Regarding the working fluid, the use of R1233zd(E) and butene is roughly comparable in terms of performance. Therefore, the choice of one over the other is likely to be motivated by other type of considerations, such as safety of operation, environmental impact, compatibility with lubricants, cost, etc.

5. Appendix A



Dimensiones del módulo en mm.

16,1% EFICIENCIA

10 AÑOS DE GARANTÍA DE PRODUCTO

25 AÑOS DE GARANTÍA LINEAL DE LA POTENCIA NOMINAL

PARÁMETROS TÉRMICOS	
Temp. de operación nominal de la célula (noct)	45,7°C (±2°C)
Coefficiente de temperatura para P _{MPP}	-0,40%/°C
Coefficiente de temperatura V _{OC}	-0,27%/°C
Coefficiente de temperatura I _{SC}	0,024%/°C

DATOS GENERALES	
Tipo de célula:	60 células policristalinas REC PE 3 cadenas de 20 células con diodos de derivación
Cristal:	Vidrio solar de 3,2 mm con tratamiento antirreflejante
Lámina posterior:	Doble capa de poliéster de alta resistencia
Marco:	Aluminio anodizado
Caja de conexiones:	IP 67 Cable solar 4mm ² , 0.90 m + 1.20 m
Conectores:	Multi-Contact MC4 (4 mm ²)
Origen:	Fabricado en Singapore

LÍMITES OPERATIVOS	
Margen de temperatura del módulo:	-40 ... +85°C
Voltaje máximo del sistema:	1000V
Máxima carga de nieve:	550 kg/m ² (5400 Pa)
Máxima carga de viento:	244 kg/m ² (2400 Pa)
Capacidad máxima del fusible:	25A
Máxima Corriente Inversa:	25A

DATOS MECÁNICOS	
Dimensiones:	1665 x 991 x 38 mm
Área:	1,65 m ²
Peso:	18 kg

¡Atención! Las especificaciones están sujetas a cambios sin notificación previa.

PARÁMETROS ELÉCTRICOS @ STC	REC240PE	REC245PE	REC250PE	REC255PE	REC260PE	REC265PE
Potencia nominal - P _{MPP} (Wp)	240	245	250	255	260	265
Clasificación de la clase de potencia - (W)	0/+5	0/+5	0/+5	0/+5	0/+5	0/+5
Tensión nominal - V _{MPP} (V)	29,7	30,1	30,2	30,5	30,7	30,9
Corriente nominal - I _{MPP} (A)	8,17	8,23	8,30	8,42	8,50	8,58
Tensión a circuito abierto - V _{OC} (V)	36,8	37,1	37,4	37,6	37,8	38,1
Corriente corto circuito - I _{SC} (A)	8,75	8,80	8,86	8,95	9,01	9,08
Eficiencia del módulo (%)	14,5	14,8	15,1	15,5	15,8	16,1

Los datos analizados demuestran que el 99,7% de los módulos tienen una tolerancia de corriente y tensión del ±3% respecto al valor nominal. Valores en condiciones estándar de medida STC (masa de aire AM1,5, irradiancia 1000W/m², temperatura de la célula 25°C). En bajas radiaciones de 200 W/m² y condiciones STC (1,5 AM y Temperatura de célula de 25°C) es posible obtener, al menos el 96% de la eficiencia.

PARÁMETROS ELÉCTRICOS @ NOCT	REC240PE	REC245PE	REC250PE	REC255PE	REC260PE	REC265PE
Potencia nominal - P _{MPP} (Wp)	183	187	189	193	197	202
Tensión nominal - V _{MPP} (V)	27,7	28,1	28,3	28,5	29,0	29,4
Corriente nominal - I _{MPP} (A)	6,58	6,64	6,68	6,77	6,81	6,90
Tensión a circuito abierto - V _{OC} (V)	34,4	34,7	35,0	35,3	35,7	36,0
Corriente de corto circuito - I _{SC} (A)	7,03	7,08	7,12	7,21	7,24	7,30

Temperatura nominal de la célula (NOCT) 800W/m²; AM1,5, velocidad del viento 1m/s, temperatura ambiente 20°C.

CERTIFICADOS

IEC 61215, IEC 61730 y UL1703; IEC 62716 (resistencia al amoníaco), IEC 60068-2-68 (degradación por tormenta de arena), IEC 61701 (corrosión en presencia de niebla salina - nivel 1 & 6).

takeaway
for an easy way

GARANTÍA

10 años de garantía de producto
25 años de garantía de la potencia nominal lineal (máxima degradación de rendimiento del 0,7% p.a.)
(Ver detalles en las Condiciones de Garantía)

Figure 77: Technical datasheet of the PV module (REC250PE) used in Ispaster case.

Summary of EN 12975 Test Results, annex to Solar KEYMARK Certificate						Certificate No.		011-7S089 R				
						Date of issue		25.06.2014				
Company			Ritter Energie- und Umwelttechnik GmbH & Co. KG			Country			Deutschland			
Brand (optional)						Website			www.ritter-gruppe.com			
Street, number			Kuchenäcker 2			E-mail			J.Budde@ritter-gruppe.com			
Postal Code			72135			Tel.		+49		715 753 591 266		
City			Dettenhausen			Fax		+49		715 753 591 269		
Collector Type (flat plate / evacuate tubular / un-glazed)						Evacuated tubular collector						
Integration in the roof possible ?						No						
Collector name	Aperture area (A _a) [m ²]	Gross length [mm]	Gross width [mm]	Gross height [mm]	Gross area (A _g) [m ²]	Power output per collector unit G = 1000 W/m ² T _m -T _a :						
						0 K	10 K	30 K	50 K	70 K		
						[W]	[W]	[W]	[W]	[W]		
CPC 14 Star azzurro	2.33	1 616	1 622	120	2.62	1 501	1 482	1 438	1 384	1 321		
CPC 21 Star azzurro	3.47	1 616	2 427	120	3.92	2 235	2 207	2 141	2 061	1 968		
CPC 30 Star azzurro*	3.00	2 033	1 622	120	3.30	1 932	1 908	1 851	1 782	1 701		
CPC 45 Star azzurro*	4.50	2 033	2 427	120	4.93	2 898	2 862	2 777	2 673	2 552		
CPC 14 INOX RP *	2.33	1 616	1 622	120	2.62	1 501	1 482	1 438	1 384	1 321		
CPC 21 INOX RP*	3.47	1 616	2 427	120	3.92	2 235	2 207	2 141	2 061	1 968		
CPC 14 INOX mono*	2.33	1 616	1 622	120	2.62	1 501	1 482	1 438	1 384	1 321		
CPC 21 INOX mono*	3.47	1 616	2 427	120	3.92	2 235	2 207	2 141	2 061	1 968		
STAR 15/26 *	2.33	1 616	1 627	122	2.63	1 501	1 482	1 438	1 384	1 321		
STAR 15/39 *	3.47	1 616	2 432	122	3.93	2 235	2 207	2 141	2 061	1 968		
STAR 19/33 *	3.00	2 033	1 627	122	3.31	1 932	1 908	1 851	1 782	1 701		
STAR 19/49 *	4.50	2 033	2 432	122	4.94	2 898	2 862	2 777	2 673	2 552		
Collector efficiency parameters related to aperture area (A _a)						η _{0a}		0.644		-		
Type of fluid and flow rate see note 1						a _{1a}		0.749		W/(m ² K)		
						a _{2a}		0.005		W/(m ² K ²)		
Stagnation temperature - Weather conditions see note 2						t _{stg}		301		°C		
Effective thermal capacity						C _{eff} = C/A _a		9.18		kJ/(m ² K)		
Max. operation pressure - see note 3						p _{max}		1000		kPa		
Incidence angle modifiers K _θ (θ)	G _{DIFF} /G _{TOT}		θ _T / θ _L	50°	10°	20°	30°	40°	60°	70°		
	min	max									K _θ (θ _T)	0.98
	-	-	K _θ (θ _L)	0.95	1.00	1.00	0.99	0.98	0.89	0.76		
G _{DIFF} /G _{TOT} : min&max - while measuring						Optional values						
Testing Laboratory						TZS, ITW University of Stuttgart						
Website						www.tzs.uni-stuttgart.de						
Test report id. number						06COL456/6						
Date of test report						25.06.2014						
Perf. test method						EN 12975-2 6.1.4 (outdoor)						
Comments of testing laboratory :												
* dimensions according to manufacturer												

Figure 78: Technical datasheet of the CPC collector (STAR 19/49) used in Ispaster case.

References

- [GNB, 2018]. GNB Industrial Power. Industrial Batteries / Network Power – Classic Solar. 2018. Available at <https://autosolar.es/baterias-estacionarias-opzs-24v/bateria-opzs-24v-2350ah-transparente-tudor-exide>.
- [Fugmann, 2015]. Fugmann H., Nienborg B., Trommler G., Dalibard A., Schnabel L.; Performance Evaluation of Air-Based Heat Rejection Systems. 2015. Energies 8, 714-741. Available at doi.org/10.3390/en8020714.